9-12-2014

Stochastic Dynamics of Cascading Failures in Electric-Cyber Infrastructures

Mahshid Rahnamay Naeini

Mahshid Rahnamay-Naeini

Candidate

Electrical and Computer Engineering

Department

This dissertation is approved, and it is acceptable in quality and form for publication:

Approved by the Dissertation Committee:

Professor Majeed M. Hayat , Chairperson

Professor Andrea Mammoli

Professor Maria Cristina Pereyra

Professor Olga Lavrova

Stochastic Dynamics of Cascading Failures in Electric-Cyber Infrastructures

by

Mahshid Rahnamay-Naeini

B.S., Computer Engineering, Sharif University of Technology, 2007
M.S., Computer Engineering, Amirkabir University of Technology (Tehran Polytechnic), 2009

DISSERTATION

Submitted in Partial Fulfillment of the
Requirements for the Degree of

Doctor of Philosophy
Engineering

The University of New Mexico

Albuquerque, New Mexico

July 2014

Dedication

To my husband, my beloved parents, and my wonderful siblings.

Acknowledgments

This work is the result of invaluable support and guidance of many, some of whom are acknowledged below. First and foremost I would like to express my deepest gratitude to my advisor Prof. Majeed M. Hayat for his excellent guidance, encouragement, support, kindness, and help which made my Ph.D. experience productive and stimulating. It has been a great honor for me to work under his guidance. I have learned immensely from him and I am so grateful to him for this great opportunity.

I would specially like to thank my committee members Dr. Andrea Mammoli, Dr. Maria Cristina Pereyra, and Dr. Olga Lavrova for their valuable suggestions and questions. In particular, I praise the enormous amount of help and guidance by Dr. Andrea Mammoli. Thank you for invaluable discussions and suggestions during the development of this work. I would like to thank Dr. Maria Cristina Pereyra for her valuable suggestions, guidance, advices and comments on this dissertation. I would also like to thank Dr. Olga Lavrova for her valuable comments and advices on this dissertation. I am greatly thankful to Dr. Nasir Ghani for his invaluable guidance, discussions, advices, and friendship. He has been very encouraging and supportive, and I owe a debt of gratitude to him. I would also like to acknowledge the helpful faculty and staff at UNM, specially Dr. Meeko Oishi, Dr. David Ramirez and Mr.James E. Prewett. I would like to greatly thank the past and present members of our research group who have contributed immensely to my personal and professional experience at UNM. I must thank Dr. Jorge Pezoa, and specially Mr. Zhuoyao Wang for the enormous amount of help he provided me in this work. Also, thank you Ghady Azar, Yasser Yasaei, Mostafa Aghaee, Shahin Abdollahy, Sebastian Godoy and Georges El-Howayek.

At last, I would like to thank my beloved husband Mostafa, my parents Mahin and Majid, my siblings, my parents-in-law and my entire family for their love, and unconditional support. Special thanks also to Prof. Hayat's family and all my wonderful friends specially Elham, Pouyan, Leila, and Nima for their support and kindness. Thank you all very much! This work has been supported by Prof. Majeed M. Hayat's projects supported by the Defense Threat Reduction Agency's Basic Research Program under grant No. HDTRA1-13-1-0020 and the Defense Threat Reduction Agency contract No. DTRA01-03-D-0009-0026, University Partnership Program: Fundamental Research and by NPRP 5 - 137 - 2 - 045 grant from the Qatar National Research Fund (a member of Qatar Foundation).

Stochastic Dynamics of Cascading Failures in Electric-Cyber Infrastructures

by

Mahshid Rahnamay-Naeini

B.S., Computer Engineering, Sharif University of Technology, 2007
M.S., Computer Engineering, Amirkabir University of Technology (Tehran Polytechnic), 2009

Ph.D., Engineering, University of New Mexico, 2014

Abstract

Emerging smart grids consist of tightly-coupled systems, namely a power grid and a communication system. While today's power grids are highly reliable and modern control and communication systems have been deployed to further enhance their reliability, historical data suggest that they are yet vulnerable to large failures. A small set of initial disturbances in power grids in conjunction with lack of effective, corrective actions in a timely manner can trigger a sequence of dependent component failures, called cascading failures. The main thrust of this dissertation is to build a probabilistic framework for modeling cascading failures in power grids while capturing their interactions with the coupled communication systems so that the risk of cascading failures in the composite complex electric-cyber infrastructures can be examined, analyzed and predicted.

A scalable and analytically tractable continuous-time Markov chain model for stochastic dynamics of cascading failures in power grids is constructed while retain-

ing key physical attributes and operating characteristics of the power grid. The key idea of the proposed framework is to simplify the state space of the complex power system while capturing the effects of the omitted variables through the transition probabilities and their parametric dependence on physical attributes and operating characteristics of the system. In particular, the effects of the interdependencies between the power grid and the communication system have been captured by a parametric formulation of the transition probabilities using Monte-Carlo simulations of cascading failures. The cascading failures are simulated with a coupled power-system simulation framework, which is also developed in this dissertation. Specifically, the probabilistic model enables the prediction of the evolution of the blackout probability in time. Furthermore, the asymptotic analysis of the blackout probability enables the calculation of the probability mass function of the blackout size, which has been shown to have a heavy tail, e.g., power-law distribution, specifically when the grid is operating under stress scenarios. A key benefit of the model is that it enables the characterization of the severity of cascading failures in terms of a set of operating characteristics of the power grid. As a generalization to the Markov chain model, a regeneration-based model for cascading failures is also developed. The regeneration-based framework is capable of modeling cascading failures in a more general setting where the probability distribution of events in the system follows an arbitrarily specified distribution with non-Markovian characteristics.

Further, a novel interdependent Markov chain model is developed, which provides a general probabilistic framework for capturing the effects of interactions among interdependent infrastructures on cascading failures. A key insight obtained from this model is that interdependencies between two systems can make two individually reliable systems behave unreliably. In particular, we show that due to the interdependencies two chains with non-heavy tail asymptotic failure distribution can result in a heavy tail distribution when coupled.

Lastly, another aspect of future smart grids is studied by characterizing the fundamental bounds on the information rate in the sensor network that monitors the power grid. Specifically, a distributed source coding framework is presented that enables an improved estimate of the lower bound for the minimum required communication capacity to accurately describe the state of components in the information-centric power grid.

The models developed in this dissertation provide critical understanding of cascading failures in electric-cyber infrastructures and facilitate reliable and quick detection of the risk of blackouts and precursors to cascading failures. These capabilities can guide the design of efficient communication systems and cascade-aware control policies for future smart grids.

Contents

List of Figures

List of Figures

Chapter 1

Introduction

1.1 Overview and motivation

A collection of systems are said to be *interdependent* if the behavior of a system affects the other systems' behavior. Many critical infrastructures are interdependent systems, wherein the reliability of each system affects the reliability of other systems. Examples of such interdependent infrastructures are power, communication, transportation, and financial market infrastructures. Reliable operation of critical infrastructures is essential as it impacts national security and the economy. Due to the importance of critical infrastructures it is important to develop frameworks for accurate prediction of their reliability and complex behavior. However, complexity and scale of critical infrastructures as well as their interdependencies make modeling and analysis of such systems challenging. Many proposed frameworks for reliability analysis of critical interdependent infrastructures consider infrastructures individually, while emerging efforts consider interdependent infrastructures jointly as a single system.

In this dissertation, the critical infrastructures under study are power and com-

munication infrastructures. While power grids are currently highly reliable, historical data suggest that their complex nature, aging, growing demands, operation near their limits, as well as lack of infrastructure investment make them vulnerable to intermittent failures. When such systems become stressed due to a small set of initial disturbances a sequence of *dependent* component failures may occur in the system. Such sequence of dependent failures is called *cascading failures*. As stated in [3], historical data indicate that many blackouts in power grids result from cascading failures. Specifically, cascading failures in power grids has gained much attention due to their cost and large impact on society. For instance, the 2003 blackout in the Northeast grid of the United States led to electrical service interruption to approximately 50 million people in eight US states and one Canadian province [2]. Also, the 2003 blackout in Italy affected approximately 57 million people in Italy and Switzerland [6].

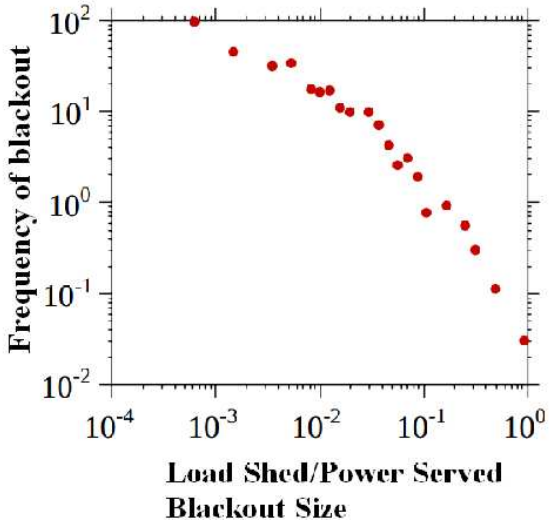

Figure 1.1: A power-law scaling of blackout frequency based on the historical data. Blackout size is measured by unserved energy (the figure is a copy borrowed from [1].)

Although severe infrastructure disruptions such as large blackouts are rare, new findings suggest that their probability is higher than what traditional risk analysis

predicts [1, 7]. Moreover, moderate size cascading failures (interruption of service to 50,000 customers or less) are surprisingly common according to [3]. Generally, a power-law scaling of blackout frequency has been observed, as shown in Fig. 1.1 from [1], based on the available historical data, when the blackout size is measured by unserved energy. The power-law behavior in the distribution of the blackout size suggests that the probability of large blackouts are larger than what can be ignored. Therefore, it is important to analyze the risk and probability of large blackouts in power grids.

Large cascading failures in the transmission grid of power grids can be triggered by a combination of a small set of initial failures and lack of proper corrective actions in a timely manner. Power grids are usually operated so that a single failure of one of the most critical components can be absorbed without cascading failures (N-1 Criterion). The ability of the grid to operate in this fashion is linked to the integrity of the sensing and communication systems, as well as to the ability of the monitoring tools to convey accurate information to human operators and automatic control systems, which are ultimately responsible for corrective actions such as load shedding. As we move toward smarter power grids, power grids rely more and more on the modern control and communication technologies to improve their reliability and efficiency. However, these gains come with their own vulnerabilities, since the correct functioning of the power grid depends not only on the integrity of the power infrastructure but also on the effectiveness of the communication system. Vulnerabilities associated with communication systems, such as physical component failures, cyber attacks and communication-protocol inefficiencies, can threaten the reliability of power grids specially when they are stressed. Historical data also suggest that power and communication infrastructures are interdependent and the reliability of one affects the reliability of the other. For instance, in the 2003 blackout in Italy on September 28th, unplanned shutdown of a power station led to failures of communication network nodes and the supervisory control and data acquisition (SCADA)

system, which were responsible for controlling the power grid. This event, in turn, led to further failures in the power grid resulting in a large cascading-failure event in the system [8]. Another example of such interdependency is observable in the 2003 blackout in the Northeast United States, where not only power-component failures contributed to cascading failures so did the computer and human events. Figure 1.2 presents the timeline of initial power, computer and human events at the start of the 2003 blackout in Ohio [2]. Here, a mishandled restart of a monitoring system led to a sequence of undetected failures. Subsequent corrective actions, such as load shedding, were also delayed as the operator had never seen requests of such a magnitude and was unaware of the rapidly developing crisis. As such, miscommunication and failures in the control and monitoring systems fueled the cascade of failures leading to a large blackout. In summary, interdependencies and extensive integration of power grids and communication systems mandate that they should be studied as a single electric-cyber system specially when the reliability of the system is of concern. Another important lesson to be learned from the past events is that human error also plays an important role in the cascading behavior of the system. Although it has not been explored in this dissertation, human-behavioral aspects of cascading failures such as the level of stress and panic, and operators susceptibility to errors are also key components to be investigated in the reliability of electric-cyber infrastructures. Our research group at the University of New Mexico in collaboration with Fraunhofer USA Center for Sustainable Energy Systems is currently working on modeling the behavior of the power-grid operators and its impact on cascading failures.

Another important point regarding cascading failures is that the time evolution of failures exhibits three phases. The first phase of cascading failures is the *precursor phase*, where the progress of failures is slow and the control actions are effective to mitigate the effects of disturbances. The second phase of cascading failures is the *escalation phase*, where failures occur very fast and preventing blackouts in this phase is very difficult. The third phase of cascading failures is *cascade phase out*, where the

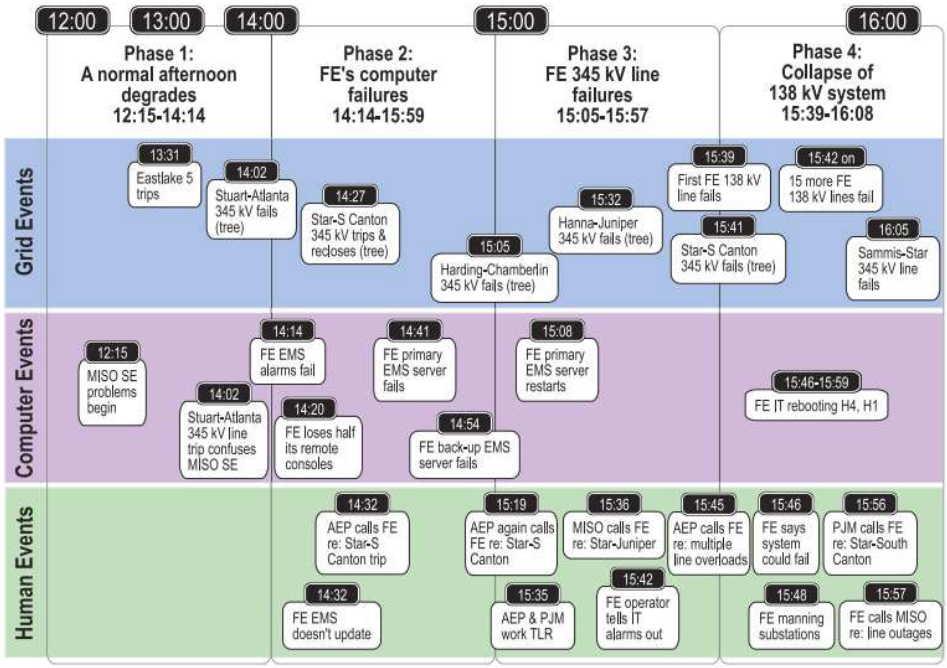

Figure 1.2: The timeline of initial power, computer and human events at the start of the 2003 blackout in Ohio (the figure is a copy borrowed from [2].)

progress of failures becomes slow again. This behavior can be attributed to the fact that a large number of components have already failed and functional islands have formed in the system leading to the termination of cascading failures. These three phases are easily observable in the time evolution of failures in the 2003 blackout shown in Fig. 1.3. Clearly, the ability to reliably and quickly detect precursors to cascading failures before the system enters the escalation phase, combined with fast and correct responses are crucial for mitigating large blackouts. Hence, it is important to build predictive tools that can identify the risk of large cascading failures in integrated power and communication infrastructures.

Nowadays, operators have become more adept at operating the grid near its physical limits by taking advantage of advances in communications and data processing. In particular, advances in sensor technologies have accelerated the use of sensors for continuously monitoring components of critical infrastructures. The employed

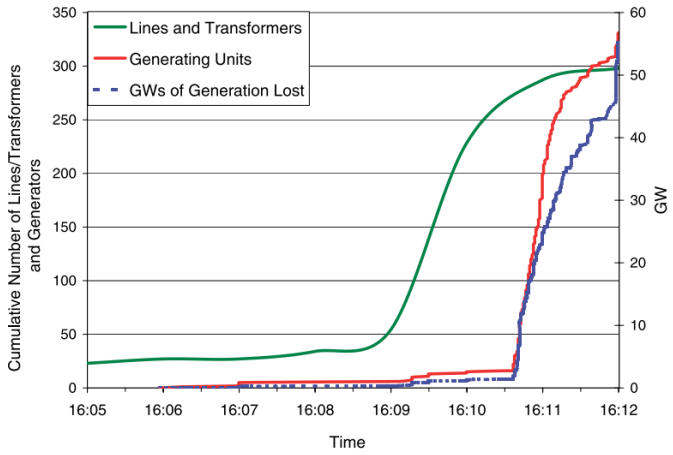

Figure 1.3: Time evolution of failure accumulation in the 2003 blackout in Northeast United States power grid (the figure is a copy borrowed from [2].)

sensors take samples of the status of components with high frequency and send the status updates to control centers, enabling them to accurately estimate the state of the system. As such, smart grids of the future will face large volume of data, which must be handled efficiently by provisioning necessary computation and communication resources.

The size of customer demands, available generation resources, and the status of the control and communication system determine the operating setting of the power grid. The operating setting can largely affect the resilience of the system in the case of contingencies. In general, cascading failures in power grids are particularly complex phenomena as they are attributable to a large number of interacting factors and stochastic events. It is essential to develop theoretical frameworks driven by the need to abstract and better understand such complex phenomena in such complex systems. The fundamental understanding of cascading behaviors guides the design of control policies for power grids as well as reliable communication networks for robustness of the power grid. It is also crucial to characterize the severity of cascading failures in terms of the operating characteristics of the power grid to avoid operating

modes that increase the probability of large blackouts. Specifically, understanding cascading failures in interdependent infrastructures is significantly important as the interdependency between infrastructures can result in new behaviors for the whole system as a single system, which are not observable in the individual systems.

1.2 Literature review

1.2.1 Prior work on modeling cascading failures in power grids

In the past two decades, a great volume of work has been devoted to understanding and analyzing cascading failures. The majority of research in cascading failures in power grids has been focused on single, non-interacting power systems. A review of different available methods for analyzing cascading failures in power grids is provided in [9]. These efforts can be categorized into three classes: analysis of cascading failures using power-system simulations [10], deterministic analytical models [11–13], and probabilistic analytical models [5, 14–18]. Each approach sheds light on certain aspects of cascading failures with various degrees of detail and complexity.

Many of the approaches that are based on power-system simulations use static line overloads with DC power flow model [10]. In simulation-based approaches there is a trade-off between complexity and simulation time, on one hand, and details and diverse scenarios that the simulator can simulate on the other hand.

In the category of deterministic approaches, the work in [12] presents a model for cascading failures in complex networks. This work is motivated in part by the propagation of failures and congestion in computer networks. The presented model for communication networks differs from power-grid models in that it considers flows

of fully controlled discrete packets of information, rather than flow of electricity in the power grid. Another example of the deterministic model is a hybrid nonlinear system model using Lyapunov methods that is proposed by DeMarco in [11] to determine cascading failures due to dynamic transients in the system. In this work a detailed RLC circuit model is used as an example to illustrate the concept of cascading failures in the context of RLC circuits (electrical circuits consisting of resistors, inductors, and capacitors). Some limitations of the deterministic approaches are their inability to capture the effects of stochastic events that may affect cascading failures and the complexity and scalability limitations to large systems.

Probabilistic models for cascading failures can elegantly capture the stochastic dynamics of cascading failures as well as the general qualitative features of cascading failures such as the risk of blackout, probability distribution of the blackout size and the asymptotic behavior of cascading failures in certain cases. In this dissertation, we focus on the probabilistic approaches for cascading failures in power grids. The CASCADE model by Dobson *et al.* [14] models cascading failures triggered by initial load increments on certain components of the system. In this model, failures occur due to overloaded components and cascading failures develop as a result of redistribution of loads among the remaining components. However, the re-distribution of loads are based upon simple assumptions; for example, loads will be added equally to the components of the system as a result of failures. The CASCADE model is a simple and analytically tractable model; however, it does not consider the topological or electrical characteristics of power grids and heterogeneity of capacity of components. Probabilistic analytical models based upon branching processes [5, 19, 20] have also emerged, providing a framework to study the statistical properties of cascading failures such as the probability distribution of the blackout size. Reported branching-process approaches model cascading failures by considering generations of failures, whereby each failure in each generation independently produces a random number of subsequent failures in the next generation, and so on. In [19, 20], the

authors estimate the failure generation parameter of the branching process model for cascading failures using historical outage datasets. Notably, in [20] the authors account for varying failure generation parameter as the cascade progresses instead of a fixed parameter as in [19]. However, authors in [20] assume that all line outages are homogeneous in their type. The models presented based on branching process have the limitation that they do not have sufficient degree of freedom to capture the effect of physical factors contributing to cascading failures, as the failure generation parameter is the only parameter used in these models.

Finally, the recent work by Wang *et al.* [17] provides a Markov-transition model for cascading failures. The transition probabilities among states are derived from a stochastic model for line overloading using a stochastic flow redistribution model based upon DC power-flow equations. The state space of the model [17] is large, as it requires tracking the functionality status of transmission lines and power flow information. This model enables simulating the progression of cascading failures and its time span. However, due to the analytical complexity of the time-varying transition probabilities the analytical and asymptotic characterization of probabilistic metrics such as the blackout probability and distribution of the blackout size is not possible.

1.2.2 Prior work on modeling cascading failures in interdependent infrastructures

Aside from efforts on understanding the reliability of individual infrastructures, there has been great interest in understanding cascading failures in interdependent infrastructures. The general concepts of interdependent infrastructures and challenges in modeling such systems have been discussed in [21–25]. We categorize the efforts for modeling cascading failures in interdependent infrastructures into three classes as described bellow.

Graph-based models – A body of work has emerged recently in understanding cascading failures in interdependent infrastructures using network theory and graph-based models. These efforts use network-theoretic tools to characterize cascading failures based on network properties and to identify vulnerable areas of the network. In such efforts, a problem that has been considered is the characterization of the minimum number of nodes/links whose removal will disrupt the functionality of the entire network [8, 26–30]. For instance, the work of Buldyrev *et al.* [31] considers a graph-based approach that utilizes percolation theory. The authors provide analytical solutions for the critical fraction of nodes that on their removal will lead to cascading failures and to a complete fragmentation of two interdependent networks. Later, Li *et al.* [32] extended the work to include geographical factors in the coupling between interdependent networks, such as considering the range of interaction between nodes from different networks. Further, the work in [33] by Wang *et al.* extended the work in [31] by taking into account the load, the load redistribution, and the node capacity in studying the robustness of two interdependent networks. In general, the graph-based models do not consider the physics of the system and they only rely on the topological connectivity of the system in their analysis.

Hybrid simulations – These approaches aim to build accurate synchronization mechanisms between the simulators of the two systems. As mentioned before, in simulation-based approaches there is a trade-off between complexity and simulation time, on one hand, and details and diverse scenarios that the simulator can simulate on the other hand. The extra challenge for the hybrid power and communication simulation is the synchronization of the continuous time power-system simulators with the discrete-event communication-system simulators. Examples of such efforts are [34–36]. The work in [37] is another example that aims to develop a simulation framework which abstracts the physical details of the services provided by the infrastructures while at the same time capturing their essential operating features. A group of efforts in this category are the approaches that focus on a specific ef-

fect of the control and communication system on the power grid and model the effects directly in the power-grid dynamics and equations. We call such approaches, *effect-driven models*. An example of such models is [38], where the role of information exchange is investigated in the transient stability of generators and the loss of generator synchronism in power grids.

Probabilistic models – Probabilistic analysis of the reliability of interdependent systems is another category of modeling cascading failures in interdependent infrastructures. The goal of these efforts is to investigate the risk of large failures as a result of interdependencies among the systems. For instance, the authors in [39, 40] introduced the Damon model in conjunction with a mean-field theory to model coupled infrastructure systems. This work suggests that the coupling between systems can make the whole system vulnerable and increase the probability of large failures. There are some intersections between the approaches in this category with the graph-based models in using probabilistic models, for instance the work by Brummitt *et al.* [41] characterizes the optimal connectivity between two interdependent networks while using the multitype branching process framework.

1.3 Contributions of this dissertation

The main thrust of this dissertation is to build a predictive capability of the reliability of a power grid while considering its interdependency with a communication system. While the majority of the work in this dissertation has been presented for power grids and communication systems, key general ideas can be applied to different interdependent infrastructures. We summaries the contributions of this dissertation as follows.

The first contribution of this dissertation is the development of *a scalable probabilistic framework for modeling cascading failures in power grids*. The key idea of the

proposed framework is to simplify the state space of the complex power system so that we can track the dynamics of cascading failures using a continuous-time Markov chain while capturing the effects of the omitted variables through the transition probabilities and their parametric dependence on the physical attributes and operating characteristics of the system. In addition to the framework's ability to predict the evolution of blackout probability in time, the asymptotic analysis of the blackout probability using this model enables the calculation of the probability mass function of the blackout size and leads to the characterization of the severity of cascading failures under different system operating characteristics. A key insight provided by this framework is that the probability distribution of size of failures in power grids has a heavy tail, which the probability of large blackouts heavily depends on the operating characteristics of the power grid. The ability to characterize the distribution of the blackout size in terms of the physical attributes and operating characteristics of the system while keeping the complexity to a minimum is a critical advantage of this approach. Other probabilistic approaches [14, 42–45] often lack a strong connection to the physical characteristics of power grids.

The second contribution of this dissertation is a generalization of the Markov chain model to another probabilistic framework for modeling cascading failures based on regeneration theory. Similarly to the Markov chain model, this model provides a strong tool for capturing the stochastic dynamics of cascading failures, albeit in a more general setting, namely non-Markovian setting. We derive, as a special case, a systems of differential equations describing the probability of the blackout for a power grid with Markovian setting using the regeneration-based framework. The analysis of this model supplements the analysis of the Markov chain model for cascading failures.

The third contribution of this dissertation is an extension of the Markov chain model to a novel interdependent Markov chain framework for modeling cascading

failures in interdependent infrastructures. To the best of the author's knowledge, interdependent Markov chains have not been proposed heretofore. The interdependent Markov chain approach proposed in this dissertation provides a probabilistic framework to capture how the stochastic dynamics of a system affects the other system's dynamics. The idea of this general approach is to build an integrated framework consisting of a system of interdependent heterogeneous Markov chains, one for each physical system. The usual approach for coupling Markov chains relies on the generation of the Cartesian product of the individual state spaces. This approach, however, has the shortcoming that the new transition probabilities among the states of the coupled Markov chain cannot be readily derived from the transition probabilities of the individual Markov chains. A more serious flaw of this approach is that it is based on the false and built-in assumption that combining two Markov chains results in a new Markov chain with its state space being the Cartesian product of the individual chains. To address these issues, we have proposed the interdependent Markov chain framework with an interleaving approach for coupling Markov chains. Meanwhile, the similar term "interactive Markov chains" [46], describes models which fall in the category of process algebra frameworks [47]. Interactive Markov chains have been introduced as a framework for analyzing concurrent systems. Generally, process algebras are abstract languages that are used to model concurrent systems as collections of entities, called agents, to describe their behaviors as well as how they communicate [48]. In these models, agents communicate by actions. The interactive Markov chain framework combines interacting agents each described by a continuous-time Markov chain by extending the standard Markov chains with action transitions and forming a stochastic process algebra framework. While these models along with an algorithm to analyze the interactions and dependencies among agents are applicable for performance analysis of systems with large number of simple agents, the complexity of the models as well as the agents increases for cases with few interacting complex systems (few very complex agents). Moreover, they do not

provide a standard probabilistic framework with its standard analytical tools. The interdependent Markov chain model presented in this dissertation enables us to characterize the impact of stochastic behavior of a system on its interdependent systems in a probabilistic framework. A key insight obtained from interdependent Markov chain framework is that interdependencies between two systems can make two reliable systems behave unreliably when they are put together, thereby increasing the probability of large failures.

The fourth contribution of this dissertation is developing a simulation framework for simulating cascading failures in electric-cyber infrastructures. Monte-Carlo simulations using this framework is used in parametric modeling of transition rates of the models for cascading failures presented in this dissertation. The proposed simulation framework is based on an integrated power-flow optimization framework, which captures certain effects of communication-system vulnerabilities in the power-flow distribution of the system. This optimization framework enables us to investigate the effects of communication vulnerabilities as well as the topology of the communication system on the reliability of the power grid.

The fifth contribution of this dissertation is developing a simulation framework that enables a systematic way of simulating correlated failures. Generally, physical infrastructures are vulnerable to spatially correlated failures arising from various physical stresses such as natural disasters (earthquakes and hurricanes) as well as malicious coordinated attacks. It is important to study the effects of spatial distribution of failures on cascading failures. As such, we present a stochastic model, based on spatial point processes, for representing stress centers on the geographical plane in order to facilitate the modeling and simulation of spatially inhomogeneous and correlated component failures in the system. This model is then used to further generate scenarios with inhibition or clustering between stress centers, which enables detailed assessment of vulnerabilities of the system to the level of inhomogeneity and

spatial correlation in the stress-event centers. This simulation framework enables us to study the effects of spatial correlation of initial failures in communication and power systems on cascading failures.

The sixth major contribution of this dissertation is developing an information-theoretic framework for characterizing the information rate of the sensor network that monitors the power grid to enhance its reliability. Due to the large number of sensors and the high frequency of sampling from the states of components, exchange of state information incurs a large communication cost on the communication system of the power grid. To characterize the minimum required information rate in the communication system, a lossless distributed source-coding framework is presented to model the exchange of state information. The framework enables the characterization of the interplay between the information rate and the correlation among the state information of various components. Moreover, the proposed framework enables an improved estimate of the lower bound for the minimum information rate necessary to accurately describe the state of components in the system. This improvement is achieved by exploiting the correlation among the state information of components as well as the available side information in the system.

In Fig. 1.4, we have summarized the contributions of this dissertation in a flow chart that shows the basic dependencies between the contributions.

1.4 Organization of the dissertation

For the convenience of the reader, whenever appropriate, the chapters provide concise review of the relevant background information and related work, as well as brief summary and our conclusions.

This dissertation is organized as follows. In Chapter 2, the structure of electric-

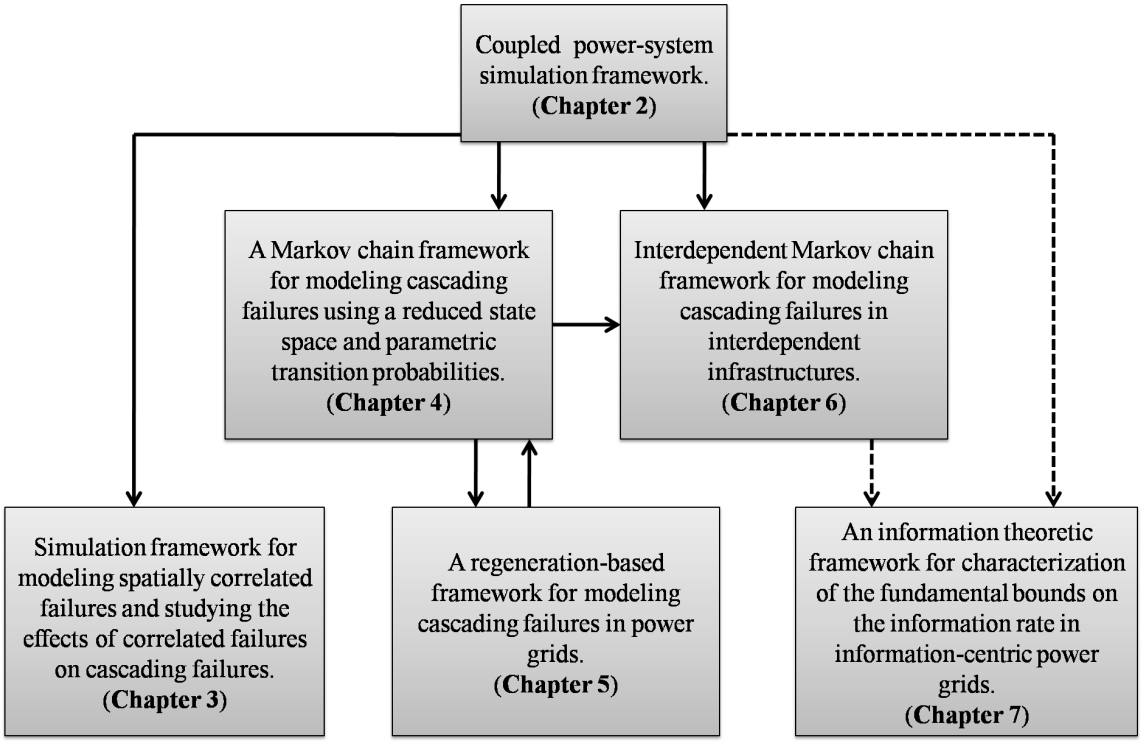

Figure 1.4: The flow chart of the basic dependencies between the contributions of this dissertation. The arrows point at the dependent contribution. The solid line represents the direct dependency between the contributions. This means certain parts of the model or the theory is used in the other contribution. The dashed line represents an indirect dependency, which means certain concepts are borrowed from the other contribution.

cyber infrastructures is reviewed. The general assumptions made about the interdependency of power grids and communication systems are stated and the interdependency parameters used in our models are introduced. In addition, the power-flow optimization framework that captures the interdependency between the power grid and the communication system and enables the simulation of cascading failures in power grids is presented. The simulation results that show the impact of interdependencies on the reliability of the power grid are also presented. Further, the effects of the connectivity of the communication system on the reliability of the communication system and the power grid is investigated.

The focus of Chapter 3 is on characterizing the effects of spatial distribution of initial failures on the reliability of communication and power systems. A probabilistic model for modeling correlated failures is provided that enables a systematic way of simulating correlated failures. Various scenarios of correlated initial failures in the communication system and their effects on the reliability of the power grid have been investigated.

In Chapter 4, a continuous-time Markov chain framework, termed Stochastic Abstract State Evolution (SASE), for modeling cascading failures in power grids is presented. The concept of equivalence classes for partitioning the state space of the power grid is introduced. The transition rates of the Markov chain capturing the effects of communication interdependencies and operating characteristics are formulated using the power-system simulations. The analytical results on the size and severity of cascading failures have been presented for various operating conditions. Finally, the conditions leading to a power-law behavior for the distribution of the blackout size in power grids are studied.

In Chapter 5, a regeneration-based approach for modeling cascading failures in power grids is presented. The integral equations describing the evolution of the blackout distribution are derived using the regeneration-based framework.

In Chapter 6, the problem of modeling cascading failures in interdependent infrastructures is formulated by extending the the Markov chain framework to an interdependent Markov chain framework. The general interdependent Markov chain approach for modeling any number of interdependent system is presented. As a specific example, the interdependent Markov chain model for power and communication infrastructures is developed.

In Chapter 7, the minimum requirement for the capacity of the communication network for tracking accurate information on the state of components in power grids

is characterized. A lossless, distributed source-coding framework is presented to model the exchange of state information. An improved estimate of the lower bound for the minimum information rate of the communication system is also derived.

Finally, in Chapter 8 possible new lines of research for this work in the future have been discussed.

1.5 Publications resulting from the dissertation

A list of our publications, related to this dissertation, is as follows:

1. M. Rahnamay-Naeini, and M. M. Hayat, "Stochastic Dynamics of Cascading Failures in Interdependent Infrastructures: An Interdependent Markov-Chain Approach", To be submitted, 2014.

2. M. Rahnamay-Naeini, and M. M. Hayat, "On the Influences of Power-Grid Operating Characteristics on Self-Organized Criticality", To be submitted, 2014.

3. M. Rahnamay-Naeini, Z. Wang, N. Ghani, A. Mammoli, and M. M. Hayat, "Stochastic Analysis of Cascading-Failure Dynamics in Power Grids", *IEEE Transactions on Power Systems,* vol. PP, no. 99, 2014.

4. M. Rahnamay-Naeini and M. M. Hayat, "On the Role of Power-Grid and Communication-System Interdependencies on Cascading Failures", *Proceedings of IEEE Global Conference on Signal and Information Processing*, pp. 527-530, 2013.

5. M. Rahnamay-Naeini, N. Ghani, and M. M. Hayat, "On the Interplay Between Resource-Management Overhead and Performance in Sensor Networks: An Information Theoretic Approach", *IEEE GLOBECOM*, 2013.

6. M. Rahnamay-Naeini, Z. Wang, A. Mammoli, and M. M. Hayat, "A Probabilistic Model for the Dynamics of Cascading Failures and Blackouts in Power Grids", *IEEE Power and Energy Society General Meeting,* San Diego, CA, 2012.

7. M. Rahnamay-Naeini, Z. Wang, A. Mammoli, and M. M. Hayat, "Impacts of Control and Communication System Vulnerabilities on Power Systems Under Contingencies", *IEEE Power and Energy Society General Meeting,* San Diego, CA, 2012.

8. M. Rahnamay-Naeini, Jorge E. Pezoa, Ghady Azar, Nasir Ghani, Majeed M. Hayat, "Modeling Stochastic Correlated Failures and their Effects on Network Reliability", *Proceedings of 20th International Conference on Computer Communications and Networks (ICCCN)*, pp. 1-6, Maui, Hawaii, August 2011.

Chapter 2

Interdependent electric and cyber infrastructures

In this chapter, we start by briefly reviewing the structure of the electric-cyber infrastructure. We then develop a simulation framework that enables simulating cascading failures in an electric-cyber infrastructure. To do so, we first introduce the overloading and failure mechanisms assumed in this dissertation for modeling cascading failures. Next, we review the general sources of interdependency among critical infrastructures and state the assumptions made about the interdependency of power grids and communication systems that lead to propagation of failures between the two systems. Based on these assumptions, we introduce interdependency parameters that will be used in our models. Further, the power-flow optimization framework that captures the interdependency between the power grid and the communication system is presented based on the general DC power-flow optimization framework [49]. Using this optimization framework, we simulate cascading failures and study the extent to which the interdependency between the two systems affects the reliability of the coupled system. We show that as the level of interdependency between the two systems increases the frequency of failures in the individual systems

increases and severe cascading behavior occurs. The simulation framework proposed in this chapter will be used for Monte-Carlo simulations of cascading failures and estimating the parameters of the model presented in Chapter 4.

2.1 Structure of the electric-cyber infrastructure

A power grid is an interconnected network that delivers electricity from generation resources to consumers. In general, power grids consist of distribution and transmission networks. The transmission network transmits electricity over long distances. We describe the transmission network as a set of nodes interconnected by high-voltage transmission lines. In the transmission network, network nodes represent load buses $\mathcal{L}$ (substations, which are connected to distribution network), generating stations $\mathcal{G}$, combinations of load and generating buses, and transmission buses that do not have any load or generating resources and only help in transmitting power in the transmission network. At a substation, the power is stepped down from a transmission level voltage to a distribution level voltage and is delivered to individual customers by distribution lines. Figure 2.1 depicts the schematics of distribution and transmission networks. As large blackouts and cascading failures are attributes of the transmission network, we focus on the transmission network of power grids in this dissertation. We use IEEE 118 bus system (Fig. 2.2) and IEEE 300 bus system (Fig. 2.3) as two examples of transmission networks for simulation and analysis purposes.

Power grids rely on their control and communication systems for efficient and reliable daily operations. The control and communication systems of power grids are hierarchical systems (see Fig. 2.1). For instance, in the distribution-network level, neighbor area networks (NAN) provide network connectivity to endpoints such as smart meters deployed at customer homes and businesses. At the next level of the

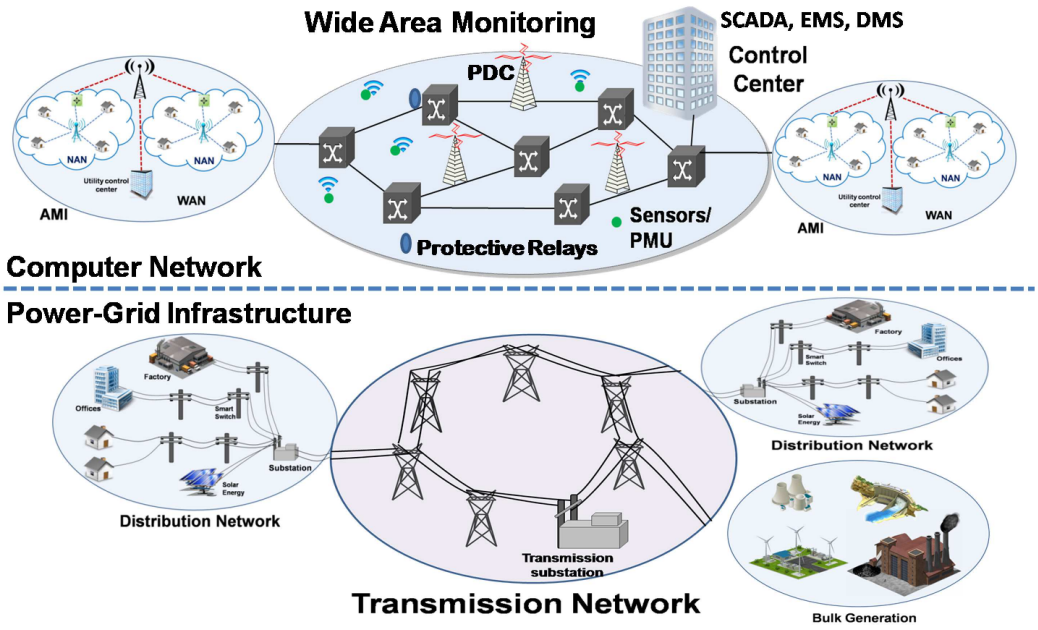

Figure 2.1: A balancing authority (BA) consisting of a transmission network and two distribution networks along with their control and communicating systems. The electric-cyber infrastructures have hierarchical structures.

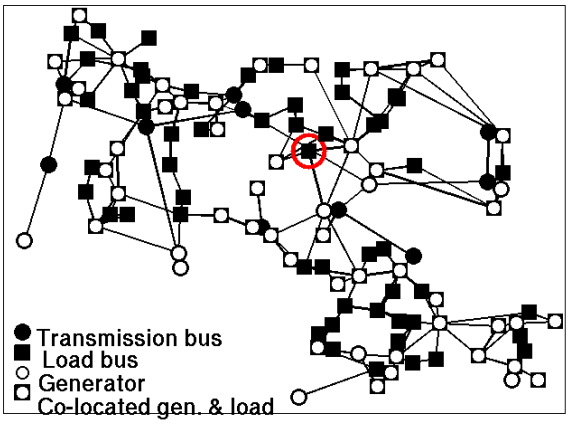

Figure 2.2: Topology of the IEEE 118 bus system. The control center for this transmission network is assumed to be co-located with the node marked by the circle.

hierarchy, wide area networks (WAN) connect multiple NANs to the control centers at the distribution-network level for monitoring and control purposes. Another level

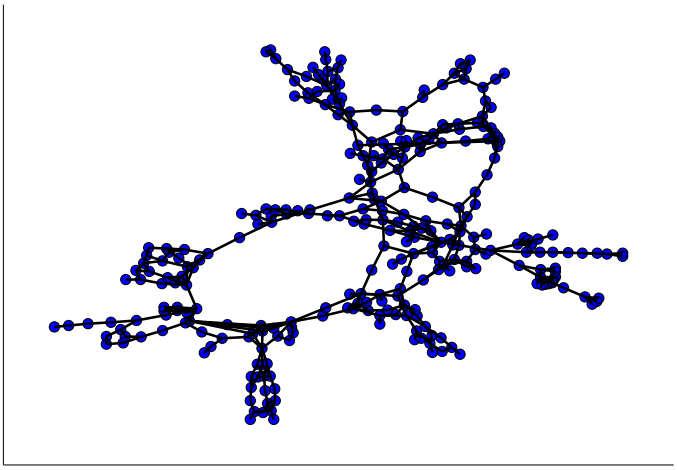

Figure 2.3: Topology of the IEEE 300 bus system. The topology is plotted based on the topology map from [3].

of the hierarchy is at the transmission-network level, where sensors, phasor measurement unit (PMU), phasor data concentrators (PDC), and protective relays connect through a wide area monitoring network that communicates the state information of transmission-network components to the control center at the transmission-network level. The control centers employ, for example, SCADA, energy management system (EMS), or distributed management system (DMS) to control and monitor the system using the information provided by the communication system.

Considerable efforts have emerged in studying smart-grid communications. A large subset of such efforts emphasize only on the communication network for the distribution level of power grids [50]. Communication networks for the transmission network of power grids have been studied in [51]. This work introduces critical attributes and technology solutions that can be employed at the transmission network level. Depending on the technology solutions and how they have been employed, the communication network may have different topologies. One possible network topol-

ogy for the communication system of the transmission grid is the same topology as the transmission grid itself, which we call such topology the *base topology*. The base topology is a communication topology with a node at each bus and communication links along transmission lines. This topology may be formed, for example, by employment of optical ground wires (OPGW) along transmission lines of the power grid.

Overall, the regional transmission sub-systems in power grids controlled by the same entity are called balancing authority (BA). For instance, Fig. 2.1 represents a BA. Each BA has a primary control center (and a set of backup control centers) responsible for maintaining the stability of the region. The control center monitors the system, for instance, by employing SCADA systems, and makes control decisions for the BA. Such decisions are, for example, about integrating and planning generation resources and finding solutions to the optimal power-flow distribution for the transmission network. Multiple BAs form a reliability coordinator region as is shown in Fig. 2.4 and finally multiple reliability coordinator regions form an interconnection, where, for example, the electrical infrastructure of the United States is composed of three interconnections as shown in Fig. 2.5 [4].

We assume that power-grid components utilize intelligent electronic devices (IEDs), which host control and measurement agents. The control agents have actuators that enable the implementation of remote control signals such as breaker tripping and adjustment of the transformer tap setting. In this dissertation, we consider two types of control and measurement agents. First, we consider control agents at substations that implement remote load-shedding control signals by sending appropriate signals to their associated distribution network. Second, we consider measurement agents that measure the temperature of high voltage transmission lines and send the measurements to the control center. We use these agents, which communicate with the control center using the communication network, to introduce certain interdepen-

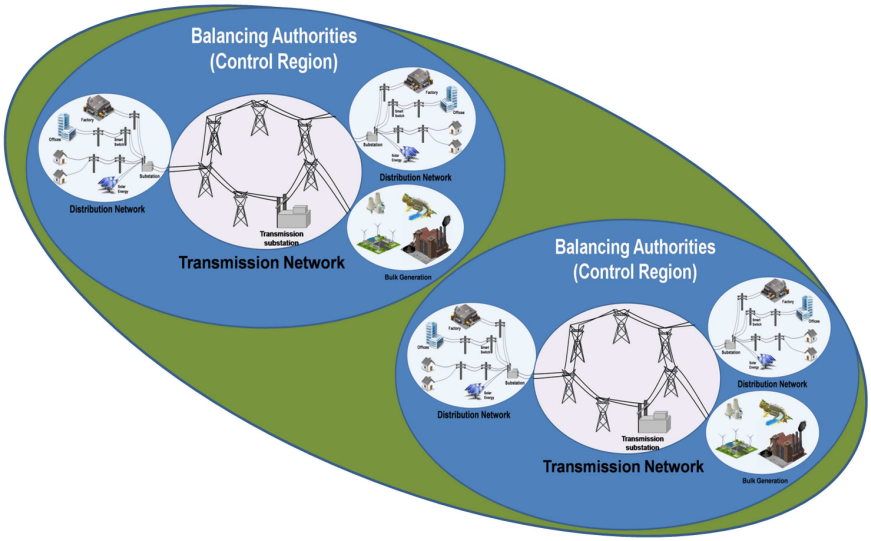

Figure 2.4: A reliability coordinator region composed of two BAs.

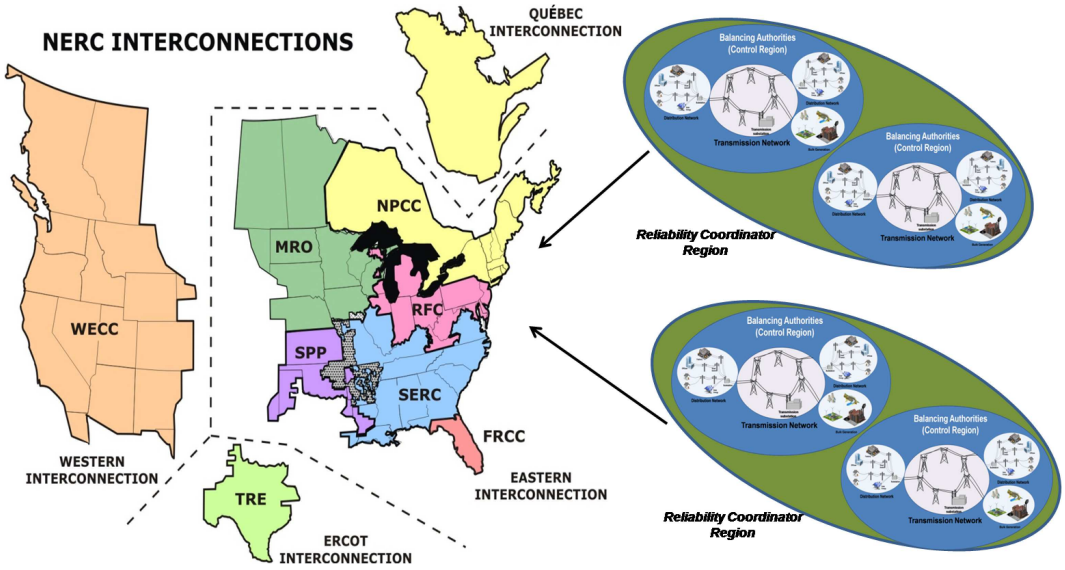

Figure 2.5: The electrical infrastructure of the United States is composed of three interconnections as described by the North American Electric Reliability Corporation (NERC). The interconnection map is from [4].

dencies between the power grid and the communication system.

2.2 Overloading and failure mechanism

Line overloading is a key mechanism in propagation of failures in power grids during cascading failures. When a line becomes overloaded, it may be tripped by protection relays or fail due to sagging into nearby trees and shorting to ground. For simplicity we call the nonfunctional lines (e.g., lines that are tripped by protection relays, overheated or physically failed) the *failed lines*. In power grids, the load of failed lines is shifted onto other lines in the system. In this section, we introduce our assumptions about line overloading and the failure mechanism.

A transmission line has a power-flow capacity that can be governed by the thermal limit, the voltage drop limit, or the steady-state stability limit of the line [52]. We denote the power-flow capacity of a transmission line, say the kth line, by C_k^{opt}. The C_k^{opt} values of the transmission lines are used by the control center of the power grid as constraints, for example, in optimizing the power flow in the system.

Similarly to the approach presented in [53], we consider a threshold α_k for the power flow through the kth line above which the protection relay (e.g., circuit breaker or impedance protective relay) trips the line. Various factors and mechanisms in the power grid may affect the threshold α for transmission lines. For example, line overloading may lead to smaller measured impedance than relay settings [54], the thermal power-flow capacity of a transmission line may vary due to changes in the surrounding temperature and ambient weather conditions [55], or problems in the communication/control system may lead to inaccurate C_k^{opt} assumption in the control center. In all of these examples, the protection relay may trip the line when the power flow exceeds the threshold α_k. Now one may interpret the discrepancy between the threshold value, α_k, which represents the true capacity of the line, and the nominal capacity, C_k^{opt}, as an error by the control center in its estimation of the true capacity of the lines. By adopting this point of view, in this dissertation we term $C_k^{\text{opt}} - \alpha_k$

the *capacity estimation error*. While the approach presented in [53] considers a fixed threshold, here we assume varying threshold to capture the effects of various parameters on the threshold and consequently on the cascading behavior. In our simulations, we quantify $C_k^{\text{opt}} - \alpha_k$ by a fraction of C_k^{opt}, i.e., $C_k^{\text{opt}} - \alpha_k = eC_k^{\text{opt}}$ for $e \in [0, 0.5]$. Therefore, we assume a line is overloaded when the power flow through the line exceeds $(1-e)C_k^{\text{opt}}$. As such, the parameter e controls the capacity estimation error. Moreover, we categorize all the transmission lines in the power grid based upon their capacity values into five categories with values from the set $\mathcal{C} = \{$20MW, 80MW, 200MW, 500MW, 800MW$\}$ [52]. Similarly to the work presented in [56], in our simulations we allow only one line trip at a time by randomly (according to the size of overload) tripping one of the overloaded lines.

Studies of major blackouts have shown that incorrect operation of protection relays contributes to cascading failures [4]. To capture this effect in our simulations, we have considered a small probability (0.04) for mis-operation of protection relays. Due to space constraints, we will not investigate the effects of the mis-operation of the protection relays on cascading behavior further. A study of such effects is presented in [57].

2.3 Interdependency parameters

In this section, we introduce interdependency parameters assumed in this dissertation based on the agents introduced in Section 2.1. The assumed interdependencies may lead to propagation of failures between the two systems; however, interdependencies can generally increase or decrease the reliability of interdependent systems. In line with the definitions presented in [23], we introduce three primary categories of interdependencies considered in this dissertation between the power grid and the communication system.

- **Physical interdependencies:** Example of such interdependency is when communication nodes rely on the power-grid energy delivery to operate. As such, failures in the power grid may interrupt the operation of the communication network.

- **Cyber interdependencies:** The efficient and reliable operation of the power grid relies on the information transfer and information processing by control and communication systems. For example, transmitting remote control signals to remote substations to implement load shedding or opening a circuit breaker in the case of contingencies relies on the communication network. Moreover, having an accurate estimate of the state of the power grid depends heavily on accurate and reliable information processing in the control and communication systems.

- **Geographical interdependencies:** Geographically correlated events can affect components of both of the systems if components of the interdependent systems are geographically co-located. In other words, a local environmental event can cause failures in both of the systems. For example, if a transmission tower collapses then both the transmission line and the OPGW communication line using that tower will fail simultaneously.

Next, we introduce the interdependency parameters assumed in this dissertation. Recall that in the previous section we introduced parameter e, which captures the effects of various factors and mechanisms that may lead to failure of transmission lines when their power flow is within a certain range of the maximum capacity assumed by the control center. We use parameter e to control the error in estimating the capacity of lines. As mentioned earlier this parameter can capture the effects of inefficiencies in the control and communication systems on the threshold. This interdependency parameter, namely *capacity estimation error*, can capture certain cyber interdependencies.

Although this interdependency parameter can capture a wide range of scenarios, here we explain its application with a specific example. A key solution in reacting to contingencies in power grids is to safely utilize the existing transmission capacity to its maximum in order to avoid over-curtailment of loads and limiting power delivery. Clearly, monitoring the transmission capacity is critical for carrying out this solution. The power-flow capacity of a transmission line can be defined, for example, by its thermal limit. The measurement agents send the measured temperatures to the control center. Estimating the temperature from the measurements and accurately estimating the capacity of the transmission lines can help in reacting to emergency scenarios more efficiently. However, error in these estimations due to error, delay and interruption in communication networks can result in either underutilization of resources or overloading of lines, which can severely affect the reliability of the power grid.

The second interdependency parameter considered in this dissertation is *load-shedding constraint level*. Load shedding is a critical control action when the system must be reconfigured to accommodate the disturbances on the grid. The efficiency of the load shedding in responding to cascading failures depends upon the constraints in implementing the load shedding in the system. The constraint level is governed, for example, by control and marketing policies, regulations, physical constraints, and communication limitations. The ratio of the uncontrollable loads (loads that do not participate in load shedding) to the total load of a substation is termed the load-shedding constraint level, denoted by $\theta \in [0, 1]$, where $\theta = 1$ means load shedding cannot be implemented and $\theta = 0$ means unconstrained load shedding. The load-shedding constraint level can also capture certain cyber interdependencies.

We explain the load-shedding constraint level with the following example. The power grid relies on the communication system for transmitting load-shedding control signals to substations in the case of contingencies. We assume that communication

irregularities may lead to the inability of control agents to efficiently implement the load shedding. Sources of such inabilities include failure of communication system to send the load-shedding control signal from the control center to the control agents, for example, due to denial of service (DoS) attack to certain servers, as well as failures at the control agents. Note that physical limitation of components and marketing policies in the power grid may also restrict the application of the optimal load-shedding controls. For example, different customers may have different interruption costs for the load curtailment; alternatively, there may exist critical loads that cannot be curtailed from the grid (based on policy or physical constraints) or the priorities that may apply to load shedding. The parameter θ can capture such scenarios and controls the level of controllability of the load shedding at substations in our simulations. To implement this constraint in the simulator, we decompose the load of a substation (represented by L_i) into a dispatchable part (controllable load) with value $(1 - \theta_i)L_i$ and a fixed load with value $\theta_i L_i$. These values are used in the power-flow optimization problem introduced in the next section.

The last interdependency parameter assumed in this dissertation is called *failure propagation probability*, which captures the dependency of the communication system on the power grid. Similarly to [31], we assume that a communication component fails probabilistically (with probability q) if a power component in its geographical vicinity fails. This dependency leads to propagation of failures from the power system to the communication network. The failure propagation probability can capture certain physical or geographical interdependencies.

To summarize, the introduced interdependency parameters are capacity estimation error, load-shedding constraint level, and failure propagation probability. The effects of these parameters on the power-flow distribution are captured by a coupled power-flow optimization framework as described in the next section.

2.4 Coupled power-flow optimization framework

Consider the transmission system of a power grid with $\mathcal{V}$ nodes (substations) interconnected by m transmission lines. The sets $\mathcal{L}$ and $\mathcal{G}$ are the set of load buses and the set of generator buses, respectively. The notation L_i represents the demand at the load bus i. The DC power-flow equations [49] can be summarized as

$$\tilde{F} = A\tilde{P}, \tag{2.1}$$

where $\tilde{P}$ is a power vector whose components are the input power of nodes in the grid (except the reference generator), $\tilde{F}$ is a vector whose m components are the power flow through the transmission lines, and A is a matrix whose elements can be calculated in terms of the connectivity of transmission lines in the power grid and the impedance of lines. This system of equations does not have a unique solution. Therefore, to find the solution to this system we use, as done in [53], a standard optimization approach with the objective of minimizing the simple cost function below:

$$Cost = \sum_{i \in \mathcal{G}} w^g{}_i g_i + \sum_{j \in \mathcal{L}} w^\ell{}_j \ell_j. \tag{2.2}$$

A solution to this optimization problem is the pair g_i and ℓ_j that minimizes the cost function in (2.2). Note that $\ell_j = \theta_j L_j + b_j$, where b_j will be determined by the optimization solution. In this cost function, $w^g{}_i$ and $w^\ell{}_j$ are positive values representing the generation cost for every node $i \in \mathcal{G}$ and the load-shedding price for every node $j \in \mathcal{L}$, respectively. We assume a high price for load shedding so that a load is to be curtailed only when there is generation inadequacy or transmission capacity limitations. The constraints for this optimization problem are listed below.

(a) DC power flow equations: $\tilde{F} = A\tilde{P}$.

(b) Limits on the generators' power: $0 \leq g_i \leq G_i^{\max}$, $i \in \mathcal{G}$.

(c) Limits on the controllable loads: $(1 - \theta_j)L_j \leq b_j \leq 0$, $j \in \mathcal{L}$.

(d) Limits on the power flow through the lines:
$|\tilde{F}_k| \leq C_k^{\text{opt}}$ for $k \in \{1, ..., m\}$.
(e) Power balance constraints (power generated and consumed must be balanced):
$\sum_{i \in \mathcal{G}} g_i + \sum_{j \in \mathcal{L}} \ell_j = 0$.

Note that in the above formulation, the quantities ℓ_js are negative and the g_is are positive by definition.

Besides the interdependency parameters that affect the solution of this optimization framework, we introduce another power grid operating setting termed *power-grid loading level*, which represents the level of stress over the grid in terms of the loading level of its components. We denote the power-grid loading level by r, defined as the ratio of the total demand to generation-capacity of the power grid. The operating parameter r affects the initial load on the system, i.e., the L_js. Furthermore, we assume that the load at substations are constant over the time interval that cascading failures occur since the duration of cascading failures is short. The solution to this optimization problem determines the amount of load shed, generation and the power flow through the lines. If failures occur in the power grid, we assume that the control center redistributes the power in the grid by solving the above optimization problem. If the new power-flow distribution overloads lines (based on the overload definition in Section 2.2), more failures will occur in the power grid. This process iterates until no more failures occur in the system.

We use MATPOWER [58], a package of MATLAB m-files, for solving the optimal power flow and simulating cascading failures. The quasi-static approaches that employ a power-flow distribution framework together with a method to identify overloaded lines and individual failures to model cascading failures have been used in several works in the literature such as [54, 56, 59].

2.5 Impact of interdependencies on reliability of the electric-cyber infrastructure

In this section, we first introduce four scenarios representing different levels of interdependencies between the power grid and the communication system. These scenarios include no-coupling, coupling through capacity estimation error, coupling through the load-shedding controllability, and coupling through both of the last two parameters. In the no-coupling scenario, the effects of failures do not propagate from the communication network to the power grid and vice versa. The no-coupling scenario is similar to the case that we consider cascading failures in the power grid alone while assuming perfect communication system. We also use the failure propagation parameter q, introduced earlier to change the strength of interdependency between the communication system and the power grid. In the introduced coupling scenarios, failures propagate to the communication system with probability q and failures in the communication network affect cascading failures in the power grid through the interdependency parameters introduced in Section 2.3, namely θ and e. In our simulations presented here, we have considered the IEEE 118 bus system along with a communication network with the same topology as the IEEE 118 bus system shown in Fig. 2.2 with the control center marked with the circle. We assume that failure of a line in the power grid results in probabilistic failure of the corresponding link in the communication network as well as its adjacent communication links, which share the communication node with that link. We set the value of parameter θ at different substations based on their connectivity to the control center, namely, if a substation is connected to the control center we assume $\theta = 0$ and otherwise $\theta = 1$. We also simply assume that the value of parameter e depends on the connectivity of the communication network and increases with the hop distance from the control center due to possible delays in the communication network as the distance increases.

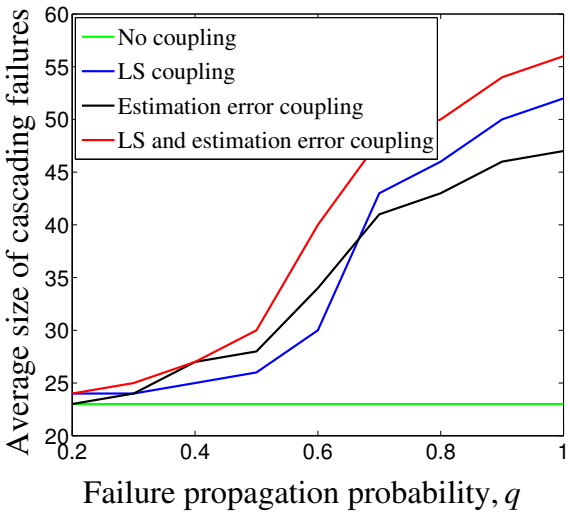

Figure 2.6: Average size of cascading failures (number of tripped lines) as a function of q and different levels of coupling between the power system and the communication network (here, LS stands for load shedding).

We have triggered cascading failures in the power grid by two or three random initial failures. The size of cascading failures is obtained by simulations of cascading failures in the power grid using the power-flow optimization framework introduced in Section 2.4. The results shown in Fig. 2.6 are obtained by averaging the size of cascading failures over 500 realizations. We measure the size of cascading failures using the number of tripped overloaded lines in the power grid. As expected, in Fig. 2.6 we observe that the size of cascading failures increases with the level of coupling between the two systems. We observe that coupling through load shedding is highly sensitive to connectivity of the communication system and the communication system disconnections make the cascading behavior more severe.

The goal of the next experiment is to study the effects of partially or fully losing control over substations for performing load shedding on the cascading behavior of the power grid. We have generated approximately 10,000 realizations of the vector θ. For each realization, we have calculated the ratio of total controllable load over the total load in the grid, $r_{c/t} \triangleq (\sum_{i\in\mathcal{L}}(1-\theta_i)L_i)/\sum_{i\in\mathcal{L}} L_i$. Next, we categorized the

realizations based on the calculated $r_{c/t}$ values into 10 equal-length sub-intervals in $[0, 1]$. In order to have the same number of realizations in each interval we selected 200 realizations in each interval. For each of the realizations we ran Monte-Carlo simulation 200 times, where in each simulation we select three transmission line failures randomly.

The average number of failed lines due to overloading is shown in Fig. 2.7-a as a function of $r_{c/t}$ for both scenarios of binary θ_i values as well as θ_i values in the interval $(0, 1]$. From the results shown in Fig. 2.7-a we observe that when full control is achievable over the loads in the grid (e.g., when there are no vulnerabilities in the control/communication system), control actions can mitigate the effects of initial disturbances and prevent the occurrence of cascading failures. Therefore, there are only few (e.g., < 5) failures on average when $r_{c/t} = 1$. However, losing control over the load buses results in an increase in the average number of failures and a high probability of cascading failures. In addition, we observe that when the power grid is operating near its maximum capacity, vulnerabilities in the control/communication system can have drastic effects. In Fig. 2.7-a we have shown the cascading-failure phenomenon, measured by the number of transmission-line failures in the system. Our simulations show a similar trend in the cascading behavior if we consider the amount of unserved loads in the system, as shown in Fig. 2.7-b. The reason for the similarity in the trends in cascading behavior in both cases (when considering the number of transmission-line failure and unserved loads) can be explained as follows. In the presence of control/communication vulnerabilities, it is more likely that lines become overloaded and hence fail. Thus the load buses disconnect from the grid in addition to the loads that have been curtailed from the system. Therefore, the total amount of unserved load in these cases are larger than that in the case when controlled load curtailment is performed. Another intuitive observation made from Fig. 2.7-a is that for a fixed amount of uncontrollable load over the grid, the scenario for which we totally lose control over certain load buses results in a more

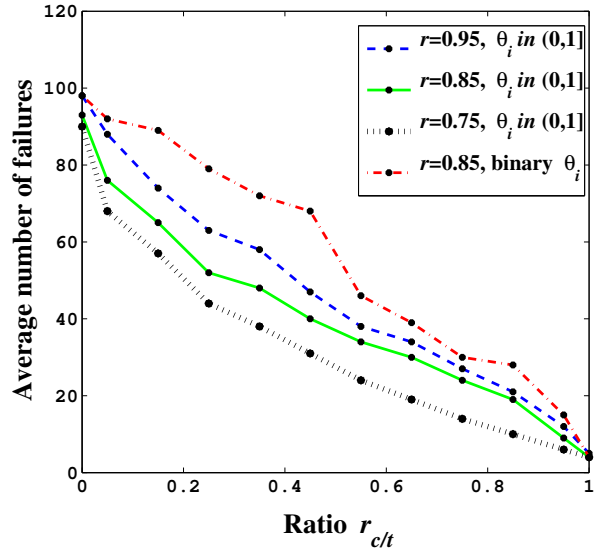

(a)

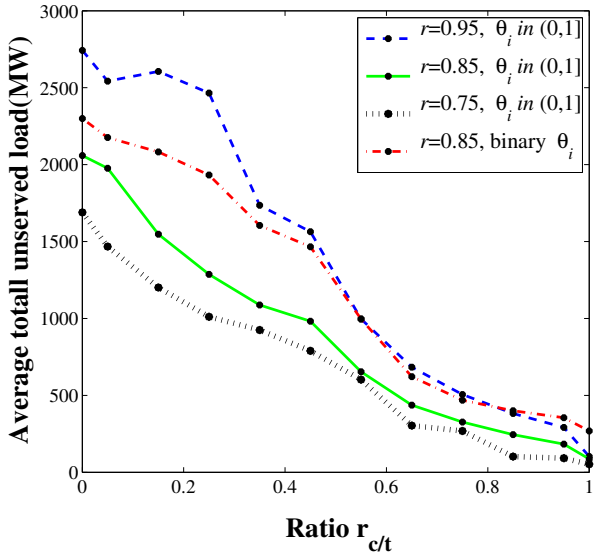

(b)

Figure 2.7: (a) Average number of failed lines, and (b) average total unserved load, due to cascading failures as a function of the ratio of total controllable loads over the total load in the grid.

severe cascading effect compared to that for the scenarios where we lose control over a portion of the load in the load buses. This may correspond to the scenario,

where the automatic relays can still perform sub-optimally without the control center interference.

2.6 Impact of communication system's connectivity on cascading failures

In this section, using the introduced simulation framework, we show that the connectivity of the communication system affects the reliability of the power grid. Using this simulation framework, we also identify characteristics of the areas of the power grid, which require more protection and communication connectivity.

In this section, we consider a set of candidate topologies for the communication system of the power grid. This set includes a network with the same topology as the power grid connectivity, the *base topology*. We also consider random variations of the base topology by generating two random sets of topologies based upon the base topology; one set with randomly removed links while maintaining the connectivity (smaller average degree of nodes, where degree is defined to be the number of nodes having direct link to the node) and one set with randomly added links (larger average degree of nodes). Note that the set of nodes in all the topologies are assumed to be the same. Similarly to the previous section, we assume that failure of a line in the power grid results in probabilistic failure of the corresponding link in the communication network as well as its adjacent communication links, which share the communication node with that link. We set the value of parameter θ at different substations based on their connectivity to the control center, namely, if a substation is connected to the control center we assume $\theta = 0$ and otherwise $\theta = 1$. In general, we assume that the communication connectivity affects the load shedding constraint level of substations.

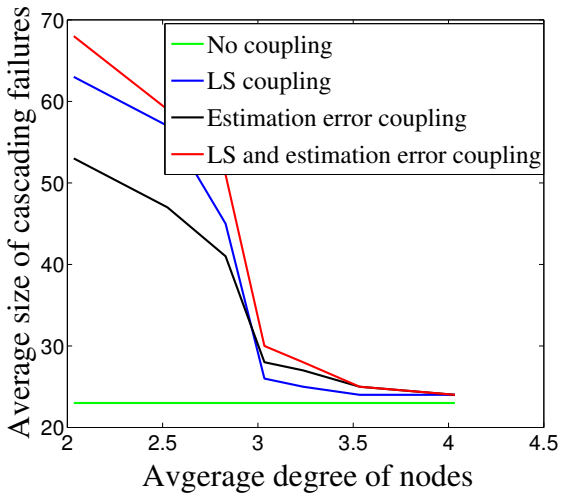

Figure 2.8: Average size of cascading failures (number of tripped lines) as a function of average degree of nodes in the communication network when probability of propagation of failures to the communication system is 0.5.

We trigger cascading failures in the power grid by two or three random initial failures. The size of cascading failures is obtained by simulations of cascading failures in the power grid using the power-flow optimization framework introduced in Section 2.4. In the simulations, for each value of the average degree of nodes we have used 20 randomly generated topologies with approximately the same average degree. In Fig. 2.8, we observe that the connectivity of the communication network affects cascading failures in power grids. The results presented in Fig. 2.8 suggest a critical value of average degree of nodes (approximately 3 in this example) for which the size of cascading failures drops sharply. We interpret this value as the minimum connectivity of the communication network that can considerably reduce the risk of large cascading failures in the power grid. Thus we conjecture that the communication network can be strengthened by adding more links to enhance the robustness of the power grid to cascading failures. Further, notice that as described earlier when the level of coupling between the two systems increases the probability of cascading failures also increases.

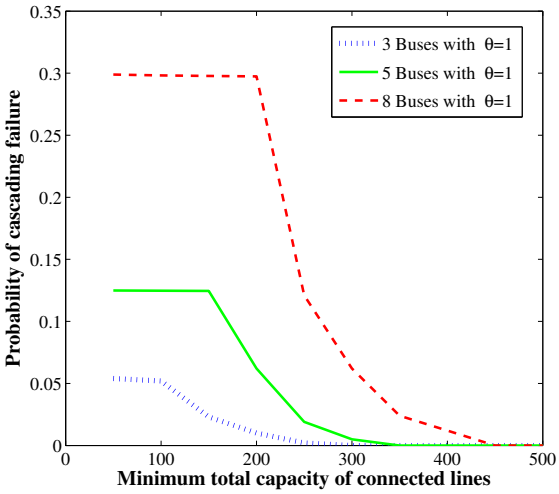

Figure 2.9: Probability of cascading failure as a function of the minimum total capacity of the connected lines to substations with communication problems for three different number of substations.

In the next study, we identify vulnerable areas of the communication system where connectivity problems (disconnections from the control center, which result in $\theta = 1$) increase the risk of cascading failures. In this study, we consider certain number of substations (specifically 3, 5, or 8) randomly selected from the power grid and assume that they are disconnected from the control center, i.e., we set $\theta = 1$ for the selected substations. We study the effects of the area, where such communication failures occur, on cascading failures and describe such areas based on the characteristics of the power system. As such, we identify the area of the power grid that requires more protection and communication connectivity. In Fig. 2.9, we present the probability of having ten or more failures beyond the initial three failures. Based on the simulation results presented in Fig. 2.9 we observe that when the minimum total capacity of the lines connected to a substation with communication problems is above a certain threshold, then the probability of having cascading failures drops sharply. The behavior observed in Fig. 2.9 can be explained as follows. Since we assume that the load-shedding control action cannot be implemented on the substations with communication problems then if they have lines with low capacities,

there is a high probability of overloading such line in the case of contingencies that necessitate load curtailments. Thus, based on these results we conjecture that the capacity of the lines connected to the substations with communication problems impact the cascading behavior. In particular, substations that have weak lines are vulnerable areas in the case of communication problems in their associated control and communication components.

2.7 Summary and conclusions

In this chapter, we stated the assumptions made about the interdependency of the power grid and the communication system that lead to propagation of failures between the two systems. We developed a simulation framework for simulating cascading failures in electric-cyber infrastructures. The proposed framework is an integrated power-flow optimization framework, which captures the effects of the introduced interdependencies on the power-flow distribution of the system. Based on the simulation results presented in this chapter, we conjecture that interdependencies between the power grid and communication system as well as the level of coupling between the two systems affect the cascading behavior in a substantial way. Furthermore, we showed that the connectivity of the communication network, measured by the average degree of nodes, does affect the cascading behavior in the power grid also in a substantial way. Thus, it is essential to consider such interdependencies in analysis of the reliability of electric-cyber infrastructures. As such, we have investigated the effects of interdependencies between power and communication systems on the stochastic dynamics of cascading failures in Chapters 4 and 6 and we have identified interdependency characteristics that largely affect the probability of large blackouts.

Chapter 3

Impact of spatial distribution of failures on the infrastructure reliability

Physical infrastructures are vulnerable to spatially correlated failures arising from various physical stresses such as natural disasters (earthquakes and hurricanes) as well as malicious coordinated attacks. Correlated component failures in physical systems, such as power and communication systems, and their effects on reliability of the system have been largely the concern of researchers for a long time [60–62]. However, there are very few effective works in modeling such real-world scenarios. In this chapter, we present a simulation framework, which provides a systematic way of simulating correlated failures. We use this framework to study the effects of spatial distribution of failures on the reliability of the power grid and the communication system.

Some disaster events such as earthquakes and terrorist attacks may occur in more than one location in a short period of time. Hence, multiple sets of correlated

failures may occur if more events occurred before the previous set of failures were repaired. Here, the statistical properties of induced-failure patterns depend upon the spatial interaction among stress centers (e.g., interaction among earthquake or attack locations). We present a stochastic model, based on spatial point processes, for representing stress centers in geographical plane in order to facilitate the modeling of spatially inhomogeneous and correlated failures in an infrastructure. This model is then used to further generate scenarios with inhibition and clustering between stress centers, which enables detailed assessment of vulnerabilities of the system to the level of inhomogeneity and spatial correlation in the stress-event centers.

3.1 Modeling spatially correlated failures

3.1.1 Related prior work

There are several works on characterizing the effects of correlated failures on the reliability of various systems. Most of the works in this area are in the context of communication networks. Meanwhile, the effects of correlated failures have not been extensively studied in the context of power grids. Here, we provide a short review of the efforts in understanding the effects of correlated failures in both contexts.

In an early work for modeling correlated failures [63], the authors considered the dependence between link failures in a communication system and presented an event-based reliability model. In their model, independent events are used to generate dependent link failures. This is achieved by defining independent events over sets of components (links), which, for example, share common equipments. Early origins of correlated failures in communication networks were primarily the common equipments between a set of components and the fact that failure of the equipment results in failure of all the components in the set. Here, the events have certain

probabilities of occurrence; however, components in the set sharing the equipment fail with certainty if the event happens. In a similar way, the concept of Shared Risk Link Group (SRLG) has been proposed in [64] in order to address multiple correlated link failures. An SRLG is a set of links sharing a common physical resource (cable, conduit, etc.) and thus a common risk of failure. Later, the authors in [65] used the concept of probabilistic SRLG to address the stochastic correlated component failures. In this model components in an SRLG fail in a probabilistic sense.

In contrast to previously mentioned works, there are other works that have focused on failures within specific geographical regions [66], [67]; such a assumption implies that the failed components do not necessarily share the same physical resources [68]. In [62], a framework is presented to model correlated failures caused by disasters on the networks using vertical cuts; nonetheless, the model is limited to bipartite networks and vertical regional disasters, making it inadequate for modeling stress from events such as attacks and earthquakes. The authors in [66] have modeled the disaster or attack using a circular cut, which is modeled as a disk of certain radius centered at the event location; they have assessed the vulnerability of fiber infrastructures to both circular and vertical cuts. In a similar approach, the authors in [68] used a probabilistic failure model in which components in the vicinity of the disaster (inside the disc) fail with some probability while other components (outside the disc) do not fail. However, using the same probability of failure for all the components inside the disc is not realistic since the effect of events reduces as the distance to the center of the event increases.

Correlated failures have also been studied in logical topologies (higher layers of network protocol stack) of networks [69] and [70]. In many of these kind of studies, random graphs and percolation theory [71] are common tools to evaluate the effect of random component failures in the network. An example of the source of such correlated failures are logical attacks such as coordinated cyber attacks, e.g., DoS

(Denial of Service) affecting higher layer components of networks such as routers. There are other works that discuss correlated failures in various contexts ([72, 73]) other than communication networks. There are also some models for temporally correlated failures [74]. Most related work to our approach is the work in [68], which considers multiple disasters with circular cuts. Akin to this effort, we have also identified the most vulnerable points of the network by defining various scenarios of events on the network.

Studies of correlated failures in the context of power grids are limited to few works [60, 61, 75]. In [60, 61], the authors study the effects of correlated failures on cascading failures. This model, which is inspired by methods developed for network-survivability analysis, is used to identify the most vulnerable location in the grid. In this work, authors consider contingency events that are initiated by geographically correlated failures modeled using a disk of certain radius. However, the vulnerable locations of the grid have been identified by computational geometric methods only based on the topological properties of the grid, which were then fed into the power-flow distribution problem as the initial trigger points for correlated failures. The effects of correlated power-line failures on the total system load shed have been investigated in [75]. This work uses Monte-Carlo simulations of cascading failures for estimating the statistics of the system load shed as a function of stochastic failures. However, correlated failures considered in this work are not spatially correlated; the correlation is based on the total correlation defined between the random binary variables representing the functionality of lines.

The model presented in this chapter is different from the above works, as it provides a powerful tool to systematically generate scenarios of multiple disaster events with various level of spatial correlation among their centers in order to accurately capture the geographical correlation that exists in real-world scenarios. This framework can be used for Monte Carlo simulations of correlated failures to study the

reliability of the system. We use this framework to first study the effects of correlated failures on communication networks and next, to investigate how correlated failures in the communication system affect the reliability of the power grid through the interdependencies introduced in Chapter 2.

3.1.2 Probabilistic model for spatially correlated failures

In this section, we present a probabilistic approach for modeling correlated failures due to multiple external stress-events in a physical system. We present this model in the context of communication network with the understanding that it is applicable to any geographically distributed physical system. In this model, we describe a technique for determining the probability of physical damages (failures) for an arbitrary collection of links due to external stress-events with spatially correlated centers. As described earlier, while disaster events are stochastic they can exhibit spatial correlations. Furthermore, there can be spatial inhomogeneity in the concentration of event centers since certain locations are more prone to host the events than others.

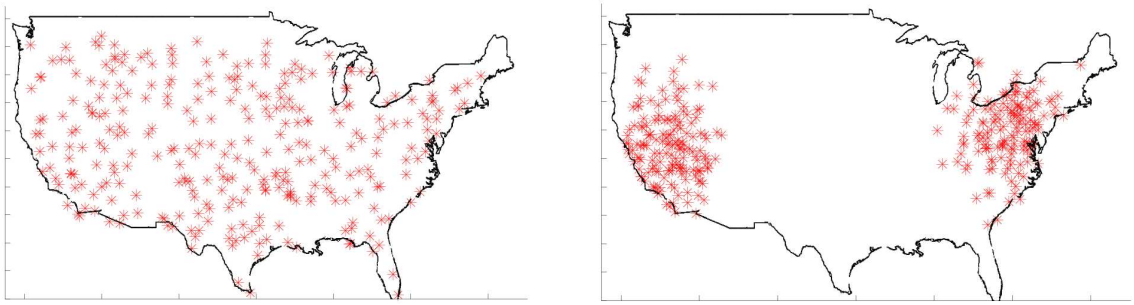

(a) (b)

Figure 3.1: Superposition of 50 realizations of a point process each having 5 event centers in the plane. (a) Points resulting from uniform (homogeneous) intensity function; and (b) points resulting from an inhomogeneous intensity function with two regions of high concentration.

Figure 3.1-a shows an example of a uniform (homogeneous) Poisson point process

in the plane. In this case, events can occur anywhere in the plane and without any spatial structure; namely, these patterns are the result of a uniform intensity function (i.e., a flat surface over the geographical plane of interest) [76]. In contrast, Fig. 3.1-b shows an inhomogeneous point process with two concentration locations for events. The inhomogeneity in the concentration of events is affected by a non-constant intensity function representing the probability of hosting individual stress-events at each point of the plane. For example, to allow more events to occur in a specific geographical area of interest, we set a peak in the probability intensity surface over the specific area.

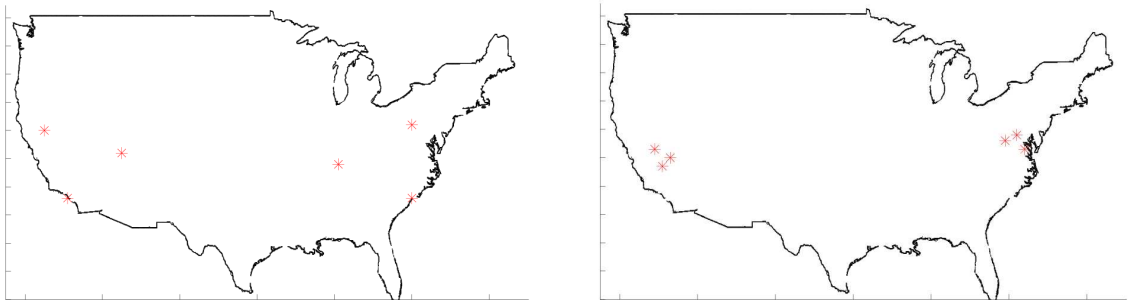

(a) (b)

Figure 3.2: Realizations of a Strauss point process with inhomogeneous intensity function and interaction between events for the cases of (a) inhibition and (b) clustering.

Next, we employ an interaction point process model [76] to capture both spatial inhomogeneity and spatial interaction between event centers. The assumption for certain events is that the occurrence of an event in a location affects the likelihood of the occurrence of other events in its vicinity. This effect is called *inhibition* if the likelihood is reduced and it is called *clustering* if the likelihood is increased. The Strauss point process is the simplest yet very effective model for inhibition and clustering effects [77]. In the case of inhibition, the probability of the occurrence of points within a fixed radius of an existing point is reduced. When this probability is zero, the inhibition is referred to as hard-core inhibition. In a similar way, in the clustering

case the probability of occurrence of events inside of a fixed radius of existing events is enhanced. To simulate the Strauss point process, we use the algorithm presented in [78]. Figure 3.2 shows realizations of Strauss point process with inhomogeneous intensity function (Fig. 3.1-b) and inhibition and clustering effects between centers. Note that the model tends to bias the event centers to be more likely to occur in the vicinity of the two regions of high concentration shown in Fig. 3.1-b. At the same time, however, there is inhibition and clustering effects between these points defined through the interaction function described bellow. Figure 3.2-a shows a realization with inhibition between event centers, while in Fig. 3.2-b there are clusters of event centers. Next, we will briefly describe pairwise interaction point-processes [76] of the type used here in order to introduce the key controls of the model in generating various interesting scenarios of events that are relevant to reliability.

Let D be a bounded subset of the plane. An interaction point process is a D^n-valued random vector, $\mathbf{v} = (V_1, V_2, ..., V_n)$, which has a probability density of the form

$$f(\mathbf{v}) = z^{-1} \prod_{1 \leq k \leq n} \Theta(v_k) \prod_{1 \leq i \leq j \leq n} \varphi(\|v_i - v_j\|), \tag{3.1}$$

where $\mathbf{v} = (v_1, ..., v_n) \in D^n$, and $\| \cdot \|$ is the Euclidean norm in the plane and z is a normalizing constant [76]. The function Θ represents the intensity function of point distributions. The function $\varphi : [0, \infty) \to [0, \infty)$ is called the *pairwise interaction function*; the pairwise behavior of events can be defined through this function. As an example, in the Strauss model [77], φ is defined to be equal to a specified value, c, for pairs of points that are within the range R, and it is set to unity otherwise. The density function of the Strauss process is then

$$f(\mathbf{v}) = z^{-1} c^{S_{\mathbf{v}}(R)}, \tag{3.2}$$

where for $R > 0$ and

$$S_{\mathbf{v}}(R) = \sum_{1 \leq i \leq j \leq n} I_{(0,R]}(\|v_i - v_j\|) \tag{3.3}$$

is the number of pairs of coordinates (points) in $\mathbf{v}$ with pairwise distance less than or equal to R, and for any set A, $I_A(a) = 1$ whenever $a \in A$ and $I_A(a) = 0$ otherwise. Based on the density function of the Strauss model, a value of c greater than 1 results in clustering and a value of c less than 1 results in inhibition. Note that when $c = 1$ we obtain the totally random (Poisson) scenario of events in the geographical plane. Furthermore, the parameter R in the Strauss model controls the range of interactions between pairs of points.

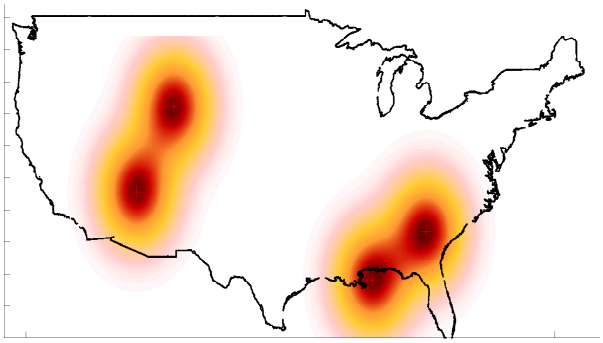

Figure 3.3: A representative CL_{pd} corresponding to a sample realization of 4 event locations.

Next, we define the *conditional likelihood function of physical damage*, $CL_{pd}(\mathbf{u})$, $\mathbf{u} \in R^2$, for all the points over the geographical plane. Specifically, we define the intensity of the damage at points of the plane using Gaussian functions placed atop each event center. The Gaussian function is a convenient and appropriate function to model the range and intensity of the disaster events over the geographical plane because of its symmetric bell shape that quickly falls off towards plus/minus infinity. The variance of the Gaussian function controls the width of the bell or the range and intensity of the disaster event. The Gaussian functions on top of multiple events are summed up and normalized (to unity) to yield $CL_{pd}(\cdot)$. Summing the Gaussian functions also captures the net result of adding the effects of multiple individual disaster events as the Gaussian functions overlap. We define the probability that a

line, say k, fails after the occurrence of a disaster event to be $\max_{u \in k}(CL_{pd}(u))$.

Figure 3.3 shows a representative CL_{pd} corresponding to a sample realization of four event locations with the Gaussian functions atop each event. Note that conditional on a particular realization of CL_{pd}, the physical failures of links (in any collection of links) are independent; however, correlation between physical damage is inherited from the correlation in the event centers associated with CL_{pd} and the geographical proximity of the links to the event centers. The c and R parameters of the Strauss model as well as the variance of the Gaussian function give us the ability to capture scenarios of events with various spatial correlations among their centers with non-uniform spatial intensity in a plane of interest. As a result, we have an effective tool to simulate desirable scenarios of spatial stress-events on the geographical plane to assess the reliability and efficiency of the network in the case of various stress scenarios.

3.2 Impact of correlated failures on communication systems

In this section, the reliability and efficiency of communication networks in the presence of geographically correlated failures due to multiple disaster events are evaluated using Monte-Carlo simulations. Specifically, a Monte-Carlo simulator for generating correlated failures based on the model presented in the previous section is developed in MATLAB. The evaluations of the reliability and efficiency of the network are presented here for different scenarios of interest for the spatial distribution of the stress centers. In our simulations, we have considered the topology of a fiber backbone operated by a major network provider in the United States as shown in Fig. 3.4. As described earlier the model enables us to control the clustering and inhibition

characteristics of the disaster events through the selection of the c and R parameters of the Strauss model. It also enables the control of the severity of the events (how strong is the disaster event in affecting the network components and the range of their impact) through the selection of the variance of the Gaussian functions. For a larger intensity of disaster events, a larger variance for the Gaussian function is used.

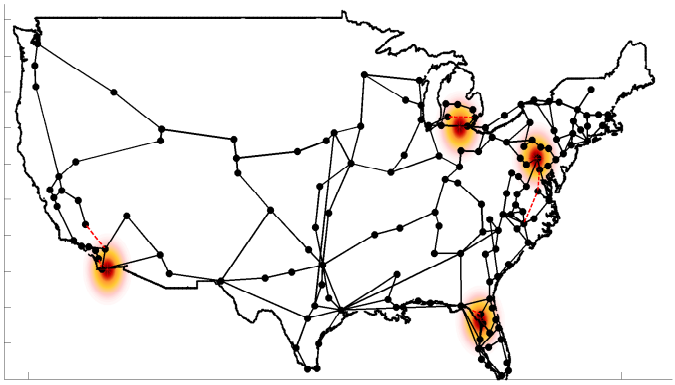

Figure 3.4: A random sample of stress-event centers with the Strauss settings of $c = 0.3$ and $R = 500$, and the variance of Gaussian function set to 600.

We shall define four scenarios of interest for the locations of stress-events and evaluate the reliability of the network in these four scenarios. In the first scenario we use the inhibition setting in the Strauss model so as to generate random realizations of event centers that are likely to be far from each other. In this scenario the probability of the occurrence of events within a fixed radius of an existing point is reduced. We define the radius to be 500 miles ($R_1 = 500$ miles), the c parameter to be 0.3 and the variance of the Gaussian functions is set to 600. A random sample of this scenario is shown in Fig. 3.4.

The rest of the scenarios are based on clustering mode in the Strauss model with the cluster radius used as a free parameter. In these scenarios, we assume that the probability of events happening farther than R miles is reduced. For each scenario we set the maximum distance between events to $R_2 = 200$, $R_3 = 100$, and $R_4 = 20$

miles, respectively, and the c parameter for all these scenarios is set to 80. Random samples of each of these scenarios are presented in Figs. 3.5, 3.6 and 3.7. Note that in the samples of the Strauss model corresponding to the fourth scenario, events are not farther than 20 miles apart; therefore, stress centers are closer than those in the remaining clustering scenarios. In all the simulations of this section we assume four number of disaster events; however, any number of events can be assumed. For comparison, we also consider the independent link failure scenario without the use of external events to represent the case of totally uncorrelated link failures in the network. (In the latter scenario we do not follow the event-center approach to insure that there is no correlation in the failures.) Next, we present our predictions of the effects of the aforementioned failure scenarios on network reliability and efficiency.

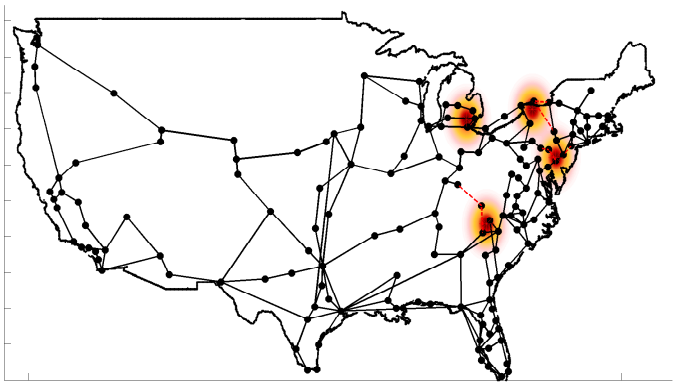

Figure 3.5: A random sample of stress-event centers with the Strauss settings of $C = 80$ and $R = 200$, and the variance of Gaussian function set to 600.

We have evaluated the reliability of the network based on two metrics: the average two-terminal reliability (ATTR) [68], which is a measure of global connectivity of the network, and the connectivity probability, which is the fraction of the number of times the network remains connected over all runs of the simulations. In Fig. 3.8, the ATTR values for the four mentioned scenarios and the independent link failure case are presented for different values of the stress effects represented by the variance of the Gaussian functions. For each scenario we have generated 500 random samples

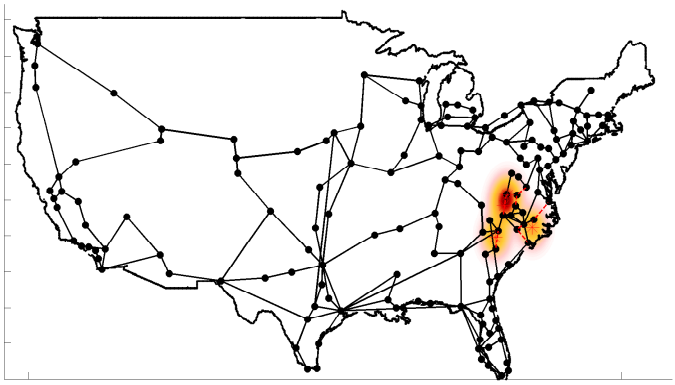

Figure 3.6: A random sample of event centers with the Strauss settings of $C = 80$ and $R = 100$, and the variance of Gaussian function set to 600.

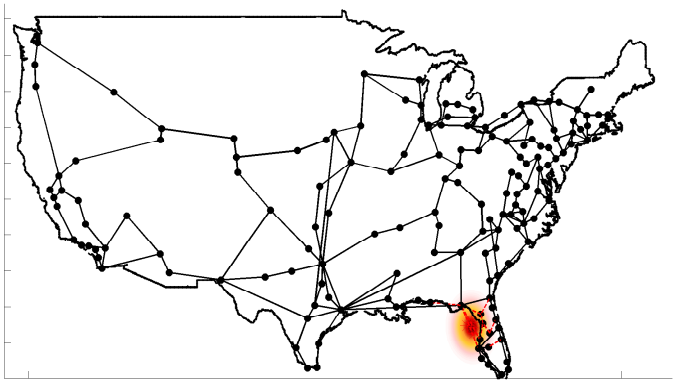

Figure 3.7: A random sample of stress-event centers with the Strauss settings of $C = 80$ and $R = 20$, and the variance of Gaussian function set to 600.

and the presented results are the average over all 500 samples. (Note that for the independent link failure scenario, we have calculated the average number of failed links in other four scenarios for each variance value and then generated the same number of failures randomly among the links.)

Based on Fig. 3.8, in the first failure scenario the ATTR is higher than those for other scenarios except for the independent link failure case. For small values of the variance of the Gaussian functions, the correlation among failures due to geographical proximity decreases. Moreover, since in the first scenario the event centers do not

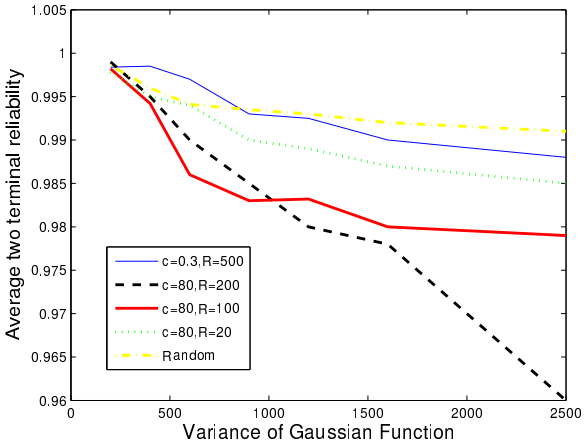

Figure 3.8: Average two-terminal reliability.

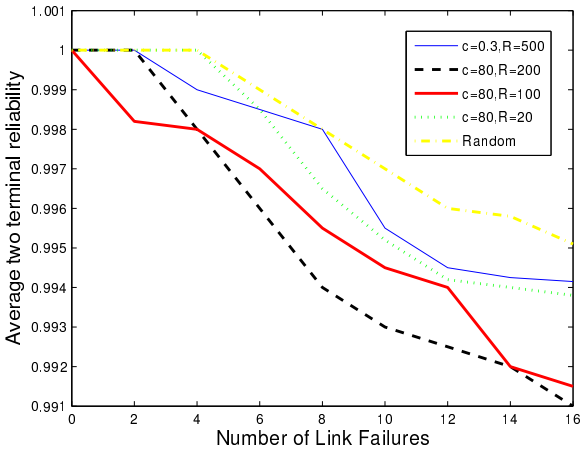

Figure 3.9: Average two-terminal reliability.

occur closer than R_1 of each other, the ATTR value is higher for smaller variances compared to independent link failure case. However, as effect-range or intensity of the disaster increases, the correlation between link failures due to geographical proximity increases, which, in turn, causes the reliability of the network to decrease compared with independent link failure scenario. The other interesting observation in Fig. 3.8 is that the reliability of the network is less affected in the scenarios with smaller cluster radius than that in the larger clusters. Note that size of clusters assumed to be less than 20 percent of the size of the geographical plane over which

the network is expanded.

Figure 3.9 shows the ATTR value for the samples with the same number of failures and for the variance of the Gaussian functions set to 1200. In this case, we have taken the average of ATTR over all the realizations with the same number of failures for the four aforementioned scenarios. As such, this plot shows that if we have the same number of failures in the network with different characteristics, they will have different effects on the network reliability. We can conclude based on these two plots that the clustering scenarios with larger effect-range, namely the second scenario ($R_2 = 200$), affect the ATTR value more significantly than the other scenarios. As before, the independent random link failure case affects the reliability less severely than other scenarios because of the lack of geographical correlation between the failures.

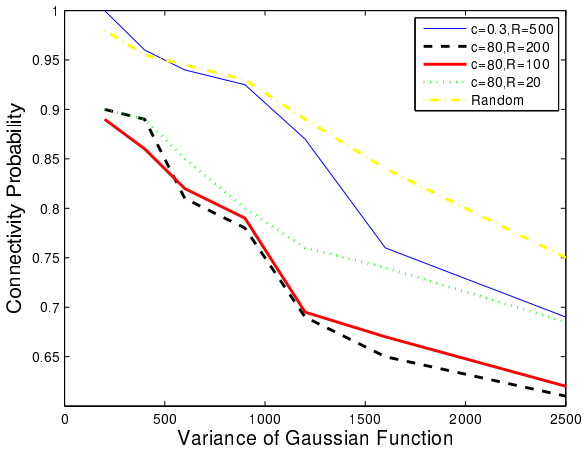

Figure 3.10: Connectivity probability.

Figure 3.10 presents the connectivity probability of the network for the different scenarios based on the variance of the Gaussian functions. Note that the clustering scenarios have lower connectivity probability than other scenarios. This is because the geographical correlation that is present amongst stress centers results in substantial geographically correlated link failures, thereby lowering reliability.

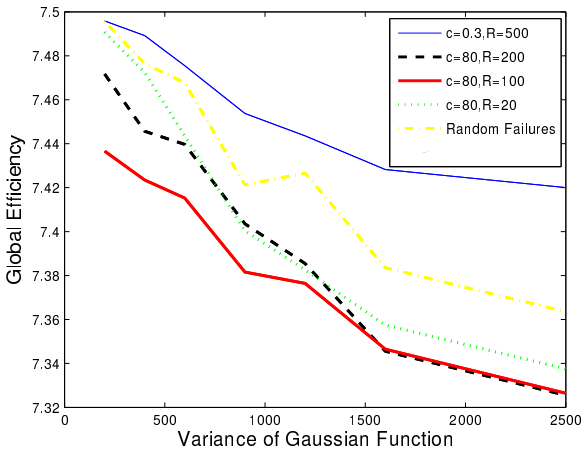

Figure 3.11: Global efficiency of the network.

In studying the network efficiency, we have adopted the global efficiency metric defined in [79], which is the average of the inverse of the shortest path length between all the nodes of the network. The results of the global efficiency of the network are presented in Fig. 3.11. Note the similarity of the behavior of the efficiency metric in this figure compared to the ATTR metric shown in Fig. 3.9.

Finally, we have also conducted a study on the most vulnerable regions of the network and the worst-case scenario of the link failures. To do this, we tested 2000 random samples of each scenario with four number of disaster events and searched for the stress-distribution scenario that resulted in the least network reliability amongst the four stress-event center scenarios. In this simulation, we fixed the intensity of the stress-event occurrence to 600. The "vulnerable" regions are identified with circles in Fig. 3.12. These regions are nearly matched with the results presented by Agarwal *et al.* [68], which did not use a stochastic approach for the distribution of stress-event centers but rather used a greedy heuristic approach that finds the vulnerable points of the network for two simultaneous events. Furthermore, the worst-case scenario for the four number of the disaster events is the second scenario, which is a clustering scenario with a radius of 200 miles.

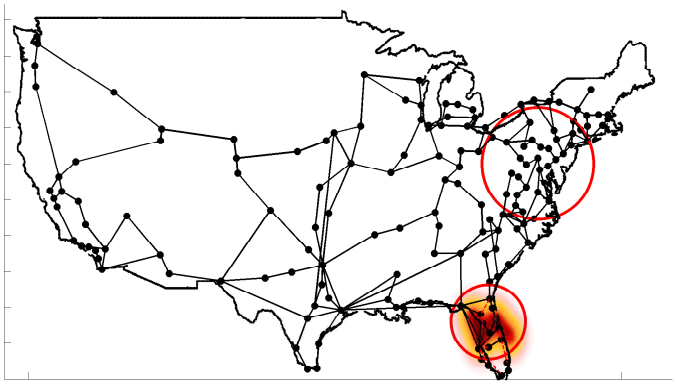

Figure 3.12: Vulnerable points of the network assuming a variance of 600 for the Gaussian functions and a random sample of the third stress-event-center scenario.

3.3 Impact of correlated failures on the reliability of electric-cyber infrastructures

In this section, we investigate the effects of spatial distribution of failures in the communication network on cascading failures in power grids using the simulation framework presented in Section 3.1.2. Specifically, we study the effects of inhibition and clustering among communication failures on cascading failures. We consider the IEEE 118 bus system as the transmission grid and assume the same topology as the power grid for the communication system. We also assume that communication node failures occur only due to external stressors such as natural disasters. In other words, we assume that failures do not propagate from the power grid to the communication system and thus the only set of failures in the communication network is the initial correlated failures. The effects of interdependencies between the power grid and communication system and propagation of failures between the two systems are studied in Chapter 2. We use the interdependency parameter, namely load-shedding constraint level, introduced in Chapter 2, to capture the effects of correlated communication failures on the power grid. We assume that communication nodes that

have been failed or disconnected from the control center due to initial external events become uncontrollable for load shedding control actions and hence we set $\theta = 1$ for such substations.

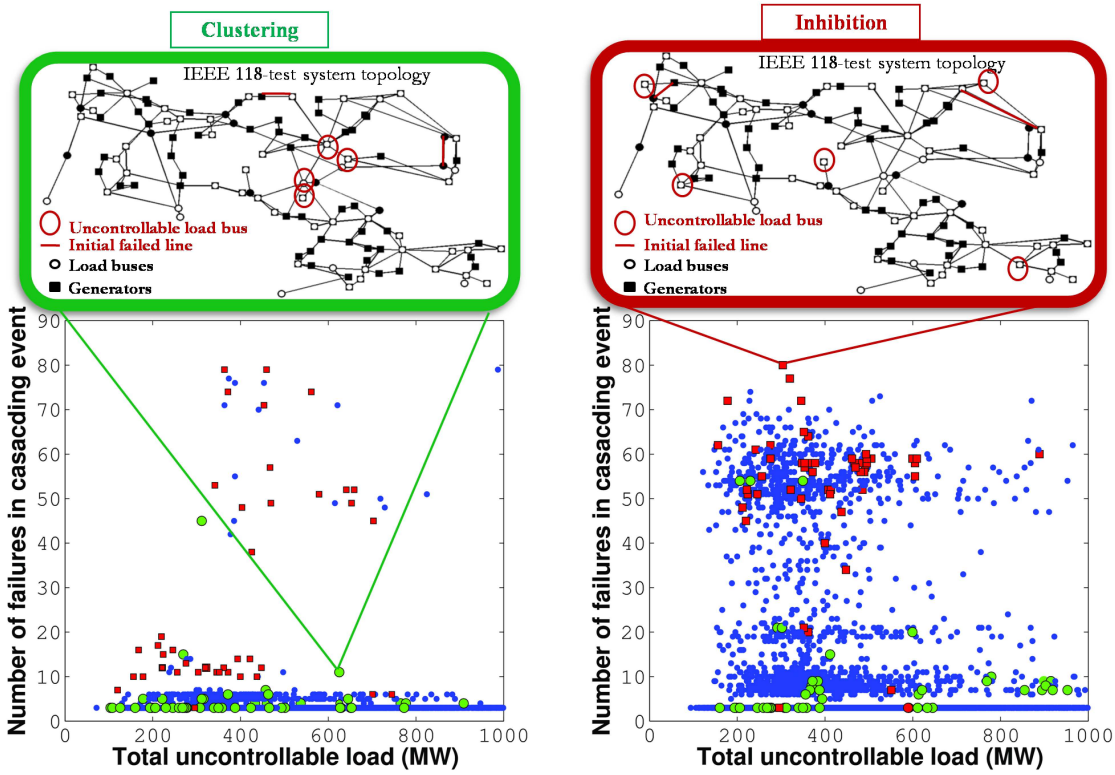

Figure 3.13: Cascading behavior of the power grid for various distributions of communication failures. Two scenarios, each shown in a sub-figure, are considered for two scenarios of two initial transmission line failures.

First, we study how the distribution of communication failures affects the cascading behavior. Understanding the effects of the spatial distribution and topological location of control/communication failures is useful in designing reliable coupled control/communication system for power grids. For this study, we use the simulation framework based on point processes in a setting with $c = 1$, which results in totally random (Poisson) and uniformly distributed scenarios of events in the geographical plane. We identify five load substations with the highest probability of failure in each

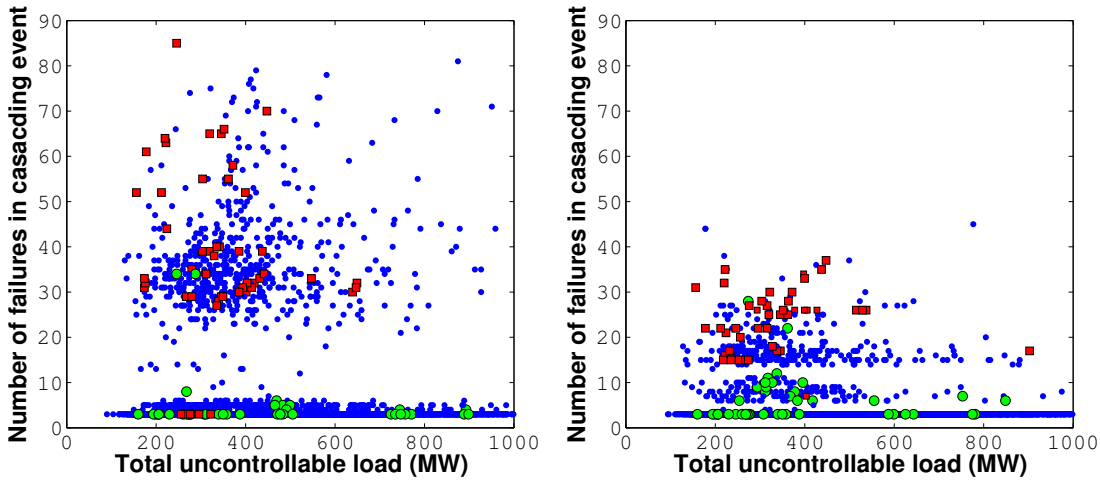

(a) (b)

Figure 3.14: Cascading behavior of the power grid for two scenarios of power-line failures in the power grid shown in each sub-figure along with various distributions of five substations with communication failures.

scenario and we assume that they are incapable of load shedding due to communication failures. We have selected the scenarios, which the value of $r_{c/t}$ (introduced in Chapter 2) for them lies in the interval $[0.9, 1)$. In other words, in this experiment we have zoomed into the interval $[0.9, 1)$ for the values of $r_{c/t}$. We run Monte-Carlo simulations for different realizations of three random initial transmission line failures for each scenario. For each of the transmission line failure realizations we carry out 1,000 iterations, each with a realization of random selection of communication failures as described above.

For better observability, the results obtained on four realizations of the initial transmission-line failures are shown in Figs. 3.13 and 3.14. Similar behavior can be seen in the rest of the samples. In each subfigure of Figs. 3.13 and 3.14, we have shown the results on the number of failures due to cascading failures for each of the 1,000 realizations of the randomly and uniformly selected load buses with uncontrollable loads with small blue dots. Note that each dot in each of the plots corresponds to one

realization from all the combinations of five communication node failures as shown in Fig. 3.13. As can be seen, the results show that both the topological location of power line failures and the spatial distribution of failures in the communication system affect the cascading behavior of the power grid. For example, the initial triggering disturbance in Fig. 3.13(b) resulted in a more pronounced cascading phenomenon compared to that in Fig. 3.13(a). Similarly, for a fixed distribution of the two initial failures (fixed sub-plot), we observe a clear change in the cascading behavior as we change the combination of communication failures.

Next, we have generated correlated communication failures using the simulation framework based on point processes. In our simulations presented here, inhibition refers to cases where the communication failures cannot be close to each other (e.g., closer than 50 miles) in a geographic sense, and clustering refers the cases where communication failures are close to each other (e.g., within a radius of 20 miles). We have assumed that IEEE 118-bus network is spanned over a 100 miles by 150 miles area. We tested cascading failures with 250 realizations with clustering effect and 250 realizations with inhibition effect. However, we have selected 50 realizations from each scenario such that the value of $r_{c/t}$ for such scenarios lies in the interval $[0.9, 1)$. These realizations are shown in Fig. 3.13: the square markers correspond to scenarios with inhibition and circles correspond to the scenarios with clustering. We observe that when there is clustering effect in the distribution of communication failures the occurrence of cascading failures are less likely compared to the case in which there is inhibition effect. This may be attributed to the ability of the power grid to isolate the problem locally in the case when the uncontrollable buses are within close proximity of one another, which may impede the propagation of subsequent failures through the grid.

3.4 Summary and conclusions

In this chapter, we developed a simulation framework that enables a systematic way of simulating correlated failures. The presented approach is based on spatial point processes, for representing stress centers on the geographical plane in order to facilitate the modeling of spatially inhomogeneous and correlated component failures in system. Using Monte Carlo simulations with the proposed framework, we showed that it is important to study the effects of spatial distribution of failures on reliability of infrastructures. We showed that correlated failures in communication networks have severe impact on the reliability of communication networks compared to random failures. We also showed that correlations among failures in the communication system affects the reliability of the power grid through the interdependencies introduced in Chapter 2. Interestingly, we observed that inhibition effect in the distribution of communication failures have severe impact on cascading failures compared to the clustering effect. Understanding the effects of distribution of failures in electric-cyber infrastructures on their reliability is important in identification of vulnerable points of the system as well as designing reliable control and communication systems for future smart grids.

Chapter 4

Markov chain framework for cascading failures

In this chapter, a scalable and analytically tractable probabilistic model for the stochastic dynamics of cascading failures in power grids is constructed while retaining key physical attributes and operating characteristics of the power grid. The operating characteristics of the power grid are defined to include the interdependency parameters, namely the load-shedding constraint level and the capacity estimation error in addition to the power-grid loading level, all introduced in Chapter 2. The key idea of the proposed framework is to simplify the state space of the complex power system so that we can track the dynamics of cascading failures using a continuous-time Markov chain while capturing the effects of the omitted variables through the transition probabilities and their parametric dependence on the physical attributes and operating characteristics of the system. To do so, we define a reduced abstraction of the state space of large scale power grids by defining a relatively small number of equivalence classes of power-grid states. The aggregate state variables used in defining the reduced state space represent critical power-grid attributes, which have been shown, from prior simulation-based and historical-databased analysis, to strongly

influence the cascading behavior. We call the proposed framework Stochastic Abstract State Evolution (SASE) as it describes the stochastic dynamics of cascading failures using the introduced abstract state space and the parametrized transition rates. The transition rates among states are formulated in terms of certain parameters that capture grid's operating characteristics. The model allows the prediction of the evolution of blackout probability in time. Moreover, the asymptotic analysis (in the limit as time tends to infinity) of the blackout probability enables the calculation of the probability mass function of the blackout size. It is shown that the probability mass function of the blackout size has a heavy tail specifically when the grid is operating under stress scenarios. We have specifically investigated the transition probabilities for the Markov chain model that lead to a power-law distribution for the blackout size. Further, a key benefit of the model is that it enables the characterization of the severity of cascading failures in terms of the operating characteristics of the power grid.

4.1 State space and equivalence classes

In general, a large number of parameters, such as voltage and frequency at various points in the grid, power-flow distribution, and the functionality of the grid's components contribute to the definition of the *state* of the power grid at each time. As such, detailed modeling of the state space of power grids for analytical modeling may not be feasible due to its prohibitively large size. For instance, even in the case where only the functionality status of the m transmission lines of the system are considered to describe the state of the system, the size of the state space of the power grid is exponential in m. The approach to overcome this challenge is to identify few key parameters that govern the cascading behavior of the system.

Our power-system simulations as well as available historical blackout data [2, 4,

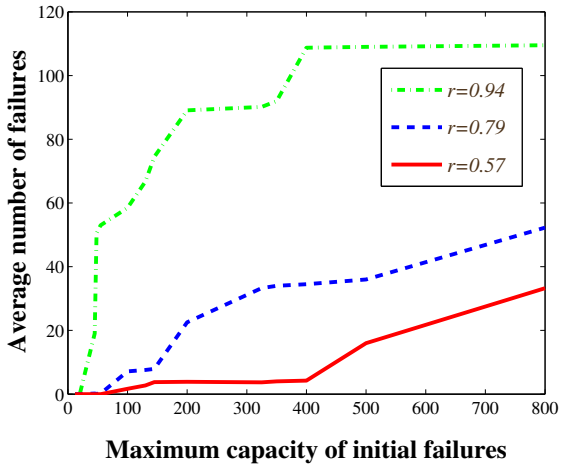

Figure 4.1: Average size of blackouts, resulting from three initial line failures, as a function of maximum capacity of the initial line failures for three different power-grid loading level.

80], together suggest that the functionality status of transmission lines and their power-flow capacities [52] are key physical attributes that should be considered in modeling cascading failures. Here, we present simulation results and two examples of real scenarios of cascading failures that support the role of the number and the capacity of the failed lines in cascading behavior of the system. The importance of these attributes are clear as line failures have always been a part of historical large blackouts and the capacity of transmission lines determine the power-delivery capacity of the grid. The results of simulations of cascading failures in the IEEE 118 bus system shown in Fig. 4.1 indicate that the size of cascading failures increases as a function of the capacity of the initial failures that trigger cascading failures.

Figure 4.2-a presents the time evolution of the cumulative line failures for the blackouts in July 1996 and August 1996 in the Western Interconnection [4]. The number of initial and final transmission-line failures are very close in these two blackouts. However, the approximate average line-failure rate in the July 1996 blackout is 1.6 failures per minute during the escalation phase of the cascading failures, while it is 4 failures per minute in the August 1996 blackout. Most notably, the initial

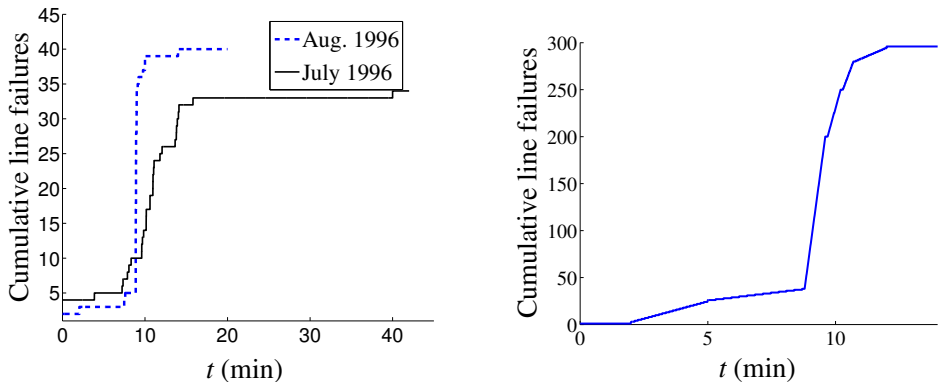

(a) (b)

Figure 4.2: Cumulative line failures in (a) July 1996 WSCC blackout (solid line), August 1996 WSCC blackout (dashed line), and (b) August 2003 blackout [2, 4]. The time of the initial failure is set to zero. Figures are reproduced in the same way as in [5].

disturbance of the blackouts were two 345KV transmission-line failures in the July 1996 blackout and two 500KV transmission-line failures in the August 1996 blackout. Next, the time evolution of the cumulative line failures for the blackout in the August 2003 in Eastern Interconnection [2] is shown in Fig. 4.2-b. Based upon the data, the average line-failure rate is approximately 1.4 failures per minute at the beginning phase while it is 18 failures per minute at the escalation phase of cascading failures. This can be described by the larger number of failures in the grid in the second phase as well as failure of some critical lines with high capacities. In summary, the aforementioned observations extracted from historical data and our simulations both support the selection of the capacity of the failed lines and the number of failures as key players in the formulation of the abstract state space.

As such, we consider the following aggregate state variables to represent the power-grid state. The first variable is the number of failed lines, F, which has been commonly considered in the probabilistic modeling of cascading failures to represent power-grid states [5, 17, 20, 53]. Next, we consider the maximum of the capacities of all the failed lines, $C^{\max}$. As shown in the simulation results presented in Fig. 4.1,

$C^{\max}$ dominates the effect of the capacity of the failed lines in cascading failures.

In addition, our simulations presented in Fig. 4.3 indicate that certain power-grid states are *cascade-stable*, defined as a state for which once entered no further failures occur in the system. The simulations of cascading failures in the IEEE 118 bus system and the IEEE 300 bus system shown in Fig. 4.3 show the probability that certain states with specific F and $C^{\max}$ are cascade stable. We will explain these figures in more detail later in this chapter. According to the cascade-stable attributes of certain states, we define a new aggregate state variable, termed cascade-stability, which collectively captures many other physical attributes of the power grid (as the physical attributes specify whether a power-grid state is cascade-stable or not). We represent the cascade-stability by a binary state variable I, where $I = 1$ indicates a cascade-stable state and $I = 0$ indicates otherwise.

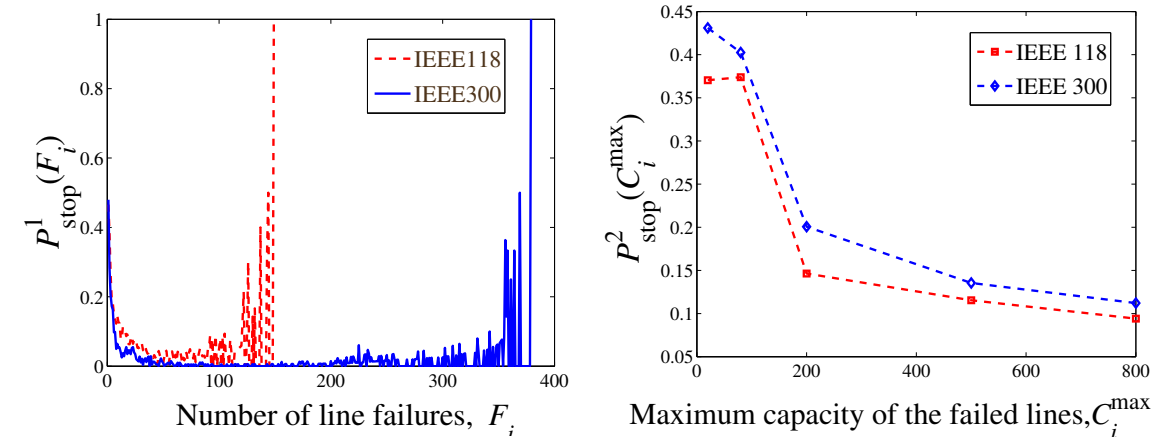

(a) (b)

Figure 4.3: (a) Probability of cascade-stability for states as a function of F_i and (b) probability of cascade-stability for states as a function of $(C_i^{\max})$ for the IEEE 118-bus system and the IEEE 300-bus system for $r = 0.7$, $e = 0.1$, and $\theta = 0$.

By utilizing the three introduced state variables as the descriptors of power-grid states, we partition the space of all detailed power-grid states into a collection of equivalence classes denoted by $\mathcal{S}$. Such coarse partitioning of the state space of the

power grid implies that detailed power-grid states with the same aggregate state-variable values (i.e., the same value of F, $C^{\max}$ and I) will belong to one class and will be indistinguishable as far as the reduced abstraction is concerned. We term each class of the power-grid states an *abstract power-grid state* or in short an *abstract state*, and label each as $S_i = (F_i, C_i^{\max}, I_i)$, where $S_i \in \mathcal{S}$.

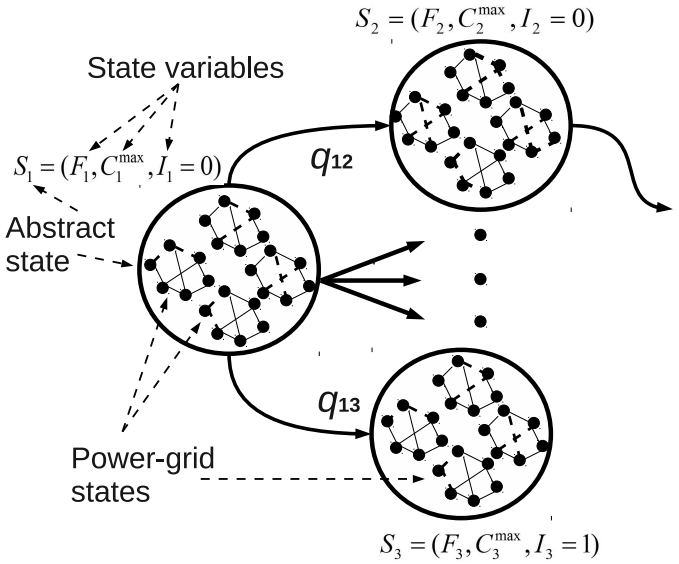

Figure 4.4: Power-grid states, abstract states and transitions between the abstract states.

The notion of power-grid states, abstract states, and transition between the abstract states is sketched in Fig. 4.4. Each large circle represents an abstract state and each of the four topological graphs inside each large circle represents a detailed power-grid state, albeit with common values for F, $C^{\max}$ and I. We assume that the power-flow capacity of the lines can be quantized into a discrete and finite set of capacity values, i.e., $\mathcal{C} = \{C_1, C_2, ..., C_K\}$. Thus, the cardinality of the abstract-state space $\mathcal{S}$ is $N = 2Km$. Therefore, the equivalence-class approach reduces the complexity associated with tracking the stochastic dynamics of the power grid from exponential (when considering the functionality status of every line in the system) to linear in m.

4.2 Stochastic Abstract State Evolution model

The Stochastic Abstract State Evolution (SASE) model describes the stochastic dynamics of cascading failures using a finite state continuous-time Markov chain whose state space is defined by the abstract states $S_i = (F_i, C_i^{\max}, I_i)$ for $i = 1, 2, \ldots, N$. Recall that the state variable I indicates whether a state is cascade-stable; hence, it is utilized to specify the *absorbing* ($I = 1$) and *non-absorbing* ($I = 0$) states of the Markov chain. We term the non-absorbing states as transitory states. We reiterate that with this definition of the state, there are two abstract states associated with any power-grid state: one is an absorbing state and the other is a transitory state. The definition of absorbing states in the state space of the Markov chain enables modeling of cascading failures, which can be terminated (with some probability) at any power-grid state with any F_i and $C_i^{\max}$ instead of continuing to induce further failures. In contrast, a pure birth chain model [81] with positive upward transition probabilities, in which each birth represents a new failure in the system, has a single absorbing state (due to the finite size of the system) corresponding to the complete failure of the system. As such, models like the pure-birth chain model are not effective in modeling the real world cascading failures as the real failure scenarios also suggest that depending on control actions and islands formed in the system, cascading failures may result in different size of failures [4]. The definition of the absorbing states in the presented Markov chain framework enables modeling of various sizes of blackouts in the system by modeling stable states in the system, which the system may enter with certain probability. On the other hand, the pure-birth model does not allow for different blackout sizes. Another way of capturing the effects of stable states in the state-space of the system is by defining *partially absorbing* states, which the system never leaves such states with certain probability. We will introduce and use the latter definition in Chapter 5.

We consider two types of state transitions in the SASE model. The first type

is termed as *cascade-stop* transition, which is from a transitory state, say S_i, to an absorbing state, say S_j, (i.e., $I_i = 0$ and $I_j = 1$) such that $F_j = F_i$ and $C_j^{\max} = C_i^{\max}$. The cascade-stop transition leads to the end of the chain of failures, which in real systems can occur as a result of the implementation of successful control actions, formation of operating islands in the power grid, or occurrence of a large blackout. The second type of transitions is termed a *cascade-continue* transition. We assume that the cascade-continue transition occurs as a result of a single line failure in the system. The single-failure-per-transition approximation is based upon the assumption that time is divided into sufficiently small intervals such that each interval can allow only a single failure event. By *cascade-continue transition* we mean transition from a transitory state, say S_i, to another transitory state, say S_j (i.e., $I_i = I_j = 0$) such that $F_j = F_i + 1$ and $C_j^{\max} \geq C_i^{\max}$. To this end, the cascading failure can be described as a sequence of Markovian transitions among transitory states with a final transition to some absorbing state.

We represent the state of the system at time $t \geq 0$ by $X(t)$, an $\mathcal{S}$-valued, continuous-time Markov chain. The transition probability matrix of the chain $X(t)$ is denoted by $\mathbf{P}(t)$, where its ijth element is $p_{ij}(t) = \mathsf{P}\{X(\tau + t) = S_j | X(\tau) = S_i\}$, $t \geq 0$. Note that the notation P is used to represent probability measure defined on the collection (σ-algebra) $\mathcal{F}$ of all events (subsets of the sample space Ω) generated by the random variables defined in this dissertation.

Let q_{ij} for $i \neq j$ represents the probability rate of transition from state S_i to state S_j, which depends upon the origin and destination states of the transition. This dependency allows for cascading behavior and will be explained in details in Section 4.3. The q_{ij} is defined as

$$q_{ij} = \begin{cases} \lim_{h \to 0^+} \frac{p_{ij}(h)}{h} & \text{for } i \neq j \\ -\lim_{h \to 0^+} \frac{1 - p_{ij}(h)}{h} & \text{for } i = j \end{cases}, \tag{4.1}$$

where q_{ii} satisfies $q_{ii} = -\sum_{j=1, j \neq i}^{N} q_{ij}$ [81]. A Markov chain $X(t)$ is completely

determined by the transition rate matrix $\mathbf{Q}$ with q_{ij} as its ijth element.

We formulate the transition rates of the SASE model based upon the transition probabilities of its embedded Markov chain (EMC). We denote the state of the EMC at discrete time instant ℓ by $X^{(\ell)}$. The one-step transition probability matrix of the EMC is denoted by $\mathbf{P}^{\text{EMC}}$. According to the definition of the SASE model, the elements of $\mathbf{P}^{\text{EMC}}$ have the following form

$$p_{ij}^{\text{EMC}} = \begin{cases} 0 & F_j < F_i \ \text{ or } \ F_j - F_i > 1 \ \text{ or } \\ & C_j^{\max} < C_i^{\max} \ \text{ or } \ (I_i = 1 \ \text{ and } \ j \neq i) \\ 1 & I_i = 1 \ \text{ and } \ j = i \\ P_{\text{trans}}(S_i, S_j) & \text{otherwise} \end{cases}, \tag{4.2}$$

where $P_{\text{trans}}(S_i, S_j)$ represents the probability that the system transits from a transitory state, say S_i, to state S_j for which the value of F_j and $C_j^{\max}$ does not violate the transition rules in (4.2). In Section 4.3, we will parametrically characterize $P_{\text{trans}}(S_i, S_j)$ based upon our observations from simulations.

We approximate q_{ij} based upon (4.1) and for a small Δt as $q_{ij} \approx \frac{p_{ij}^{\text{EMC}}}{\Delta t}$ for $i \neq j$. We consider Δt as (the small) unit of time approximating the average time between failures during the rapid escalation phase of the cascading behavior, which is relatively small compared to the total duration of cascading failures. We estimate such Δt using the historical blackout data provided in [4,5]. Note however that based upon the individual blackout events, Δt may vary depending on the power system and its operating characteristics. For example, historical data suggest approximately 18 transmission-line failures per minute on average during the rapid escalation phase of the cascading failure for the August 2003 Eastern Interconnection blackout ($\Delta t \approx 0.055$ min) [4] while this number is 4 failures per minute for the August 1996 Western Interconnection blackout ($\Delta t \approx 0.25$ min) [5]. In our calculations we have selected an intermediate value of $\Delta t = 0.1$ min. We emphasize that while we consider a fixed Δt for the system, it is the state-dependent nature of the transition probabilities, p_{ij}^{EMC},

that inherently adjusts the transition rates to accommodate all phases of cascading failures, such as the precursor and escalation phases.

In the next section, we use our power-system simulation methodology introduced in Chapter 2 for parametric formulation of p_{ij}^{EMC}.

4.3 Parametric modeling of transition rates

In this section, we parametrically model $P_{\text{trans}}(S_i, S_j)$ introduced in (4.2). In order to simplify the formulation of the $P_{\text{trans}}(S_i, S_j)$, we consider the probability components depicted in Fig. 4.5. We will introduce the components represented in Fig. 4.5 as we go through this section and refer to this figure as necessary.

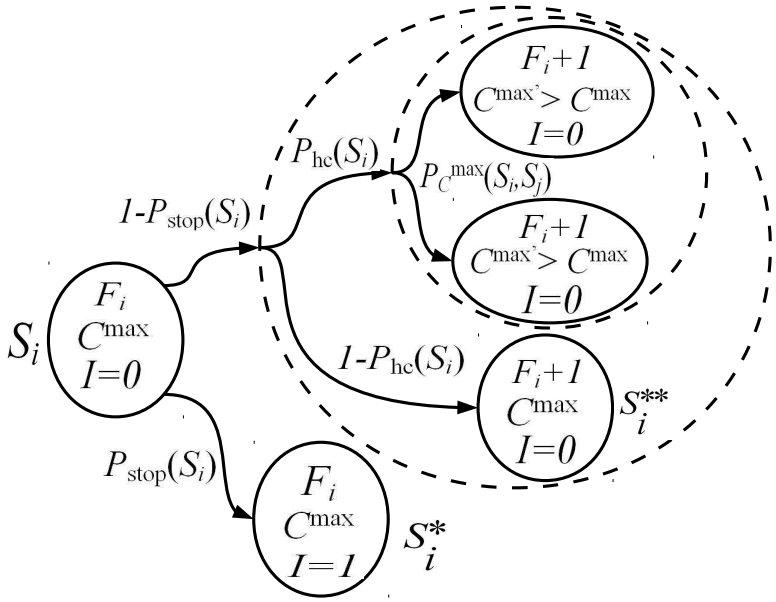

Figure 4.5: The components of $P_{\text{trans}}(S_i, S_j)$. First, transition from a transitory state S_i is divided into two categories: transition to an absorbing state S_i^* and transition to a transitory state (states in the dashed circles are transitory states). Next, the transition to a transitory state is also divided into two categories: transition to a state S_i^{**} with the same $C^{\max}$ values as that of S_i, and transition to a state whose maximum capacity of the failed lines is larger than $C^{\max}$ associated with the state S_i.

Note that for every transitory state, say $S_i \in \mathcal{S}$, there is a single associated absorbing state, which we denote by S_i^* (see Fig. 4.5). Note that state S_i^* has the same F and $C^{\max}$ values as those for S_i but it has $I_i^* = 1$ (where as $I_i = 0$). Based upon whether the next state of the transition is an absorbing state or not, we decompose the transition probability as follows:

$$\begin{aligned} &P_{\text{trans}}(S_i, S_j)= \\ &\mathsf{P}\{X^{(\ell+1)}{=}S_j | X^{(\ell)}{=}S_i, X^{(\ell+1)}{=}S_i^*\}\mathsf{P}\{X^{(\ell+1)}{=}S_i^* | X^{(\ell)}{=}S_i\} \\ &+\mathsf{P}\{X^{(\ell+1)}{=}S_j | X^{(\ell)}{=}S_i, X^{(\ell+1)}{\neq}S_i^*\}\mathsf{P}\{X^{(\ell+1)}{\neq}S_i^* | X^{(\ell)}{=}S_i\}. \end{aligned} \tag{4.3}$$

Note that $X^{(\ell+1)} = S_i^*$ implies that cascading failure ends in the system. As such, we define the probability of cascade-stop transition as $P_{\text{stop}}(S_i) \triangleq \mathsf{P}\{X^{(\ell+1)}{=}S_i^* | X^{(\ell)}{=}S_i\}$. Clearly, $\mathsf{P}\{X^{(\ell+1)}{=}S_j | X^{(\ell)}{=}S_i, X^{(\ell+1)}{=}S_i^*\} = \delta_{S_i^*,S_j}$, where $\delta_{S_i^*,S_j} = 1$ when S_j is equal to S_i^* and $\delta_{S_i^*,S_j} = 0$ otherwise. Moreover, we define $\mathsf{P}\{X^{(\ell+1)}{=}S_j | X^{(\ell)}{=}S_i, X^{(\ell+1)}{\neq}S_i^*\} \triangleq (1 - \delta_{S_i^*,S_j})P_{\text{cont}}(S_i, S_j)$, where $P_{\text{cont}}(S_i, S_j)$ is the conditional cascade-continue transition probability. Thus, we rewrite (4.3) as

$$\begin{aligned} P_{\text{trans}}(S_i, S_j) &= \delta_{S_i^*,S_j} P_{\text{stop}}(S_i) \\ &\quad + (1 - \delta_{S_i^*,S_j}) P_{\text{cont}}(S_i, S_j)(1 - P_{\text{stop}}(S_i)), \end{aligned} \tag{4.4}$$

for S_i, S_i^*, $S_j \in \mathcal{S}$. Note that $\sum_{j=1}^{N} P_{\text{trans}}(S_i, S_j) = 1$.

The rest of this section is devoted to the parametric representation of $P_{\text{stop}}(S_i)$ and $P_{\text{cont}}(S_i, S_j)$, and therefore, the parametric formulation of $P_{\text{trans}}(S_i, S_j)$ due to (4.4).

4.3.1 Cascade-stop probability

In this section, we present simulation results that show the dependency of $P_{\text{stop}}(S_i)$ on F_i and $C_i^{\max}$. To simplify the observation of the effects of F_i and $C_i^{\max}$ on $P_{\text{stop}}(S_i)$, we

have studied $P_{\text{stop}}(S_i)$ as a function of F_i and $C_i^{\max}$ individually represented, respectively, by $P_{\text{stop}}^{(1)}(F_i)$ and $P_{\text{stop}}^{(2)}(C_i^{\max})$. In Appendix A, we present a simple approach similar to the approach presented in [82] in conjunction with certain reasonable assumptions (originated from the simulations of the power grid and power grid characteristics) to approximately represent $P_{\text{stop}}(S_i)$ in terms of a weighted superposition of $P_{\text{stop}}^{(1)}(F_i)$ and $P_{\text{stop}}^{(2)}(C_i^{\max})$ as

$$P_{\text{stop}}(S_i) = wP_{\text{stop}}^{(1)}(F_i) + (1-w)P_{\text{stop}}^{(2)}(C_i^{\max}), \tag{4.5}$$

where in our formulation we simply set $w = 0.5$.

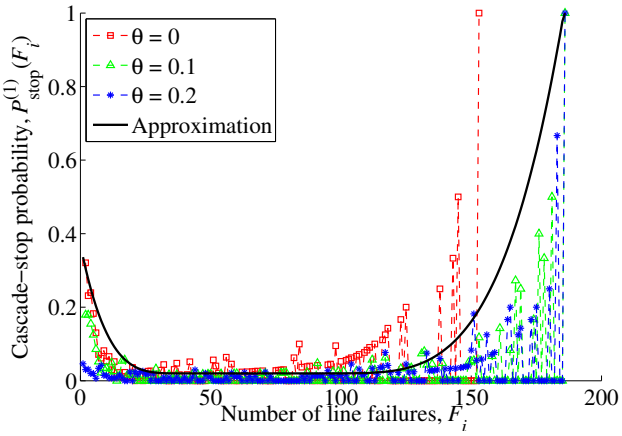

Figure 4.6: Simulation results of $P_{\text{stop}}^{(1)}(F_i)$ for $r = 0.7$, $e = 0.1$ and three values of θ. The solid line is the parametric approximated function when $\theta = 0$.

Figures 4.3-a and 4.3-b show the simulation results of $P_{\text{stop}}^{(1)}(F_i)$ and $P_{\text{stop}}^{(2)}(C_i^{\max})$, respectively, for the IEEE 118-bus and the IEEE 300-bus systems. The IEEE 118-bus system has 186 transmission lines and the IEEE 300-bus systems has 411 transmission lines. Note that $P_{\text{stop}}^{(1)}(F_i)$ and $P_{\text{stop}}^{(2)}(C_i^{\max})$ exhibit the same general behavior in both grids. Due to the space constraints, we will limit our presentation to the IEEE 118-bus system with the knowledge that a similar approach for the parametric modeling of transmission rates can be applied to larger scale grids by adjusting the parameters of the model.

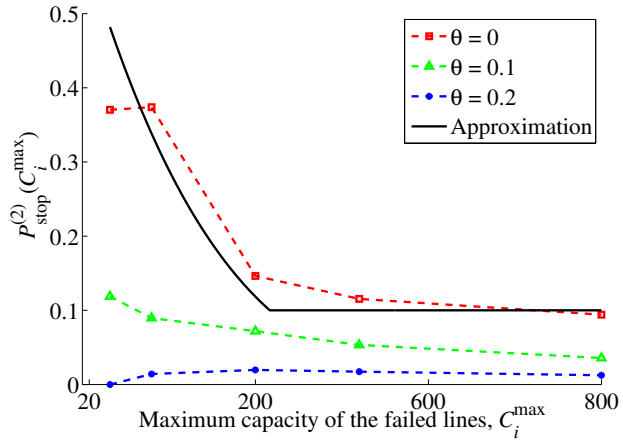

Figure 4.7: Simulation results of $P^{(2)}_{\text{stop}}(C_i^{\max})$ for $r = 0.7$, $e = 0.1$ and three values of θ. The solid line is the parametric approximated function when $\theta = 0$.

Figures 4.6 and 4.7 show the simulation results of $P^{(1)}_{\text{stop}}(F_i)$ and $P^{(2)}_{\text{stop}}(C_i^{\max})$ for the IEEE 118-bus system, respectively, for different operating settings of the grid. The results of our simulations are obtained using 1,000 scenarios of random initial disturbances with two or three random line failures. We considered three different values of load-shedding constraint level θ in order to show that operating characteristics of the power grid affect the stability probabilities while the value of r and e are fixed to be 0.7 and 0.1, respectively (the effects of r, and e are discussed in Section 4.3.3).

From Fig. 4.6, we observe that $P^{(1)}_{\text{stop}}(F_i)$ is bowl shaped, with three identifiable phases, which are described in detail below. The importance of the bowl-shape form is that it reflects the general cascading behavior as failures accumulate. Similar three-phase behavior can be observed in the historical cascading-failure data presented in Fig. 4.2. Specifically, we will revisit the bowl-shape function in Section 4.5.1.1 and explain that the bowl-shape form for the cascade-stable probability generally increases the size of large blackouts and leads to heavy-tail property for the distribution of the blackout size.

First phase– This phase represents the regime when the likelihood of an additional

failure increases substantially as a function of the number of failures. A qualitatively similar increase in the failure propagation probability has also been observed by Dobson [20]. This phase starts at $F_i = 2$ (due to N-1 criterion). To this end, we define the parameter a_1 as $P^{(1)}_{\text{stop}}(2)$, which represents, intuitively speaking, the reliability of the power grid to initial disturbances with two failures. Also in the first phase, $P^{(1)}_{\text{stop}}(F_i)$ decreases from a_1 to a small $P^{(1)}_{\text{stop}}(F_i)$ value, ϵ (our results suggest $\epsilon = 0.05$), as the number of failures increases and reaches a critical $F_i = a_2 m$ value.

Second phase– This phase represents the escalated phase of cascading failures. During this phase $P^{(1)}_{\text{stop}}(F_i)$ is small (we assume $P^{(1)}_{\text{stop}}(F_i) = \epsilon$ during this phase) and the power grid is highly vulnerable. This phase starts at $F_i = a_2 m$, which represents the number of failures in the power grid after which the cascading failure enters the escalated phase. As expected, our results show that during this phase the efficiency of the control action (represented by θ) hardly affects $P^{(1)}_{\text{stop}}(F_i)$.

Third phase– As F_i increases further, the probability of having an additional failure decreases as cascading-failure behavior begins to phase out. This behavior can be attributed to the finite size of the power grid or the fact that as more failures occur "functional islands" may form in the grid, leading to the termination of cascading failures. Therefore, in this phase the value of $P^{(1)}_{\text{stop}}(F_i)$ rises and finally $P^{(1)}_{\text{stop}}(m) = 1$. Note that here we simply consider a fixed parametric model for the third phase of $P^{(1)}_{\text{stop}}(F_i)$, which only roughly approximates the average scenario of various operating settings.

We propose the following parametric model to capture the three aforementioned phases in $P^{(1)}_{\text{stop}}(F_i)$:

$$P^{(1)}_{\text{stop}}(F_i) = \begin{cases} a_1 \left(\frac{a_2 m - F_i}{a_2 m}\right)^4 + \epsilon & 2 \leq F_i \leq a_2 m \\ \epsilon & a_2 m < F_i \leq 0.6m \\ \min\left\{\left(\frac{F_i - 0.6m}{m - 0.6m}\right)^4 + \epsilon, 1\right\} & 0.6m < F_i \leq m \end{cases} . \tag{4.6}$$

The parametric $P^{(1)}_{\text{stop}}(F_i)$ is shown in Fig. 4.6 for $\theta = 0$. Recall that we have judiciously selected a common parametric model for the third phase of the bowl-shaped function across various operating settings. Consequently, the parametric function $P^{(1)}_{\text{stop}}(F_i)$ shown in Fig. 4.6 does not accurately match the simulation results for $\theta = 0$ scenario in the third phase.

The empirically calculated $P^{(2)}_{\text{stop}}(C^{\max}_i)$ is shown in Fig. 4.7. The value of $P^{(2)}_{\text{stop}}(C^{\max}_i)$ indicates, intuitively speaking, the reliability of the power grid when the maximum capacity of the failed lines in the grid is $C^{\max}_i$. Note that $P^{(2)}_{\text{stop}}(C^{\max}_i)$ decreases as $C^{\max}_i$ increases, which means that the power grid is more vulnerable to additional failures when it has lost at least a line with a large capacity value. We also observe that $P^{(2)}_{\text{stop}}(C^{\max}_i)$ decreases for all $C^{\max}_i$ values as θ increases; however, the effect of θ on the reliability is larger when $C^{\max}_i$ is smaller. This is because control actions are most effective when they are implemented in the beginning phase of cascading failures where $C^{\max}$ is more likely to be small.

The $P^{(2)}_{\text{stop}}(C^{\max}_i)$ is formulated parametrically as

$$P^{(2)}_{\text{stop}}(C^{\max}_i) = \max\left\{ a_3 \left(\frac{C^{\max}_i - \max\{\mathcal{C}\}}{\max\{\mathcal{C}\}} \right)^4, a_4 \right\}, \tag{4.7}$$

where $a_3 \triangleq P^{(2)}_{\text{stop}}(\min\{\mathcal{C}\})$ and $a_4 \triangleq P^{(2)}_{\text{stop}}(\max\{\mathcal{C}\})$. The parametric function of $P^{(2)}_{\text{stop}}(C^{\max}_i)$ is also shown (in solid line) in Fig. 4.7. This completes the parametric modeling of $P_{\text{stop}}(S_i)$ based on (4.5). In Section 4.3.3 we show that the value of $a_1, ..., a_4$ are affected by r, e, and θ. In the SASE model we will perceive the parameters $a_1, ..., a_4$ beyond abstract model parameters but as parameters that govern the cascading behavior while maintaining a physical connection to the operating characteristics of the system.

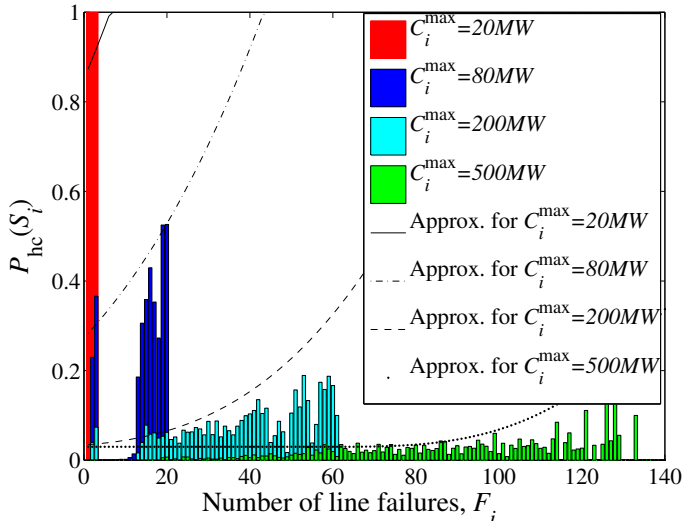

Figure 4.8: Simulation results of $P_{\rm hc}(S_i)$ as a function of F_i and $C_i^{\max}$ for $r = 0.7$, $e = 0.1$ and $\theta = 0.1$.

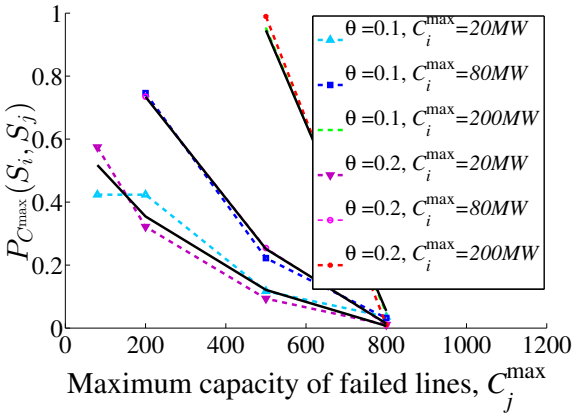

Figure 4.9: Simulation results of $P_{C^{\max}}(S_i, S_j)$ as a function of $C_i^{\max}$ and $C_j^{\max}$ for $r = 0.7$ and $e = 0.1$ and two values of θ. The parametric approximations are represented by solid lines.

4.3.2 Cascade-continue probability

Recall that for every transitory state S_i there is only one transitory state with the same $C^{\max}$ as that of state S_i and exactly one more failure than that for state S_i. We denote such state by S_i^{**} (see Fig. 4.5). Failure of a line with capacity smaller than

or equal to $C_i^{\max}$ results in transitioning from state S_i to state S_i^{**}. Similarly to (4.3), depending on whether the next line failure has larger capacity than $C_i^{\max}$ or not, we can write the conditional cascade-continue transition probability by conditioning on S_i^{**} as

$$\begin{aligned} P_{\text{cont}}(S_i, S_j) &= (1 - P_{\text{hc}}(S_i))\delta_{S_i^{**},S_j} \\ &\quad + (1 - \delta_{S_i^{**},S_j})P_{C^{\max}}(S_i, S_j)P_{\text{hc}}(S_i), \end{aligned} \tag{4.8}$$

for S_i, S_i^{**}, $S_j \in \mathcal{S}$ and $I_j = 0$, where P_{hc} is defined as the probability of having a line failure that results in a higher capacity of the failed lines than $C_i^{\max}$. In (4.8) $P_{\text{hc}}(S_i) \triangleq \mathsf{P}\{X^{(\ell+1)} \neq S_i^{**} | X^{(\ell)} = S_i, X^{(\ell+1)} \neq S_i^{*}\}$ and $(1 - \delta_{S_i^{**},S_j})P_{C^{\max}}(S_i, S_j) \triangleq \mathsf{P}\{X^{(\ell+1)} = S_j | X^{(\ell)} = S_i, X^{(\ell+1)} \neq S_i^{**}, X^{(\ell+1)} \neq S_i^{*}\}$.

The empirically calculated $P_{\text{hc}}(S_i)$ as a function of F_i and $C_i^{\max}$ is shown in Fig. 4.8 with the same simulation settings as that of the previous subsection. Our simulation results show strong evidence that F_i and $C_i^{\max}$ affect $P_{\text{hc}}(S_i)$. Results suggest that regardless of the $C_i^{\max}$ value of the power-grid state, as F_i increases the probability that a line with capacity larger than $C_i^{\max}$ fails increases. This is meaningful because as the number of failures increases the power grid becomes vulnerable and hence large transmission lines may be affected by contingencies. Moreover, the ratio of the number of transmission lines with capacity larger than $C_i^{\max}$ to the total number of functional lines increases with F_i. The next general observation from Fig. 4.8 is that for the same F_i value, as $C_i^{\max}$ increases the probability that a line with capacity larger than $C_i^{\max}$ fails decreases. This is mainly due to decrease in the number of lines with capacity value larger than $C_i^{\max}$ (as $C_i^{\max}$ increases). Furthermore, it is less likely to have states with $C_i^{\max}$ value after F_i reaches a certain threshold denoted by Γ_i (the value of Γ_i increases as $C_i^{\max}$ increases). This means that as F_i approaches Γ_i, line failures with capacity larger than $C_i^{\max}$ become highly likely.

Based upon our simulations the role of θ, r and e in $P_{\text{hc}}(S_i)$ is subtle. Therefore, here we approximate $P_{\text{hc}}(S_i)$ for different operating characteristics of the power grid

with a fixed function. The above trends in $P_{\rm hc}(S_i)$ are captured by:

$$P_{\rm hc}(S_i) = \begin{cases} \alpha(F_i+\beta)^3 & 2 \le F_i \le \Gamma_i \\ 1 & \Gamma_i < F_i \end{cases}, \tag{4.9}$$

for $S_i \in \mathcal{S}$, where $\alpha = 6 \times 10^{-7}$ and β is $C_i^{\max}$ dependent. The parametric $P_{\rm hc}(S_i)$s are shown in Fig. 4.8. Note that the over-estimation of the curves in Fig. 4.8 is due to employing a common parametric model for various operating settings as well as the introduced parameter Γ_i (there is no simulation data when F_i is beyond Γ_i.)

Next, we find the parametric formulation for $P_{C^{\max}}(S_i, S_j)$. Our simulation results suggest that $C_i^{\max}$ and $C_j^{\max}$ play key roles in determining $P_{C^{\max}}(S_i, S_j)$. Figure 4.9 shows the empirically calculated $P_{C^{\max}}(S_i, S_j)$ as a function of $C_i^{\max}$ and $C_j^{\max}$. From Fig. 4.9 we observe that conditional on the occurrence of an additional failure with capacity larger than $C_i^{\max}$ the probability of transitioning to state S_j decreases as $C_j^{\max}$ increases. The results suggest that lines with capacity value close to $C_i^{\max}$ have a higher probability of failure than those with much larger capacities than $C_i^{\max}$. We also observe that the probability of transitioning to state S_j increases as $C_i^{\max}$ increases. This is because the power grid becomes more vulnerable when $C_i^{\max}$ is large. By comparing the simulation results correspond to two values of θ in Fig. 4.9 we conclude that role of θ in $P_{C^{\max}}(S_i, S_j)$ is also subtle and similarly to $P_{\rm hc}(S_i)$, the effect of operating characteristics on $P_{C^{\max}}(S_i, S_j)$ is not considered. To capture the described trends, $P_{C^{\max}}(S_i, S_j)$ is modeled parametrically as

$$P_{C^{\max}}(S_i, S_j) = \frac{w(C_j^{\max})}{\sum\limits_{k:C_k > C_i^{\max}} w(C_k)}, \tag{4.10}$$

where $w(C_k)$ is what we term the weight of transition to a state with the maximum capacity of the failed line equal to C_k. We have assigned these weights such that they approximate the simulation results presented in Fig. 4.9 using (4.10). Here, the value of the weights are set to $w(80\text{MW}) = 2.2$, $w(200\text{MW}) = 1.5$, $w(500\text{MW}) = 0.5$, and $w(1500\text{MW}) = 0.01$. This completes the modeling of $p_{ij}^{\rm EMC}$ presented in (4.2).

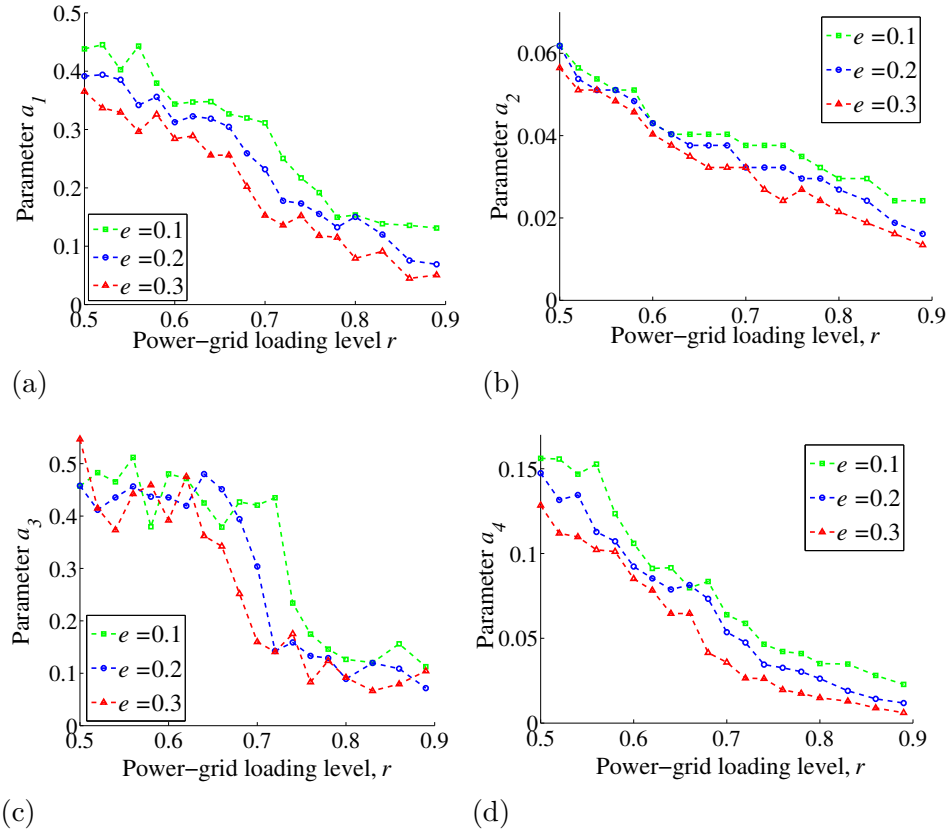

Figure 4.10: SASE-model parameters (a) a_1, (b) a_2, (c) a_3, and (d) a_4 as a function of r parameterized by e.

4.3.3 Effects of operating characteristics on parameters of the SASE model

The SASE model parameters $a_1, ..., a_4$ determine different cascading behaviors. These parameters may vary under different operating conditions and also across different power grids due to different connectivity pattern and components characteristics. Recall that we made the general observation that the power grid is more reliable when $a_1, ..., a_4$ are larger. To illustrate the effects of operating characteristics on $a_1, ..., a_4$, the values of these parameters (obtained based upon simulation results) are shown in Fig. 4.10 and Fig. 4.11 for different values of the load-shedding constraint level θ,

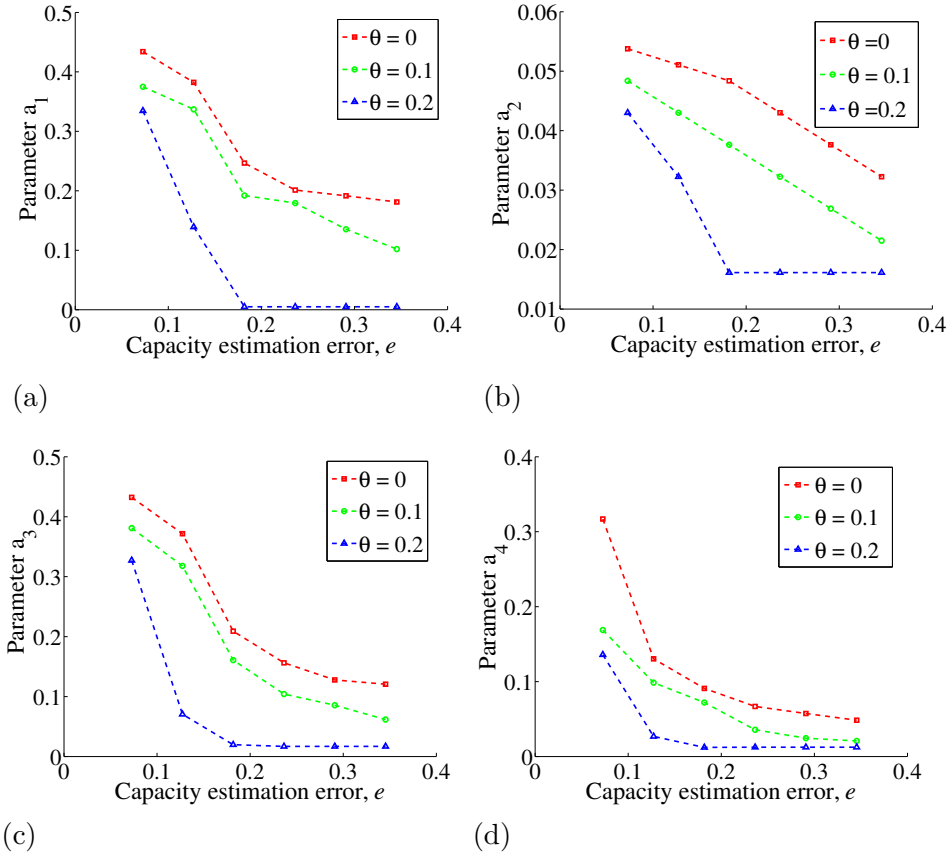

Figure 4.11: SASE-model parameters (a) a_1, (b) a_2, (c) a_3, and (d) a_4 as a function of e parameterized by θ.

the power-grid loading level r and the transmission capacity estimation error e. Our simulation results suggest that the power grid is more reliable ($a_1, ..., a_4$ are larger) when r, e, and θ are small. We observe that when any of the r, e, and θ parameter increase they add more stress to the system and the effect of contingencies becomes larger. Therefore, the probability of an additional failure in the system increases (a_1, a_3, and a_4 decrease). We also observe that when any of r, e, or θ increase, the cascading failure enters the rapid escalation phase with smaller number of failures (a_2 decreases).

4.4 Analysis of the SASE model

In this section, we analyze the SASE model by understanding the properties of the transition probability matrix $\mathbf{P}(t)$. To simplify the analysis, we first rearrange the indices of states in $\mathcal{S}$ by following three simple rules so that $\mathbf{Q}$ becomes upper diagonal matrix denoted by $\mathbf{Q}^d$. The three rules pertain the indices of states in $\mathbf{Q}^d$ such that: (1) $i < j$ if $F_i < F_j$; (2) $i < j$ if $F_i = F_j$ but $C_i^{\max} < C_j^{\max}$; and (3) $j = i + 1$ if $F_i = F_j$ and $C_i^{\max} = C_j^{\max}$, but $I_i = 0$ and $I_j = 1$. Note that the SASE Markov chain is not irreducible (and hence not ergodic) because $\mathbf{Q}^d$ is upper diagonal. This further implies that there is no stationary distribution for the SASE model and the canonical limit theorems of ergodic Markov chains are not applicable. Regardless, $\mathbf{P}(t)$ is governed by

$$\mathbf{P}'(t) = \mathbf{Q}^d\mathbf{P}(t), \tag{4.11}$$

where $\mathbf{P}'(t)$ denotes the matrix whose elements are time derivative of $p_{ij}(t)$ [81]. In principle, the solution of (4.11) is given by $\mathbf{P}(t) = e^{\mathbf{Q}^d t}\mathbf{P}(0)$. While the numerical solutions of $\mathbf{P}(t)$ can be easily obtained, to have better insight we pursue an analytical approach which can result in the asymptotic solution of $\mathbf{P}(t)$. To do so, the eigenvalues $\lambda_1, \lambda_2, \ldots, \lambda_N$ of $\mathbf{Q}^d$ and a complete system of associated right eigenvectors $\mathbf{u}_1, \mathbf{u}_2, \ldots, \mathbf{u}_N$ need to be determined. Then, $\mathbf{P}(t)$ can be represented as $\mathbf{P}(t) = e^{\mathbf{Q}^d t} = \mathbf{U}\Lambda(t)\mathbf{V}$, where $\mathbf{U}$ is the matrix whose column vectors are $\mathbf{u}_1, \mathbf{u}_2, \ldots, \mathbf{u}_N$ and $\mathbf{V} = \mathbf{U}^{-1}$. The matrix $\Lambda(t)$ is diagonal with $e^{\lambda_i t}$ as its ith diagonal element.

Due to the upper diagonal form of $\mathbf{Q}^d$ and by carrying out simple matrix manipulations, we can express $p_{ij}(t)$ as

$$p_{ij}(t) = \beta_{ij} + \sum_{i<k<j} \alpha_{ik} e^{\lambda_k t}, \tag{4.12}$$

where $\beta_{ij} \triangleq \mathbf{U}(i,j)\mathbf{V}(j,j)$ and $\alpha_{ik} \triangleq \mathbf{U}(i,k)\mathbf{V}(i,k)$. Notice that $\mathbf{V}(j,j) = 1/\mathbf{U}(j,j)$

for $j = 1, 2, \ldots, N$. Since $\mathbf{Q}^d$ is upper diagonal λ_k is negative for all k, and hence $\lim_{t\to\infty} p_{ij}(t) = \beta_{ij}$.

Further, using the asymptotic analysis, we can derive the conditional probability that a power grid *eventually* reaches a state with n failures from an initial state S_i defined as

$$D(n|S_i) \triangleq \sum_{j\in\mathcal{J}_n} \lim_{t\to\infty} p_{ij}(t) = \sum_{j\in\mathcal{J}_n} \beta_{ij}. \tag{4.13}$$

Hence, the probability mass function (PMF) of the blackout size, conditional on the initial state, can be computed by calculating $D(n|S_i)$ for $n = F_i, \ldots, m$.

Now, let $B(t, M|S_i)$ be the conditional probability of reaching a state with M or more failures by time t starting from an initial state S_i. Then $B(t, M|S_i)$ can be obtained as follows:

$$B(t, M|S_i) = \sum_{n=M}^{m} \sum_{j\in\mathcal{J}_n} p_{ij}(t), \tag{4.14}$$

where $\mathcal{J}_n$ represents the set of indices of states with n failures, i.e., $\mathcal{J}_n \triangleq \{j : F_j = n\}$. $B(t, M|S_i)$ estimates the evolution of the risk of cascading failures in time. Theorem 4.4.1 represents a more elegant representation of $B(t, M|S_i)$ with a system of differential equations. Before stating Theorem 4.4.1, we introduce the notation used in this theorem. Recall that $P_{\text{stop}}(S_i)$ represents the cascade-stop probability introduced in Section 4.3.1, γ_W represents the transition rate corresponding to $(1 - P_{hc}(S_i))$, γ_{U_j} represents the transition rate corresponding to $P_{hc}(S_i)P_{C^{\max}}(S_i, S^{u_j})$ and $\gamma = \sum_{j\in\mathcal{J}} \gamma_{U_j} + \gamma_W$. Further, S^W and S^{u_j} denote states with the same $C^{\max}$ as the initial state S_i and with larger $C^{\max}$ than the initial state S_i, respectively. Here, if C_f represents the capacity of the new failure in the system then the subscript j in U_j is for $j \in \mathcal{J}$, where $\mathcal{J} \triangleq \{j|C_f = C_j, C_j \in \mathcal{C} \text{ and } C_j > C^{\max}\}$.

Theorem 4.4.1. *The probability of reaching a blackout of size M or larger in a time interval t and from an initial state S_i (with $F_i < M$) is characterized by the following*

system of differential equation:

$$\frac{dB(t,M|S_i)}{dt} = -\gamma B(t,M|S_i) + (1-P_{stop}(S_i))\Bigg(\gamma_W B(t,M|S^w) + \sum_j \gamma_{U_j} B(t,M|S^{u_j})\Bigg), \tag{4.15}$$

with the following initial conditions:

$$B(t,M|S_i) = 1, \textit{if } F_i \geq M. \tag{4.16}$$

The approach to prove Theorem 4.4.1 is based on regeneration theory presented in Chapter 5. We will therefore postpone the proof of Theorem 4.4.1 to Chapter 5. As the probability of reaching blackout for a power-grid state S_i is expressed based on the probability of reaching a blackout starting form states S^{u_j} and S^w, we have a set of coupled differential equations which must be solved simultaneously. We can also use asymptotic analysis to derive the asymptotic behavior of $B(t,M|S)$ based on (4.13) as following:

$$\rho_i(M) \triangleq \lim_{t\to\infty} B(t,M|S_i) = \sum_{n=M}^{m} D(n|S_i). \tag{4.17}$$

4.5 Analytical results

In this section, we present results obtained from the SASE model applied to IEEE-118 bus system.

4.5.1 Conditional blackout probability

The PMF of the blackout size conditional on the initial state, $D(n|S_i)$, is calculated using (4.13) and shown in Fig. 4.12 for a fixed initial state with $F_i = 2$ and $C_i^{\max} =$

20MW. Figure 4.12 also shows the effects of the operating characteristics of the power grid on $D(n|S_i)$. The results suggest that when the power grid operates under a reliable operating configuration (small values of r, e and θ) the PMF of the blackout size shows an exponential decay, which has also been observed empirically by Dobson (see Figs. 1, 2 in [20]) using real outage datasets [80]. On the other hand, when the power grid is stressed (large values of r, e and θ) the probability of large blackouts increases and a hump appears near the tail of the PMF. Note that the hump represents a heavy tail property in the distribution of the blackout size. The analysis of historical blackout data [1, 39, 83] has been suggested that the PMF of the blackout size for power grids has a heavy tail property, specifically, when they are operating close to their critical limits (see Fig. 1.1). Another example of the heavy tail distributions is the power-law distribution, which has gained attention as it is attributed to the complex system dynamics. We will discuss the power-law distribution of the blackout size in Section 4.5.1.1.

These conclusions from the analytical SASE model are confirmed by power-system simulation results as shown in Fig. 4.13. Note that the set of simulation results used to validate these conditional probabilities are different from the set of results used to identify the model parameters. All in all, these results validate that the SASE model with its low-dimensional, abstract state space is effective in capturing the dynamics of cascading failures in the power grid.

Note that the average size of cascading failures is approximately four in the scenario without stress (Fig. 4.13-a) while this number is approximately 61 in the scenario with stress (Fig. 4.13-b). Therefore, one could use the SASE model to characterize the conditions for occurrence of large blackouts by identifying the operating characteristics that result in a heavy tail PMF for the size of failures.

Next, consider the conditional probability of reaching a blackout state with at least M failures from an initial state S_i, i.e., $\rho_i(M)$, as introduced in (4.17). For a

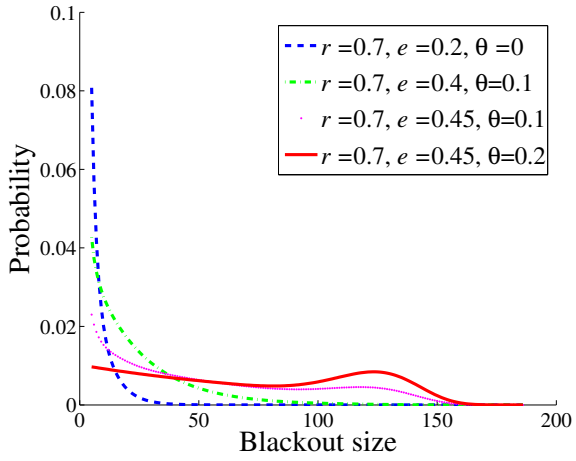

Figure 4.12: Conditional PMF of the blackout size for four operating-characteristic settings and $F_i = 2$ and $C_i^{\max} = 20$MW.

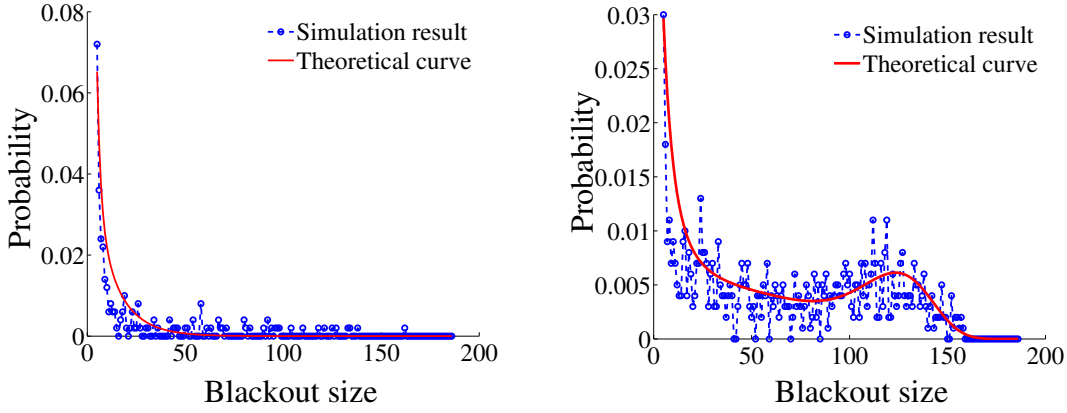

(a) (b)

Figure 4.13: The analytical and empirical conditional PMF of the blackout size (a) without stress, i.e., $r = 0.7$, $e = 0.25$ and $\theta = 0$, and (b) with stress, i.e., $r = 0.7$, $e = 0.35$ and $\theta = 0.2$, for the initial state with $F_i = 2$ and $C_i^{\max} = 20$MW.

fixed M and $F_i = 2$ and $C_i^{\max} = 20$MW, the dependence of $\rho_i(M)$ on r and e is shown in Fig. 4.16-a and on e and θ in Fig. 4.16-b. As expected, $\rho_i(M)$ increases with r, e, and θ. The results also suggest that at certain settings of the operating characteristics, a phase transition occurs in the blackout probability. This represents

the critical operating settings for which the power grid becomes highly vulnerable to cascading failures.

4.5.1.1 A discussion on the power-law distribution

Power grids are believed to exhibit some attributes associated with complex systems [1,39,83]. It has been suggested that the PMF of the blackout size for these systems has a heavy tail, specifically, when they are operated near their critical limits. In the analytical results presented in Fig. 4.12 we showed that the PMF of the blackout size has a heavy tail when the operating characteristics of the power grid introduce stress to the system and the size of the hump at the tail increases as the stress increases in the system.

Another example of the heavy tail distributions is the power-law distribution, which has gained attention as it is attributed to complex-system dynamics. In this subsection, we identify attributes of the transition probabilities for the Markov chain modeling cascading failures that lead to the power-law distribution for the blackout size. To simplify the analysis, we simplify the SASE model to a Markov chain that considers the number of failures F and stability variable I as the state variables. This simplified Markov chain model is presented in Fig. 4.14.

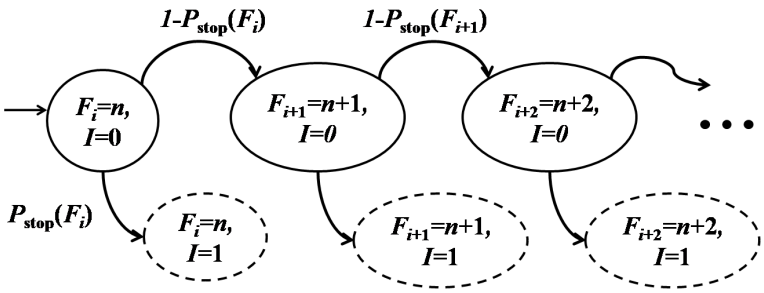

Figure 4.14: A simplified Markov chain model with F and I state variables, which models the stochastic dynamics of cascading failures in a power grid.

Recall that in Section 4.3.1 we described how power-system simulations produce a bowl-shape form for the cascade-stop probability as a function of number of failures in the system, i.e., $P^{(1)}_{\text{stop}}(F_i)$. The attributes of the bowl-shape function depend on the operating characteristics of the power grid (see Fig. 4.6). In this subsection, by using the simplified Markov-chain model presented in Fig. 4.14, we back calculate the cascade-stop probability $P_{\text{stop}}(F_i)$ for the model that precisely results in the power-law distribution for the blackout size. Interestingly, we will show that the numerically calculated $P_{\text{stop}}(F_i)$, based on this simplified analytical model, is necessarily of a bowl-shape form for $P_{\text{stop}}(F_i)$; the detail is given below.

As before, we denote the probability of a blackout with n failures by $D(n|S_i)$, which can be easily derived in the following difference equation using the model presented in Fig. 4.14,

$$D(n+1|S_i) = \frac{P_{\text{stop}}(n+1)(1-P_{\text{stop}}(n))}{P_{\text{stop}}(n)} D(n|S_i). \tag{4.18}$$

If we assume, without loss of generality, that the initial state of the power grid has one failure with $I = 0$, i.e., $S_i = (1, 0)$, then the boundary condition for (4.18) is $D(1|S_i) = P_{\text{stop}}(1)$

Based on (4.18) if the transition probabilities of the Markov chain are constant, i.e., $P_{\text{stop}}(F_i)$ is constant, then the chain can model cascading failures in a system for which the PMF of the blackout size follows an exponential distribution. Next, to identify the $P_{\text{stop}}(F_i)$ function which results in a power-law distribution for the blackout size, we input the values of $D(n|S_i)$ using the corresponding values of the PMF of a discrete power-law distribution, namely Zipf's law. The PMF of this distribution is as follows

$$P(n, s, m) = \frac{1}{\sum_{i=1}^{m} i^{-s}} n^{-s}, \tag{4.19}$$

where s is the parameter of the distribution and m is the number of lines in the power grid. In other words, we set $D(n|S_i) = P(n, s, m)$, where s is the free parameter of the

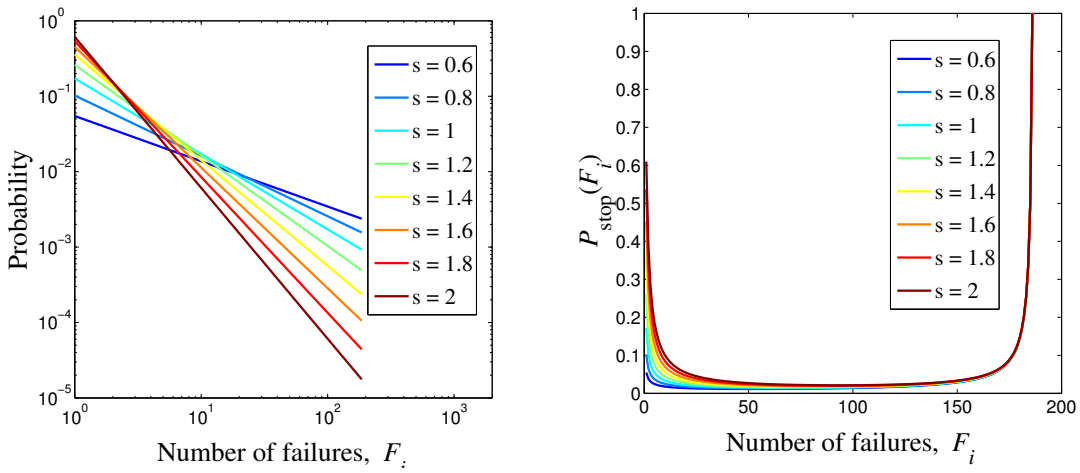

(a) (b)

Figure 4.15: (a) PMF of the blackout size, $D(n|S_i)$, in log-log scale following the power-law distribution with various s parameters, and (b) $P_{\text{stop}}(F_i)$ function deduced from $D(n|S_i)$s of part (a).

model. We have shown the distribution of blackout size, i.e., $D(n|S_i) = P(n, s, m)$, for different values of n and s in log-log scale in Fig. 4.15-a.

As mentioned in [1,39] the NERC historical data indicates a power law scaling of blackout frequency, when the blackout is measured by unserved energy and the power-law exponent s of this scaling is approximately between 0.6 to 1.9. Many probabilistic models have attempted to capture the power-law behavior for the distribution of size of failures in cascading failures [5,14]. For instance, the PMF of failures for the CASCADE model presented in [14] is a power law distribution with exponent 1.4.

We have numerically calculated $P_{\text{stop}}(F_i)$ using the difference equation in (4.18) for the distributions shown in Fig. 4.15-a. The results for function $P_{\text{stop}}(F_i)$ are shown in Fig. 4.15-b. An important point to notice here is that the results presented in Fig. 4.15-b using the difference equation (4.18) also represent a bowl-shape function similar to the one plotted using power-system simulations in Fig. 4.6. Due to the lack of sufficient parameters that parametrically model the simulation results in

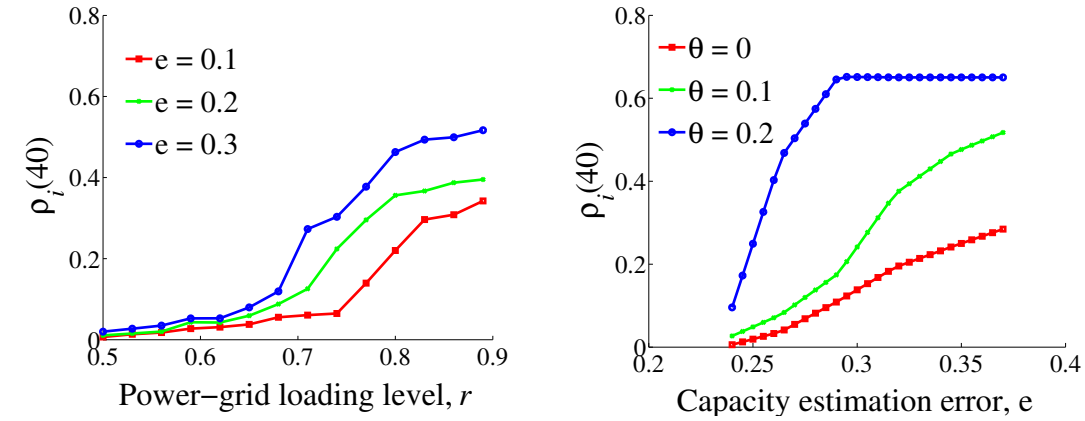

Figure 4.16: Conditional blackout probability $\rho_i(M)$ for $M = 40$ as a function of (a) r parameterized by e, and (b) e parameterized by θ, for the initial state with $F_i = 2$ and $C_i^{\max} = 20$MW.

Fig. 4.6, we cannot fit the parameters of the SASE model to the bowl-shape functions obtained here; however, based on the results presented in Section 4.3.3, we can conjecture that the attributes of the bowl-shape function depend on the operating characteristics of the power grid and thus certain operating characteristic of the system may lead to the bowl-shape functions that obtained in this subsection. Further, we conclude that the bowl-shape behavior for the state-dependent transition probabilities $P_{\text{stop}}(F_i)$ increases the probability of larger blackouts. In particular, certain bowl-shape functions result in the power-law distribution for the PMF of the blackout size. Moreover, as the simulation results in Fig. 4.6 suggest certain operating characteristics of the system set the system in critical conditions that lead to a heavy tail, specifically, the power-law distribution for the blackout size. We wish to emphasize here that the state-dependent transition probabilities are key elements of the Markov chain framework for modeling cascading failures to capture a wide range of stochastic behaviors for complex systems such as power grids.

4.5.2 Conditional blackout probability as a function of time

The numerical results of the conditional blackout probability $B(t, M|S_i)$ are calculated using (4.11) and (4.14). The same results can be obtained using Theorem 4.4.1. As a representative example, we have calculated $B(t, 30|S_i)$ for $r = 0.7$, $e = 0.2$ and $\theta = 0.1$ for different initial states, S_i, as shown in Fig. 4.17. As the results show, the values of F_i and $C_i^{\max}$ associated with the initial state affect the evolution of the blackout probability. In particular, both the probability of reaching a power-grid state with M or more failures and its rate of change during escalation phase increase with F_i and $C_i^{\max}$. We reiterate that while we have assumed a single-line failure at a time in our model, the escalation phase in the cascading failure occurs as a result of shorter time between failures due to higher transition rates for such states (as the transition rates are state dependent). Also, note that $B(t, M|S_i)$ exhibits three phases. Interestingly, the three-phase theme of cascading failures were also seen in the behavior of the cascade-stop probability as well as the evolution of the accumulative number of failures.

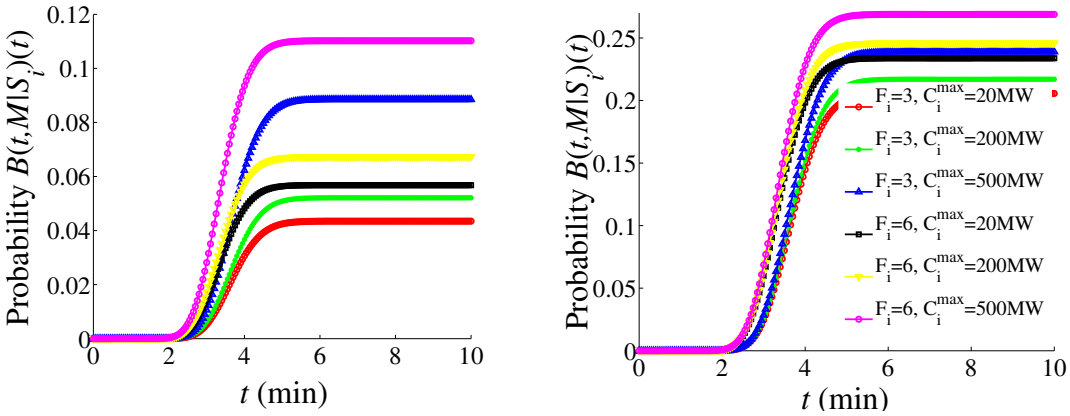

Figure 4.17: Probability of reaching a blackout, $B(t, M|S_i)$, with $M = 30$ or more failures for $r = 0.7$, $e = 0.2$, $\theta = 0.1$, and initial states (a) with $F_i = 3$, and (b) with $F_i = 6$, and different values of $C_i^{\max}$.

4.5.3 Failure evolution

Figure 4.18 shows four realizations of the cascading-failure scenarios in terms of the evolution of the cumulative number of failures obtained using the SASE Markov chain. The initial state of the power grid in all the four realizations has two line failures with $C_i^{\max} = 80$MW. Note that in the realization with 163 eventual failures, the number of failures increases relatively gently at the beginning; however, failure of a line with large capacity at $t = 10$ min results in rapid increase in the number of failures in the power grid. In contrast, the number of failures in other realizations increases rapidly right from the beginning but they transit to stable state earlier as the value of $P_{stop}(S_i)$ in these cases is larger. Note that from Fig. 4.18 we observe similar forms to those shown in Fig. 4.2 for the historical blackouts.

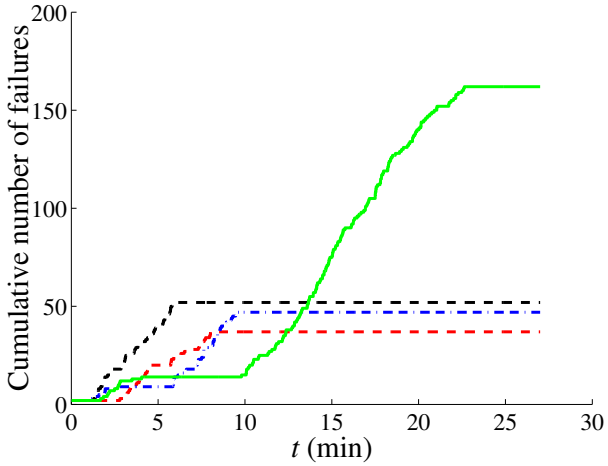

Figure 4.18: Realizations of the evolution of the cumulative line failures using the SASE model for $r = 0.7$, $e = 0.2$, $\theta = 0.1$, $F_i = 2$, and $C_i^{\max} = 80$MW.

4.5.4 Size of cascading failures

To assess the severity of cascading failures we consider the number of subsequent failures induced by each initial failure. For a given initial state S_i with F_i initial

failures, we define $R_{S_i} \triangleq (F_i - F_i^{\text{end}})/F_i$, where F_i^{end} is the random variable for the final number of failures in the power grid after cascading failure ends. Here, we study the mean of R_{S_i} as a metric representing the severity of cascading failures, which can be calculated as $\mathsf{E}[R_{S_i}] = \sum_{j=1}^{N} \lim_{t\to\infty} p_{ij}(t)(F_j - F_i)/F_i$. (For this metric to be meaningful the initial number of failures F_i must be small, which in general is met in most real scenarios.) Figures 4.19 and 4.20 show that $\mathsf{E}[R_{S_i}]$ (for $F_i = 3$) increases with r, e and θ. From results in Fig. 4.19 we observe that there is a critical value of load-shedding constraint level (approximately $\theta = 0.2$) above which strong cascading behavior is observed. Furthermore, this trend becomes more evident and aggressive as the capacity estimation error e increases. Similarly, the results in Fig. 4.20 suggests that there is a critical loading level (approximately $r = 0.8$) for which the rate of change in $\mathsf{E}[R_{S_i}]$ increases abruptly for all values of e. Here, we reiterate that the N-1 criterion has been ensured in all loading levels of the power grid; therefore, the initial contingency is assumed to have at least two initial failures.

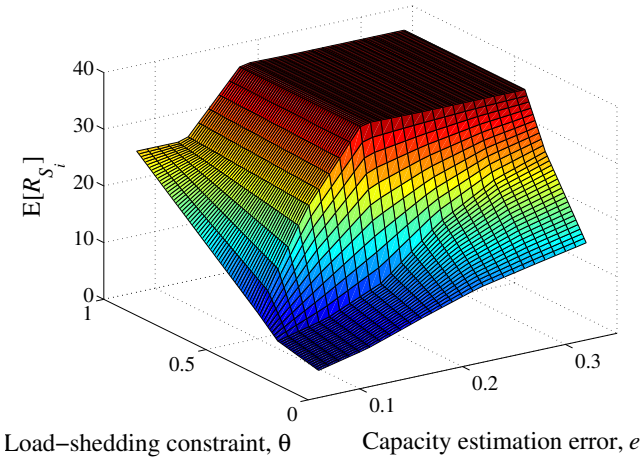

Figure 4.19: $\mathsf{E}[R_{S_i}]$ for the IEEE 118-bus system as a function of load-shedding constraint level θ and the capacity estimation error e for $r = 0.7$ and the initial state with $F_i = 3$ and $C_i^{\max} = 20$MW.

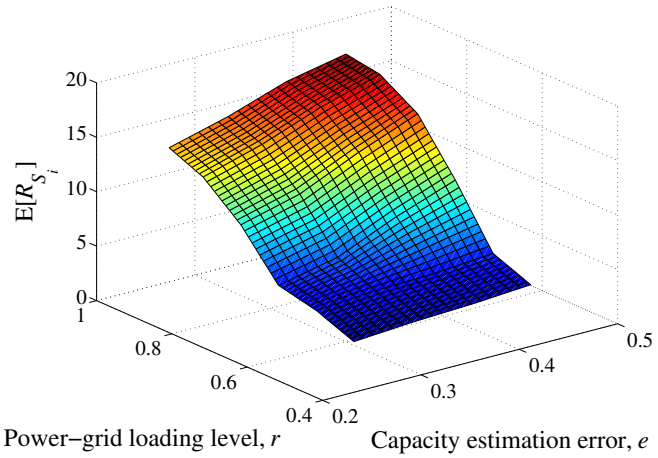

Figure 4.20: $\mathsf{E}[R_{S_i}]$ for the IEEE 118-bus system as a function of the power-grid loading level r and the capacity estimation error e for $\theta = 0$ and the initial state with $F_i = 3$ and $C_i^{\max} = 20$MW.

4.6 Summary and conclusions

We have developed a scalable and analytically tractable probabilistic model, termed the stochastic abstract-state evolution (SASE) model, which describes the stochastic dynamics of cascading failures using Markov chains. The state space of the SASE model is a reduced, abstract state space extracted from the large space of all possible power-grid states. The definition of the abstract states retains key physical attributes of the power grid. We introduced absorbing states in the state space to model the stable states of the system. In contrast to the models that are based on pure birth-chains, the definition of the absorbing states in the state-space of the Markov chain enables modeling of various blackout sizes in the system. We have formulated the state-dependent transition rates associated with the SASE model in terms of key operating characteristics of the power grid including the power-grid loading level, the load-shedding constraint level and the capacity estimation error. The analysis of the SASE model and its asymptotic behavior together enable determining the PMF of the blackout size, the evolution of the blackout probability from a specific initial

state, as well as assessing the severity of the cascading behavior as a function of various operating settings of the power grid. The SASE model also enables the identification of critical regions of the space of key power-grid operating characteristics for which severe cascading behavior may occur. A key insight provided by this model is that the PMF of the blackout size has a heavy tail specifically when the grid is operating under stress scenarios. We also identified the transition probabilities for the Markov chain model, which result in power-law distribution for the blackout size. Numerical results based on the analytical model and the power-system simulations both indicate that the probability that cascading phenomenon terminates in a state (cascade-stop probability) has a bowl-shape form as a function of number of failures in the system. The importance of the bowl-shape function is that it results in the heavily tail distribution for the blackout size and thus represents a condition for the critical behavior in the system. To the best of our knowledge, this important fact about the critical form for cascade-stop probability that leads to the heavy-tail distribution for the blackout size was not known heretofore.

Chapter 5

Regeneration-based framework for cascading failures

In Chapter 4, we introduced Markov chains with state-dependent transition probabilities as a strong tool to model cascading failures. In this chapter, we present another probabilistic framework for modeling cascading failures based on regeneration theory, which similarly to the Markov chain model, provides a strong tool for capturing the stochastic dynamics of cascading failures, albeit in a more general setting, as described next. Although exponential distribution for events (e.g., failures) in power grids is a well-accepted assumption, the presented model in this chapter is sufficiently general to capture an arbitrarily specified probability distribution for the events in the system in a non-Markovian setting. Here, we formulate a general regeneration-based framework for modeling the stochastic dynamics of cascading failures in power grids. We also derive, as a special case, a systems of differential equations describing the probability of the blackout for a power grid with Markovian settings using this framework, which supplements the analysis in Section 4.4. Specifically, this framework provides an elegant approach for proving Theorem 4.4.1 describing the probability of reaching a blackout with a specified number of failures

in a time interval.

5.1 Preliminaries

Similarly to the Markov-chain model, the presented framework in this chapter describes the stochastic dynamics of the system by a sequence of transitions among the states of the system. Similarly to the SASE model, we define the state space of this framework based on extracting a reduced abstraction of large-scale power grids using a small number of aggregate state variables.

In this framework, we use the number of failed lines F and the maximum capacity of the failed lines $C^{\max}$ as the descriptor of the state of the power grid. We denote the state of the power grid by $S_i = (F_i, C_i^{\max})$. Note that compared to the state space introduced for the SASE model in Chapter 4 we do not consider the stability parameter I as a state variable. This point simplifies the regeneration equations introduced in this chapter. Meanwhile, we capture the effect of stability of certain states through the probability of transiting out of states. In other words, the probability that transiting out of a state never occurs is equal to the cascade-stability probability introduced in Chapter 4. As such, the states of this model are *partially absorbing*, which we define to be states that when hit then the system will never leave them with certain probability (cascade-stop probability).

The idea of regeneration is that the occurrence of an event regenerates, or stochastically replicates, the same problem albeit with new initial conditions. The problem considered here is the characterization of the probability of reaching a blackout of an arbitrary size in any time interval starting from an initial grid state. In our model, the event that regenerates the problem is the first line failure in a power-grid state. Before formulating this problem theoretically, let us review the failure events in the system.

In this dissertation, we assume at most a single failure occurs at any time instant in the system. Recall from Chapter 4 that when a single line failure occurs in the system with state $S_i = (F_i, C_i^{\max})$ then the state of the system changes in one of the following ways. First, if the capacity of the newly failed line, C_f is larger than $C_i^{\max}$ then the new grid state becomes $S_{i+1}^u = (F_{i+1}^u, C_{i+1}^{u,\max})$ where $C_{i+1}^{u,\max} = C_f$ and $F_{i+1}^u = F_i + 1$. Second, if $C_f \leq C_i^{\max}$ then the new grid state becomes $S_{i+1}^w = (F_{i+1}^w, C_{i+1}^{w,\max})$ where $C_{i+1}^{w,\max} = C_i^{\max}$ and $F_{i+1}^w = F_i + 1$. Hence, we can categorize the events that transpire after a line failure, starting from state $S_i = (F_i, C_i^{\max})$, into two types. These categories of events are introduced to simplify the characterization of the transition rates among the states as introduced in Chapter 4. Let U_j and W represent the time of the transition of state S_i to state $S_{i+1}^{u_j}$ and to state S_{i+1}^w, respectively. The subscripts of the first random variable is for $j \in \mathcal{J}$, where $\mathcal{J} \triangleq \{j | C_f = C_j, C_j \in \mathcal{C} \text{ and } C_j > C_i^{\max}\}$.

The key point in the regeneration-based model is to define a certain special random variable, called the *regeneration time,* τ, defined as $\tau \triangleq \min_j\{U_j, W\}$, which represents the time to the first failure, or equivalently, the time of transition to a new state. To reiterate, the key feature of the event at time τ is that its occurrence will regenerate the problem at τ, which has the same statistical properties and dynamics as the original problem but with different initial configurations, viz., different number of failures with possibly different maximum capacity of the failed lines. Next, we present the general regeneration-based framework for the introduced problem.

5.2 Regeneration-based formulation

Similarly to Chapter 4, we use the notation $B(t, M|S_i)$ to represent the probability of reaching blackout size M or larger (a blackout with M or more line failures) in a time interval t and initial grid state $S_i = (F_i, C_i^{\max})$. We denote the probability density

function (pdf) of τ by $f_\tau(s)$. In the non-Markovian setting $f_\tau(s)$ can follow arbitrarily specified probability distributions. Note that when $F_i \geq M$ then $B(t, M|S_i) = 1$. This is because the state has at least M failures and the probability of reaching a blackout state of size M or larger is one. Now, we consider the case $F_i < M$ and state the general integral equations describing $B(t, M|S_i)$ in Theorem 5.2.1.

Theorem 5.2.1. *The probability of reaching a blackout of size M or larger in a time interval t and from an initial state $S_i = (F_i, C_i^{\max})$, where $F_i < M$ and the probability distribution of events in the system follows an arbitrary distribution $f_\tau(s)$ can be characterized by the following differential equation:*

$$B(t, M|S_i) = (1 - P_{stop}(S_i)) \int_0^t \Big(\mathsf{P}\{\mathcal{E}_\tau = W|\tau = s\} B(t-s, M|S^w) + \sum_{j \in \mathcal{J}} \mathsf{P}\{\mathcal{E}_\tau = U_j|\tau = s\} B(t-s, M|S^{u_j}) \Big) f_\tau(s) ds, \tag{5.1}$$

with the following initial conditions:

$$B(t, M|S_i) = 1, \text{ if } F_i \geq M. \tag{5.2}$$

Next, we present the proof of Theorem 5.2.1.

Proof. By exploiting the properties of conditional expectations we can write,

$$B(t, M|S_i) = (1 - P_{\text{stop}}(S_i)) \int_0^t B(t, M|S_i, \tau = s) f_\tau(s) ds. \tag{5.3}$$

Note that $B(t, M|S_i, \tau = s)$ is the probability of reaching a blackout with at least M failures in the time interval t conditioning on τ being equal to s (first event occurs at s). We write this probability as

$$B(t, M|S_i, \tau = s) = \mathsf{P}\{\mathcal{E}_\tau = W|\tau = s\} B(t, M|S_i, \tau = s, \mathcal{E}_\tau = W) + \sum_{j \in \mathcal{J}} \mathsf{P}\{\mathcal{E}_\tau = U_j|\tau = s\} B(t, M|S_i, \tau = s, \mathcal{E}_\tau = U_j), \tag{5.4}$$

where $\mathcal{E}_t$ represents the category of the event that occurred at time t. The conditional probabilities in (5.4) for the event $\{\mathcal{E}_\tau = U_j\}$ can be written as follows, which represents the regeneration of a new problem with new initial conditions.

$$B(t, M|S_i, \tau = s, \mathcal{E}_\tau = U_j) = B(t - s, M|S^{u_j}). \tag{5.5}$$

The new problem that has been regenerated based on (5.5) is the characterization of the probability of reaching a blackout of size M or large in a time interval with length $t - s$ and the initial power-grid state as S^{u_j}. Similarly, we can write $B(t, M|S_i, \tau = s, \mathcal{E}_\tau = W) = B(t - s, M|S^w)$. The proof of the regeneration equation of (5.5) is similar to the approach presented in [84]. Substituting (5.5) in (5.4) and substituting the result in (5.3) completes the proof. □

The general framework presented in this section describes a system of integral equations, where for each state S_i as the initial state we have an equation in the form of (5.1). We have to solve this system of coupled equations simultaneously in order to numerically calculate $B(t, M|S_i)$.

5.3 Regeneration-based formulation with Markov property

As a special case of the general framework presented in Theorem 5.2.1, in this section, we derive the closed form differential equations for $B(t, M|S_i)$ when $f_\tau(s)$ has Markov property (i.e., follows an exponential distribution). The discussion here based on the framework presented in Section 5.2 leads to the proof of Theorem 4.4.1.

Assume that random variables U_j and W are mutually independent and follow an exponential distribution with parameters (inverse of the mean) γ_{U_j} and γ_W, respectively. As mentioned in Chapter 4, we assume that γ_{U_j} and γ_W are state dependent

and also depend on the operating characteristics of the grid. If we assume that random variables in the system are independently and identically distributed following exponential distribution (i.e., having Markov property) then this implies that the minimum of these random variables is also an exponential random variable. As such, τ is also an exponential random variable with rate $\gamma = \sum_{j \in \mathcal{J}} \gamma_{U_j} + \gamma_W$. Further, $\mathsf{P}\{\mathcal{E}_\tau = W | \tau = s\} = \gamma_W/\gamma$, and $\mathsf{P}\{\mathcal{E}_\tau = U_j | \tau = s\} = \gamma_{U_j}/\gamma$. Based on our discussion in Section 4.3, γ_W represents the transition rate among the states corresponding to $(1 - P_{hc}(S_i))$ (probability that a new failure in the system has a smaller or equal capacity compared to the current $C_i^{\max}$) and γ_{U_j} represents the transition rate among the states corresponding to $P_{hc}(S_i)P_{C^{\max}}(S_i, S^{u_j})$, (where $P_{C^{\max}}(S_i, S^{u_j})$ represents the probability of transiting to state S^{u_j} with larger capacity compared to $C_i^{\max}$).

For completeness we restate Theorem 4.4.1, which describes $B(t, M|S_i)$ using a system of differential equations.

Theorem 4.4.1 The probability of reaching a blackout of size M or larger in a time interval t and from an initial state S_i (with $F_i < M$) and $f_\tau(s)$ following an exponential distribution is characterized by the following system of differential equation:

$$\frac{dB(t, M|S_i)}{dt} = -\gamma B(t, M|S_i) + (1 - P_{\text{stop}}(S_i))\Bigg(\gamma_W B(t, M|S^w) + \sum_j \gamma_{U_j} B(t, M|S^{u_j})\Bigg), \tag{5.6}$$

with the following initial conditions:

$$B(t, M|S_i) = 1, \text{if } F_i \geq M. \tag{5.7}$$

Proof. Following the steps presented for the proof of Theorem 5.2.1, we can write

$$B(t, M|S_i) = (1 - P_{\text{stop}}(S_i)) \int_0^t \Big(\gamma_W B(t-s, M|S^W) + \sum_{j \in \mathcal{C}} \gamma_{U_j} B(t-s, M|S^{u_j}) \Big) e^{-\gamma s} ds. \tag{5.8}$$

Now, by using the Leibnitz integral rule and change of variables in (5.8), we can derive (5.6). □

Because the probability of reaching a blackout for a power-grid state S_i is expressed based on the probability of reaching a blackout starting form states $S_{i+1}^{u_j}$ and S_{i+1}^{w}, we have a set of coupled differential equations which must be solved simultaneously to obtain the numerical results for $B(t, M|S_i)$.

5.4 Summary and conclusions

In this chapter, we presented a probabilistic regeneration-based framework for the stochastic dynamics of cascading failures in power grids. This general framework is applicable to more general settings where the system variables can be non-Markovian random variables. Similarly to the Markov-chain model, the state space of this framework is defined based on extracting a reduced abstraction of large-scale power grids using a small number of aggregate state variables. In this chapter, we first formulated a general regeneration-based framework for modeling the stochastic dynamics of cascading failures in power grids. Then, as a special case, we derived the system of differential equations based on the general regeneration-based framework, describing the probability of the blackout for a power grid in a Markovian setting. The discussions in this chapter supplement the analysis in Section 4.4 describing the probability of reaching a blackout with a specified number of failures in a time interval. The regeneration-based approach presented in this chapter is sufficiently general

to capture the stochastic dynamics of cascading failures in systems with arbitrary distribution for the random events in the system.

Chapter 6

Interdependent Markov chain framework for cascading failures

In this chapter, we present an extension of the Markov chain model presented in Chapter 4 to a novel interdependent Markov chain framework for modeling cascading failures in interdependent infrastructures. The interdependent Markov chain approach proposed in this chapter provides a probabilistic framework to capture the effects of interdependencies among physical systems on stochastic dynamics of the interdependent infrastructure. The idea of this general approach is to build an integrated framework consisting of a system of interdependent heterogeneous Markov chains, one for each physical system. In this chapter, we consider discrete time Markov chains as it simplifies the modeling of the interaction between interdependent systems by characterizing the transition probabilities of the interdependent Markov chain based on individual chains. Here, we first present the general interdependent Markov chain framework in Section 6.1. Then, we derive an interdependent Markov chain model for cascading failures in electric-cyber infrastructures in Section 6.3. A key insight obtained from the interdependent Markov chain model for the power grid and the communication system is that interdependencies between the two systems

can make two reliable systems behave unreliably, thereby increasing the probability of large failures. For instance, we specifically show that two individual systems with exponential distribution for the size of failures can be coupled together to have a power-law distribution for the size of failures in an interdependent setting.

6.1 Interdependent Markov chains

In this section, we propose interdependent heterogeneous Markov chains to model stochastic dynamics of cascading failures in a collection of systems comprising interdependent physical infrastructures. To do so, starting from individual Markov chains that approximate the stochastic dynamics of each of the physical systems, we develop a minimal Markov chain that encompasses the individual chains and approximates the stochastic dynamics of the entire collection of systems as a single system while capturing the interdependencies among the systems.

6.1.1 Preliminaries

We describe the interdependent Markov chain approach using two interdependent systems A and B with the understanding that the same approach can be applied to any finite number of interdependent systems. Here, we consider a Markov chain for each of the physical systems similar to the one presented in Fig. 4.14. We have shown the Markov chains of systems A and B in Fig. 6.1. Note that in Fig. 6.1 a transition to the same state has been added to the model compared to Fig. 4.14 in order to simplify the modeling of interdependencies between the Markov chains. The model presented in Fig. 6.1 can be simplified to the one in Fig. 4.14 by adjusting the transition probabilities. In these Markov chains the state of the system is denoted by the number of failures and the stability variable as $S_i^A = (F_i^A, I_i^A)$ for system A

and $S_i^B = (F_i^B, I_i^B)$ for system B. The state-space of the Markov chain for system A is denoted by $\mathcal{S}_A$, where $\mathcal{S}_A = \{1, \ldots, m_A\} \times \{\text{absorbing}, \text{non-absorbing}\}$ and m_A is the number of components in system A. Similarly, we denote the state space of the Markov chain for system B by $\mathcal{S}_B = \{1, \ldots, m_B\} \times \{\text{absorbing}, \text{non-absorbing}\}$. Notice that in general the state space of the Markov chains representing different physical systems are not the same, neither is their cardinality nor their state variables. The random process $X(t)$ and $Y(t)$ respectively represent the state of the system A and B at time $t \geq 0$.

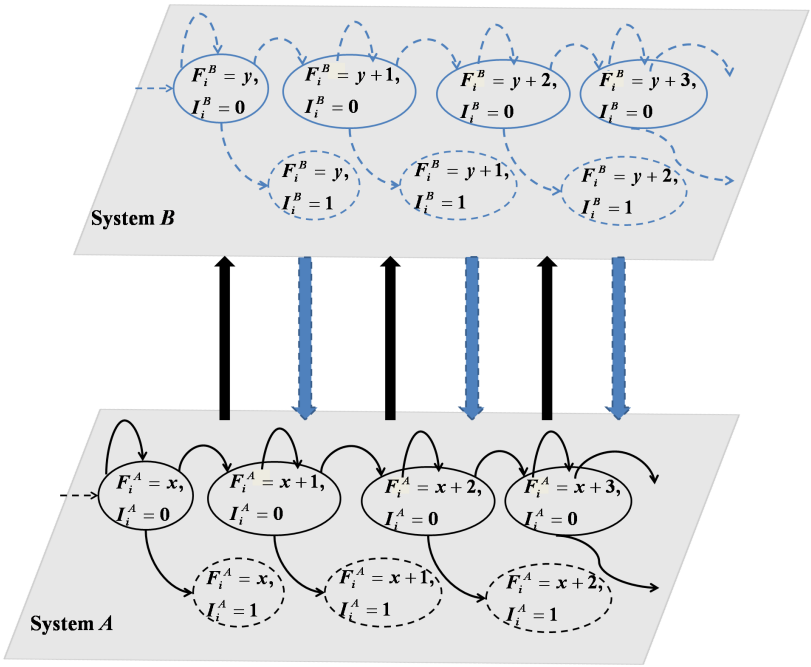

Figure 6.1: Two Markov chains representing the stochastic dynamics of cascading failures in each of the interdependent physical systems and the coupling effect between Markov chains.

Clearly, the most naïve way to couple two Markov chains is to develop a *combined Markov chain* with the state space $\mathcal{S}_C$ formed by the Cartesian product of the state space of each of the individual systems, i.e., $\mathcal{S}_C = \mathcal{S}_A \times \mathcal{S}_B$. With this approach,

we denote the state of the system comprising system A and B at time instant i by $S_i^C = (F_i^A, I_i^A, F_i^B, I_i^B)$. Transition probabilities of the combined Markov chain depend on the state of both of the individual systems.

This approach, however, has the shortcoming that the new transition probabilities among the states of $\mathcal{S}_C$ cannot be readily derived from the transition probabilities of the individual Markov chains. A more serious flaw of this approach is that it is based on the false and built-in assumption that combining two Markov chains results in a new Markov chain with its state space being the Cartesian product of the individual chains. In actuality, even if we assume that marginal processes X and Y are Markovian it does not necessarily imply that their joint process (X, Y), as defined above, is Markovian. To verify this point we present the following simple example. Let $X_1, X_2, ...$ be independent and identically distributed (i.i.d.) sequence. Next, we define the process Y_n as $Y_n = X_{n-1} + X_{n-2}$ for $n > 2$ and $Y_2 = Y_1 = X_1$.The process Y_n is Markov because

$$\begin{aligned}\mathsf{P}\{Y_n|Y_{n-1}, ..., Y_1\} = \mathsf{P}\{X_{n-1} + X_{n-2}|X_{n-2} + X_{n-3}, ..., X_1\} = \\ \mathsf{P}\{X_{n-1} + X_{n-2}|X_{n-2} + X_{n-3}\} = \quad \mathsf{P}\{Y_n|Y_{n-1}\},\end{aligned} \tag{6.1}$$

where the step before last follows from the i.i.d. property of the sequence X_n. Therefore, both X and Y individually have the Markovian property. However, their joint distribution does not have the Markovian property because

$$\begin{aligned}\mathsf{P}\{Y_n, X_n|Y_{n-1}, ..., Y_1, X_{n-1}, ..., X_1\} &= \mathsf{P}\{X_{n-1} + X_{n-2}, X_n|X_{n-2} + X_{n-3}, ..., X_1, X_{n-1}, ..., X_1\} \\ &= \mathsf{P}\{X_{n-1} + X_{n-2}, X_n|X_{n-2} + X_{n-3}, X_{n-1}, X_{n-2}\} \\ &= \mathsf{P}\{Y_n, X_n|Y_{n-1}, X_{n-1}, X_{n-2}\}.\end{aligned} \tag{6.2}$$

The extra term X_{n-2} in the last line cannot be dropped, as Y_n is not independent of X_{n-1}, X_{n-2}, and Y_{n-1} due to their common terms, denying the joint distribution of X and Y of being Markovian. In general, if the random process $X(t)$ and $Y(t)$

represent the state of the system A and B, respectively, then the interdependencies between the two systems will result in correlation between processes X and Y.

Moreover, as the definition of interdependent systems implies stochastic dynamics of each of the systems is affected by the dynamics of the other systems. As such, the one-step transitions in the whole system can be generally dependent on multiple previous transitions (past dynamics or multiple-step history) of its constituent subsystems A and B. As a result, defining the new state space simply by the Cartesian product of the state space of each system does not provide sufficient information to fully capture the interdependency between the systems and to characterize the transition probabilities among the states of the combined Markov chain. Hence, in modeling interdependent systems, besides the knowledge from the current state of each of the systems, we also need to incorporate *memory* from the past transitions to adequately characterize the stochastic dynamics of the whole system.

6.1.2 State space and transition probabilities

We denote the probability of transiting to state $s_{i+1}^C \in \mathcal{S}_C$ conditional on all the history of the transitions for the system by $f_{S_{i+1}^C|S_i^C,...,S_1^C}(s_{i+1}^C|s_i^C,...,s_1^C) \triangleq \mathsf{P}\{S_{i+1}^C = s_{i+1}^C|S_i^C = s_i^C,...,S_1^C = s_1^C\}$, where s_i^C represents the current state of the system and the remainder variables represent all the states that the system has visited in the past. Let us assume that for each $a \in \mathcal{S}_C$, $f_{S_{i+1}^C|S_i^C,...,S_1^C}(a|\cdot,\ldots,\cdot)$ is a one-to-one function on $(\mathcal{S}_C)^i$. When a system exhibits the Markovian property, we have $f_{S_{i+1}^C|S_i^C,...,S_1^C}(s_{i+1}^C|s_i^C,...,s_1^C) = \mathsf{P}\{S_{i+1}^C = s_{i+1}^C|S_i^C = s_i^C\} \equiv \tilde{f}_{S_{i+1}^C|S_i^C}(s_{i+1}^C|s_i^C)$. In this case, the function $f_{S_{i+1}^C|S_i^C,...,S_1^C}(a|\cdot,\ldots,\cdot)$ cannot be one-to-one in general on $(\mathcal{S}_C)^i$ since it maps all different history sequences with the same current state to the same value. In contrast, when we consider M-step memory then $f_{S_{i+1}^C|S_i^C,...,S_1^C}(s_{i+1}^C|s_i^C,...,s_1^C) = \mathsf{P}\{S_{i+1}^C = s_{i+1}^C|S_i^C = s_i^C,...,S_{i-M+1}^C = s_{i-M+1}^C\} \equiv \tilde{f}_{S_{i+1}^C|S_i^C,...,S_{i-M+1}^C}(a|s_i^C,...,s_{i-M+1}^C)$.

In this case, the function $\tilde{f}_{S_{i+1}^C|S_i^C,...,S_{i-M+1}^C}(a|\cdot,...,\cdot)$ can be one-to-one on $(\mathcal{S}_C)^M$. For further discussion on, for example, the two-step Markov point processes we refer the reader to [85]. The incorporation of memory in the model beyond one step provides a mean for capturing the detail of dynamics of the system that is required to fully capturing the interdependencies between the two systems.

As we pointed in the previous section, stochastic dynamics of system A and B generally depends upon the M_1-step and M_2-step memory from the system B and A, respectively. For simplicity of notation and without loss of generality, we assume that $M_1 = M_2 = M$. The standard Markov chains are assumed to have one state memory (namely 1-step memory). To capture the effects of the M-step memory for each of the systems in stochastic dynamics of the combined system, the transition probability function must be

$$f : (\mathcal{S}_C)^M \times \mathcal{S}_C \to [0, 1], \tag{6.3}$$

where $(\mathcal{S}_C)^M$ captures the information from the current state (1-step memory) as well as the previous M-1 states. The last $\mathcal{S}_C$ in the domain of transition probability function f captures the destination space of transitions.

In summary, the transitions among the states of the $\mathcal{S}_C$ are not independent of the past transitions of the system. To build the equivalent Markov chain for the finite state machine with the state space $\mathcal{S}_C$ and transition probabilities that are functions of the previous states of the system, we need to extend the state space $\mathcal{S}_C$ to incorporate the memory of the past states. For instance, to build an interdependent Markov chain while capturing M-step memory the state-space can be defined as $\mathcal{S}_I = (\mathcal{S}_A \times \mathcal{S}_B)^M$. Due to the embedded memory in the definition of the states the size of the state space $\mathcal{S}_I$ can be prohibitively large in general. Next, we introduce a quantization approach to reduce the size of the state space while capturing the memory. Finally, note that the interdependent Markov chain with the state space $\mathcal{S}_I$ can be reduced to the combined Markov chain with the state space $\mathcal{S}_C$ at the cost

of losing the detail of interaction between the systems.

6.1.3 Memory quantization

In this section, we introduce a memory quantization approach for reducing the size of the state space of the interdependent Markov chains. In this approach, we quantize the information about the history of the dynamics of the system by defining equivalence classes of behaviors for the dynamics. For instance, if we can conjecture that the system is stable or unstable based on the history of its dynamics then we can categorize the history of the dynamics of the system into two classes of behaviors. We denote the set of behavior classes for the system by $\mathcal{H}_I$, for which in this example, it is given by $\mathcal{H}_I = \{\text{stable, unstable}\}$. We define a quantization function as $g : (\mathcal{S}_A \times \mathcal{S}_B)^M \to \mathcal{H}_I$, where $\mathcal{H}_I$ is the range of g. The function g compresses the memory from the past into equivalence classes. Clearly, the most detailed $\mathcal{H}_I$ is when we exactly know the previous M-steps of the system, i.e., $\mathcal{H}_I = (\mathcal{S}_A \times \mathcal{S}_B)^M$. Note that a quantization function can also be employed for classification of the individual system's behaviors. If we use function g to quantize the memory instead of the M-step detailed memory then we can represent the state space of the interdependent Markov chain by $\mathcal{S}_I = \mathcal{H}_I \times (\mathcal{S}_A \times \mathcal{S}_B)$, which can significantly reduce the size of $\mathcal{S}_I$.

6.1.4 Capturing the impact of interdependencies

Recall that modeling interactions among interdependent systems requires the knowledge of the behavior of the two systems. Up to this point we have discussed how to capture the knowledge about the behavior of each of the systems in the model. The next step is to determine how a specific behavior of a system affects the behavior of the other system. At a coarse level, the effects of the behavior of a system on another system can be divided into three categories: (1) improve, (2) worsen, and

(3) do not change. In the Markov-chain framework presented in Fig. 6.1, these effects can be translated into: (1) reducing the probability of extra failures, (2) increasing the probability of extra failures, and (3) not changing the probabilities. Therefore, the effects of interdependencies can be captured in the transition probability function f in (6.3), which can associate such effects with the transition probabilities in the combined system using the knowledge of the current state as well as the past dynamics of the system. Note that the effects of interdependencies may be constant in time (homogeneous) but it may change depending on the state of the system.

6.1.5 Interdependency strength

We define the strength of interdependency between two systems based on two factors: (1) how much the knowledge of the behavior of a system affects the dynamics of the other system (e.g., the absolute value of change in transition probabilities), and (2) how much memory of the states of each system is required to capture the interdependency effects on the other system. For instance, we define a metric δ to measure the first factor as follows:

$$\delta = \sup_{x_i, x_{i+1} \in \mathcal{S}_A, y_j \in \mathcal{S}_B, i-M+1 \leq j \leq i} \Big\{ |\mathsf{P}\{X_{i+1} = x_{i+1} | X_i = x_i\} - \mathsf{P}\{X_{i+1} = x_{i+1} | X_i = x_i, Y_i = y_i, ..., Y_{i-M+1} = Y_{i-M+1}\}| \Big\}. \quad (6.4)$$

In (6.4) metric δ characterizes the maximum influence of the behavior of system B on system A. Note that when δ is large the interdependency is strong and when it is zero it implies that the two systems are not interdependent. To measure the second factor, we introduce $\mathcal{K}$ as the smallest integer j such that for all n and for $i > j$, X_n and Y_{n-i} are independent. Here, $\mathcal{K}$ is the minimum memory required to be included in the interdependent Markov chain to capture the interdependencies between the two systems. Note that when $\mathcal{K}$ is large the interdependency is strong. $\mathcal{K} = 0$ means that the knowledge of the current state of system A and B would

be enough in modeling the interdependencies. In this case, $\mathcal{K} = -1$ represents the scenario in which the systems are not interdependent.

6.2 Interleaving approach

In this section, we present a new perspective in modeling the interdependent systems using the interdependent Markov chain approach, which enables us to see the "cause and effect" of interactions between the systems more clearly. In order to clarify the interactions between the systems we propose an interleaving approach, which captures the effects of every single transition in a physical subsystem on the other physical subsystem right after it occurs. In other words, when a transition occurs in system A then we need to evaluate how system B transits as a result of the new transition in system A before more transitions occur in system A. Note that the transition in system B due to the new transition in system A can even be transiting back to the current state of system B (no change in the state of system B) when the new failure has no impact on system B. This is the reason we introduced the transition back to the state itself in the model presented in Fig. 6.1 compared to Fig. 4.14. Following the above discussion, we can assume that the two systems take turns in changing their states. In Fig. 6.1, we have represented the back and forth mechanism (cause and effect model), which represents this assumption. Every transition in Fig. 6.1 represented with a solid arrow will be followed by a transition represented with a dashed arrow and vice versa. We call this approach *interleaving* as it interleaves the transitions in system A and B in an order as is shown in Fig. 6.1. The interleaving approach simplifies the modeling of interdependencies between the systems by capturing the immediate effects of each transition on the other system.

Moreover, the interleaving approach adds an extra level of detail to the general interdependent Markov chain model introduced in Section 6.1. We explain this point

by the following example. Consider an interdependent Markov chain model with two-step memory, which is partially shown in Fig. 6.2. Note that we have only shown the number of failures in each system and we have assumed that the other state variable I equals to zero for both of the systems (we have considered non-absorbing states). In this example, we observe that in the sequence of transitions a failure in system A is followed by two failures in system B and again a failure in system A. Here, the effects of individual failures in system B on system A is not clear. For instance, one can conjecture that the first failure made system A vulnerable and the second failure added an extra level of vulnerability and resulted in the extra failure in system A. Further, one can also conjecture that the first failure did not have any effect on system A and the second failure was the only reason for the extra failure. This implies that the interdependent Markov chain model can capture the combined effects while the interleaving approach can break the combined effects into more detailed cause and effect scenarios. Note that the interleaved model can be reduced to the original interdependent Markov chain framework if we aggregate the effects by allowing multiple transitions in a subsystem.

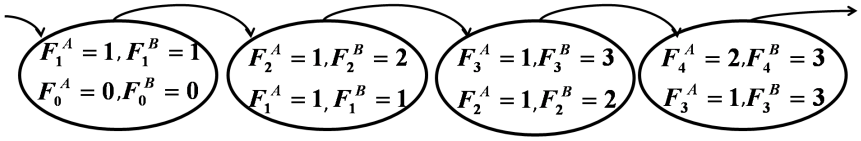

Figure 6.2: An example of sequence of transitions in an interdependent Markov chain model with two-step memory. In this example, we have only considered non-absorbing states.

All the definitions for the interdependent Markov chain model presented in Section 6.1 are valid for the interleaving framework. The only difference is the assumption of the back-and-forth mechanism for modeling the interdependencies. This assumption only affects the definition of the state space. In other words, in order to keep track of the transition turns we require an auxiliary variable, for instance, a binary variable for two interdependent systems, which increases the size of the state space by two. We have provided an example of the interleaving approach for the

interdependent power and communication infrastructures in the next section.

6.3 An interdependent Markov chain model for cascading failures in electric-cyber infrastructures

In this section, we develop an interdependent Markov chain framework based on the interleaving approach, introduced in Section 6.1, for modeling cascading failures in interdependent power and communication infrastructures. As described in Chapters 1-3, the available historical data and simulation results both suggest that the power system and the communication network are interdependent infrastructures. While such interdependencies can increase the reliability and efficiency of both systems, it can also increase the risk of failures in the individual systems. In this dissertation, we consider the interdependencies that lead to propagation of failures between the two systems. Considering such interdependencies are specifically important in analyzing the reliability of the whole system.

6.3.1 Individual Markov chains

In this section, we refer to the power system by System A and the communication system by System B. We consider the Markov chains represented in Fig. 6.1 and assume that they represent the stochastic dynamics of power and communication infrastructures individually. To simplify the notation, we represent the number of failures in the power grid, i.e., F^A, and in the communication system, i.e., F^B, by the variables x and y, respectively. Further, we denote the probability of transiting to a stable power-grid state in Markov chain A with $p(x)$, i.e., $p(x) = P_{\text{stop}}(x)$,

where $P_{\text{stop}}(x)$ is the cascade-stop probability as a function of number of failures in the system as introduced in Chapter 4. Also, in the Markov chain representing the communication system, we denote the probability of transiting to a state with an extra failure in the communication network by $q(y)$. We wish to reiterate that based on our discussions in Chapter 4, the state-dependent transition probabilities are key in modeling various stochastic behaviors for the system. Thus the state dependent $p(x)$ and $q(y)$ enable us to study various behaviors for the individual systems as well as the whole system.

Without loss of generality, we assume that the first failure occurs in the power grid. We also assume that cascading failures terminate only when no more failures occur in the power grid. Therefore, only the Markov chain representing the power grid has the absorbing states. Moreover, we assume that an extra failure in the communication system may occur only if a failure has occurred in the power grid in the last transition. This means that we assume that the communication system is more reliable than the power grid and that the cascading failure phenomenon grows faster in the power grid. This is a reasonable assumption based the historical data for cascading failures [4]. The above assumptions enable us to simplify the Markov chains in Fig. 6.1 to the ones represented in Fig. 6.3.

Before moving to the next section to build the interdependent Markov chain model, consider the case where we study the interdependent systems by studying their Markov chains individually, while capturing the effects of the interdependencies in the transition probabilities of each of the Markov chains separately. An example of the latter approach is the SASE model presented in Chapter 4. Specifically, this approach can consider a general description of communication system (without its dynamics) and embed the effects of the description (e.g., operating characteristics θ and e) in the transition probabilities of the power system. As another example, we may describe the state of the communication system by "efficient" or "inefficient"

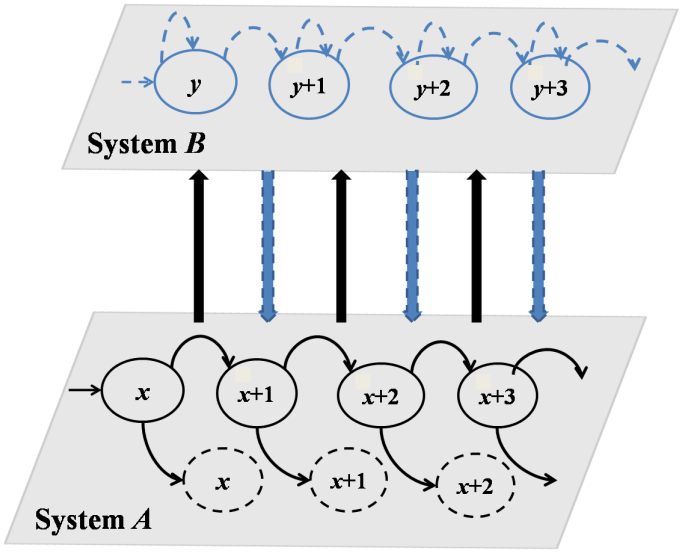

Figure 6.3: The individual Markov chains of the power grid and the communication system and the coupling effect between them in an interdependent electric-cyber infrastructure.

based on certain operating characteristics such as θ and e. Then, we can study the Markov chain of the power grid with transition probabilities determined by the knowledge of efficient or inefficient communication system. This is a special case of the interdependent Markov chain approach, in which one of the Markov chains is maximally compressed to have a state space of size one.

6.3.2 State space of the interdependent Markov chain

Here, we use the interleaving approach for coupling the individual Markov chains representing stochastic dynamics of cascading failures in electric-cyber infrastructures. As discussed in Section 6.1.2, the state space of the interdependent Markov chains should contain the state of both of the systems $\mathcal{S}_A \times \mathcal{S}_B$ as well as the memory of the past transitions. The information from the past transitions enables us to identify if a system is behaving stable or unstable. We assume that when the communica-

tion system becomes less stable by experiencing a new failure then the power-grid becomes vulnerable to extra failures. Also, when the power grid becomes less stable due to a new failure then it may trigger an extra failure in the communication system. The above discussion explains the dynamic behavior of each system in terms of the last transition in the whole system. As such, we need to capture at least the last transition in the system to capture the effect of interdependencies. Therefore, we assume that the minimum memory required to capture the dynamic behavior of the system is two-step memory, i.e., $\mathcal{K} = 2$ (the history consist of the current state plus the previous state of the system). Hence, the state space of the interdependent Markov chain is $\mathcal{S}_I = (\mathcal{S}_A \times \mathcal{S}_B)^2$. However, due to the assumption of a single failure at a time in the system, many states are not allowed to be the previous state for the system. This reduces the size of the state space to $4(\mathcal{N}_A \times \mathcal{N}_B)$, where $\mathcal{N}$ represent the cardinality of the state space. As the interleaving approach suggests, we also need an auxiliary variable to keep track of the transition turns in the system, which will double the size of the state space to $\mathcal{S}_I = 8(\mathcal{N}_A \times \mathcal{N}_B)$. The concept of interleaving Markov chain for the power grid and the communication system is shown in Fig. 6.3 is depicted in Fig. 6.4.

In summary, we define the state of the new interdependent Markov chain at discrete time n by $S_n = (X_n, I_n, Y_n, L_n, M_n)$ where, X_n and I_n are the state variables of the power grid and Y_n is the state of the communication system. We have also introduced two auxiliary variables L_n and M_n in the definition of the states. Here, $L = 0$ and $L = 1$ indicate that the last failure occurred in the power grid and the communication system, respectively. As such the first auxiliary variable L captures the 'transition turn' in the interleaving framework. The variable M_n captures the memory of the dynamics by indicating whether any component failed in the last transition. In other words, the dynamic memory quantization function g introduced in Section 6.1.3 maps the history of dynamics to $\mathcal{H}$ ={new failure, no new failure}.

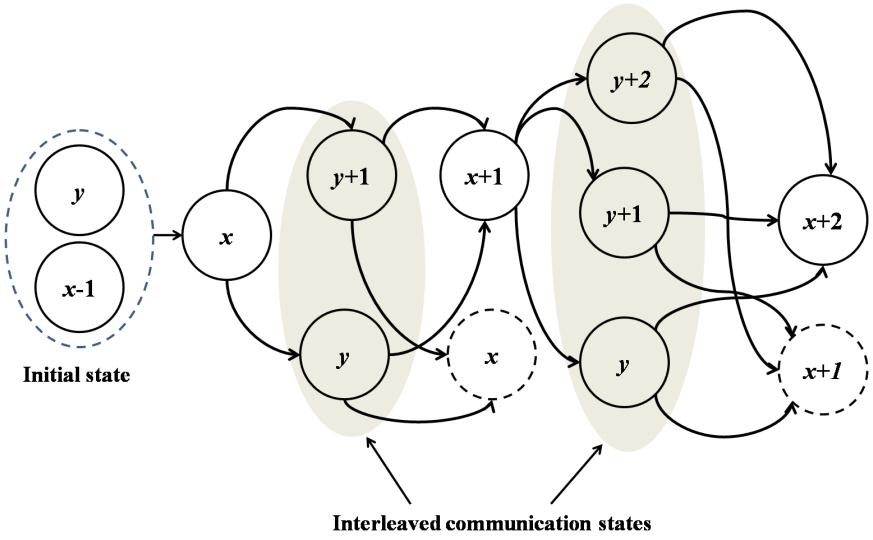

Figure 6.4: The concept of interleaving approach for coupling the Markov chains of the power grid and the communication system in Fig. 6.3 is depicted by interleaving the communication states among power-grid states.

6.3.3 Transition probabilities of the interdependent Markov chain

To characterize the interdependencies between the power and communication systems, we need to define how the behavior of a system affects the behavior of the other system. Here, we characterize the transition probabilities of the interdependent Markov chain based on the transition probabilities of the individual Markov chains and the interdependencies between the two systems. First, we define a function that captures the dependency of the power grid on the communication system. We denote such function by $d : \{0, 1, 2, ..., m_1\} \times \{0, 1, 2, ..., m_2\} \rightarrow [0, 1]$, where m_1 and m_2 denote the number of components in power and communication systems, respectively. If the failure in the communication system does not affect the power grid then $d(.,.) = 1$, and when the failure of communication component results in a failure in the power grid deterministically then $d(.,.) = 0$. The closer the value of $d(.,.)$ to zero the more it reduces the cascade-stop probability of the power grid.

As such d modifies transition probabilities for the power grid based on the dynamics of the communication chain. Further, we assume that transition probabilities of the communication system do not change due to failures in the power grid. However, the interleaving approach explicitly implies that only failures in the power grid can trigger an extra failure in the communication system. Thus, we can assume that failures in the power grid also change the transition probabilities in the communication system. Based on the above assumptions, we define the transition probability from a random state $S_n = (X_n, I_n, Y_n, L_n, M_n)$ to state $S_{n+1} = (X_{n+1}, I_{n+1}, Y_{n+1}, L_{n+1}, M_{n+1})$ at discrete time instance n as follows.

$$f(S_{n+1}|S_n) = \begin{cases} 0 & I_n = 1 \\ 0 & L_{n+1} = L_n \\ q(Y_{n+1}) & I_n = I_{n+1} = 0, \\ & L_n = 0, X_{n+1} = X_n \\ & Y_{n+1} = Y_n + 1, \\ 1 - q(Y_{n+1}) & I_n = I_{n+1} = 0, \\ & L_n = 0, X_{n+1} = X_n \\ & Y_{n+1} = Y_n, \\ 1 - \frac{p(X_n)d(X_n,Y_n)}{M_n + d(X_n,Y_n)(1-M_n)} & I_n = I_{n+1} = 0, \\ & L_n = 1, Y_{n+1} = Y_n, \\ & X_{n+1} = X_n + 1 \\ \frac{p(X_n)d(X_n,Y_n)}{M_n + d(X_n,Y_n)(1-M_n)} & I_n = 0, I_{n+1} = 1 \\ & L_n = 1, Y_{n+1} = Y_n, \\ & X_{n+1} = X_n \\ 0 & \text{otherwise.} \end{cases} \tag{6.5}$$

Based on the above discussion we can calculate the strength of interdependency based on the definition of δ in (6.4) for these two systems as $\delta = \max_{x_n \in \mathcal{S}_A, y_n \in \mathcal{S}_B} p(x_n)d(x_n, y_n)$.

To clarify the interdependent Markov chain model for the power and communication systems, a portion of the Markov chain with transition probabilities among

the states is shown in Fig. 6.5. Although the size of the state-space in this example is in the order of Cartesian product of the individual spaces, which can be large, but we can analyze this Markov chain using difference equations as presented in the next section.

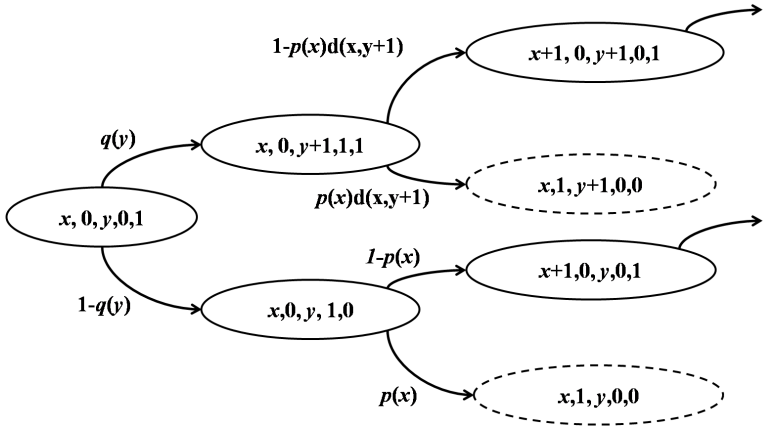

Figure 6.5: Portion of the interdependent Markov chain model for the power and communication system with transition probabilities among the states.

6.3.4 Analysis of the interdependent Markov chain

In this section, we derive a system of difference equations describing stochastic dynamics of the interdependent Markov chain presented for the interdependent power and communication system in Section 6.3. We introduce $\mathcal{P}_{\mathcal{I}}(s)$ as the asymptotic probability of reaching to state $s \in \mathcal{S}_I$ from the initial state $\mathcal{I} \in \mathcal{S}_I$. In our analysis, we are interested in the probability of reaching to stable states in the power grid in which cascading failures terminate (i.e., $\tilde{s} = (x, 1, y, 0, 0)$). We denote $\mathcal{P}_{\mathcal{I}}(\tilde{s})$ by $\mathcal{F}(x, y)$. We also define $\hat{s} = (x, 0, y, 0, 1)$ and denote $\mathcal{P}_{\mathcal{I}}(\hat{s})$ by $\mathcal{G}(x, y)$. In the analysis presented in this section, we assume that function d depends only on the state of the communication system. Based on the structure of the interdependent Markov chain model presented in Section 6.3 and following the steps in Appendix B, we derive a

system of difference equations for $\mathcal{F}(x,y)$ and $\mathcal{G}(x,y)$ as stated in Theorem 6.3.1. Here, we assume that $p(.)$, $q(.)$ and $d(.)$ functions are nonzero at every point to avoid the undefined expressions.

Theorem 6.3.1.

$$\begin{aligned}\mathcal{F}(x,y) &= \alpha_1(x,y)\mathcal{F}(x-1,y) + \alpha_2(x,y)\mathcal{F}(x-1,y-1) \\ &\quad + \alpha_3(x,y)\mathcal{G}(x-1,y-1), \\ \mathcal{G}(x,y) &= \alpha_4(x,y)\mathcal{F}(x-1,y) + \alpha_5(x,y)\mathcal{G}(x-1,y-1).\end{aligned} \tag{6.6}$$

The boundary conditions for this set of difference equations are

$$\begin{aligned}\mathcal{F}(x_0,y_0) &= (1-q(y_0))p(x_0), \\ \mathcal{F}(x_0,y_0+1) &= q(y_0)p(x_0)d(y_0+1), \\ \mathcal{G}(x_0,y_0) &= 1.\end{aligned} \tag{6.7}$$

In addition, $\mathcal{F}(x,y)$ and $\mathcal{G}(x,y)$ are equal to zero for the cases where $x < x_0$ or $y < y_0$. Moreover, $\mathcal{F}(x,y) = 0$ when $y > x$.

The coefficients in (6.6) are given by for the general case:

$$\begin{aligned}
\alpha_1(x,y) &= \frac{p(x)(1-q(y))(1-p(x-1))}{p(x-1)},\\
\alpha_2(x,y) &= \frac{p(x)d(y)q(y-1)(1-p(x-1)d(y-1))}{p(x-1)d(y-1)}\\
\alpha_3(x,y) &= (1-q(y-1))p(x)d(y)q(y-1)\\
&\quad \big((1-p(x-1)) - \frac{(1-p(x-1)d(y-1))}{d(y-1)}\big)\\
&\quad + q(y-1)p(x)(1-q(y))(1-d(y))\\
\alpha_4(x,y) &= \frac{(1-p(x-1))}{p(x-1)},\\
\alpha_5(x,y) &= q(y-1)\big((1-p(x-1)d(y))\\
&\quad - \frac{d(y)p(x-1)(1-p(x-1))}{p(x-1)}\big).
\end{aligned} \tag{6.8}$$

The coefficients are different as following for three special cases:

First–*The case where $y = 1$:*

In this case α_1 and α_4 is same as (6.8) but

$$\begin{aligned}
\alpha_2(x,y) &= \frac{p(x)d(y)q(y-1)(1-p(x-1))}{p(x-1)}\\
\alpha_3(x,y) &= q(y-1)p(x)(1-q(y))(1-d(y))\\
\alpha_5(x,y) &= 0.
\end{aligned} \tag{6.9}$$

Second–*The case where $y = x$:*

In this case all α values are zero except α_2, which is:

$$\alpha_2(x,y) = \frac{d(y)p(x)q(y-1)(1-p(x-1)d(y-1))}{p(x-1)d(y-1)} \tag{6.10}$$

Third–*The case where $y = x - 1$:*

In this case the coefficients are as following:

$$\begin{aligned}
\alpha_1(x,y) &= \frac{p(x)(1-q(y))(1-p(x-1)d(y))}{p(x-1)d(y)},\\
\alpha_2(x,y) &= \frac{p(x)d(y)q(y-1)}{p(x-1)d(y-1)},\\
\alpha_3(x,y) &= (1-q(y-1))d(y)p(x)q(y-1)\times\\
&\qquad \big((1-p(x-1))-\frac{1}{d(y-1)}\big),\\
\alpha_4(x,y) &= \frac{(1-p(x-1))}{p(x-1)},\\
\alpha_5(x,y) &= (1-d(y))q(y-1).
\end{aligned} \tag{6.11}$$

For proof see Appendix B.

The system of difference equations in (6.6) can be solved numerically using the boundary conditions introduced in Theorem 6.3.1 in (6.7). The system of difference equations in (6.6) enables the direct calculation of the probability of different size of failures in each system.

We denote the probability of blackout with x failures in the power grid by $\mathcal{R}_p(x)$, which can be written as

$$\mathcal{R}_p(x) = \sum_{0\leq y\leq x} \mathcal{F}(x,y). \tag{6.12}$$

Further, we denote the probability of y failures in the communication system by $\mathcal{R}_c(y)$ as

$$\mathcal{R}_c = \sum_{y\leq x\leq N_1} \mathcal{F}(x,y). \tag{6.13}$$

The time complexity of the numerical calculations of (6.6) is in the order of the number of components in the system, which makes the model to be scalable to large systems even though the analytical state space of the problem is large.

This model enables the identification of different stochastic behaviors for the system based on various state dependent transition probabilities for each system as well as the introduced interdependency function.

6.4 Numerical results

In this section, we present the numerical results about the distribution of the failure size in the interdependent power and communication systems based on the numerical solutions of the system of difference equations in (6.6). We term a system, whose distribution of the blackout size follows an exponential distribution, a *reliable* system as the probability of large blackouts is small compared to the heavy-tail distribution. We also term a system, whose distribution of the blackout size follows a heavy-tail distribution, such as the power-law distribution, an *unreliable* system. Using the numerical results, we show that the interdependency between two systems can introduce vulnerabilities in the whole system and increase the probability of large blackouts. We specifically show that the interdependencies between two individually reliable systems may lead to an unreliable coupled system.

6.4.1 Impact of interdependency on the distribution of the blackout size

Here, we consider the IEEE 118 bus system for the power grid, which has 186 transmission lines. Without loss of generality, we assume that there are equal number of components in the communication system, i.e., 186 communication components. As described earlier in Chapter 4 when a Markov chain model (whose distribution described by the difference equations in (4.18)), has constant (i.e., state independent) transition probabilities then the blackout size distribution is exponential. We

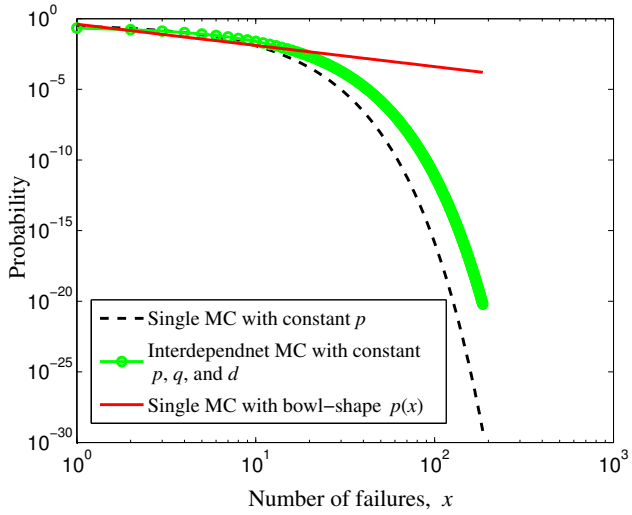

Figure 6.6: Probability mass function of the failure size in the power-grid in a log-log scale for a reliable power system with exponential blackout distribution (the dashed line), an unreliable power grid with power-law distribution (solid line) and an interdependent Markov chain with constant p, q, and d in (a doted line).

also asserted that the bowl-shape function for the cascade-stop probability for the Markov chain lead to a heavy-tail distribution for the blackout size. In particular, special forms of the bowl-shape function for P_{stop} result in a power-law distribution of the blackout size. The results presented in Fig. 6.6 represent the scenarios discusses above. In summary, in Fig. 6.6, we have presented the PMF of the failure size for a reliable power system with constant P_{stop} and exponential blackout distribution (the dashed line), an unreliable power grid with bowl-shape form for P_{stop} and power-law distribution of the failure size (solid line), and an interdependent Markov chain with constant p, q and d in with exponential distribution for the failure size (a doted line).

Next, we assume that the Markov chain for the power grid has the specific bowl-shape form for P_{stop}, that results in the power-law distribution for the blackout size. This distribution is shown by solid line in a log-log scale in Fig. 6.7. Next, we use the interdependent Markov chain model presented in Section 6.3 for the power and communication systems to study how the interdependency between the two systems

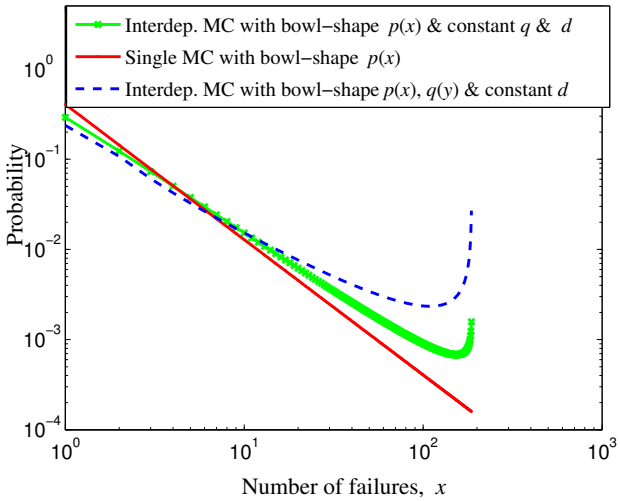

Figure 6.7: Probability mass function of the failure size in the power-grid in a log-log scale for various scenarios of $p(x)$, $q(y)$, and $d(y)$. The results are obtained based on the interdependent Markov chain model and using (6.12) and (6.6).

affects the distribution of the blackout size in the power grid. The distribution of the blackout size in the power grid, $\mathcal{R}_p$ is calculated using (6.12) and (6.6). As the first example, we couple the Markov chain of the power grid with a Markov chain for the communication system, which has constant transition probabilities. This means that we have a reliable communication system. The results shown in the doted line in Fig. 6.7 suggest that the interdependencies between the two systems increase the probability of large blackouts and also preserve the heavy tail characteristic except at the end. In other words, the blackout distribution for the power-grid $\mathcal{R}_p$ in this case also follows the power-law distribution, but with a smaller parameter s. This means that the probability of large blackouts increases as a result of the interdependency between the two systems. The sharp increase at the end of the distribution represents the critical behavior of the system, which increases the probability of larger blackouts even more that other values. As the next example, we couple the Markov chain of the power grid with a Markov chain for the communication system, which has the bowl-shape function for the probability of no extra communication failures due to

power-grid failures, i.e., $(1-q(y))$. The effect of an unreliable communication system is more severe on the reliability of the system as is shown in a dashed line in Fig. 6.7. In both of the interdependent examples presented here, the function d is assumed to be constant and equal to 0.4.

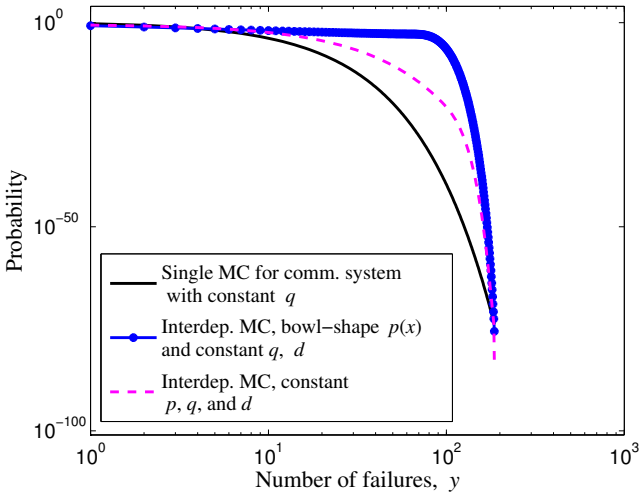

Figure 6.8: Probability mass function of the failure size in the communication system in a log-log scale for various scenarios of $p(x)$, $q(y)$, and $d(y)$. The results are obtained based on the interdependent Markov chain model and using (6.13) and (6.6).

The distribution of the failure size in the communication system $\mathcal{R}_c$, is calculated using (6.13) and (6.6) and is presented in Fig. 6.8. In Fig. 6.8, we have presented the distribution of failures in the communication system for various scenarios of interdependencies with different $p(x)$ and $q(y)$. In these scenarios, the function d is assumed to be constant and equal to 0.4. Similarly to the results in Fig. 6.7, the results in Fig. 6.8 also suggest that the interdependencies increase the probability of large failures. Specifically, when one of the systems are unreliable.

Figure 6.9 shows $\mathcal{R}_p$ when P_{stop} for the power grid follows the bowl-shape obtained from the simulation results presented in Fig. 4.6. As discussed in Chapter 4, this bowl-shape function for P_{stop} results in another heavy-tail distribution with a hump near the tail of the distribution for the blackout size as shown in Fig. 6.9. The results

presented in Fig. 6.9 indicate that the interdependencies between the communication system and the power grid with constant q and d parameters increase the size of the hump.

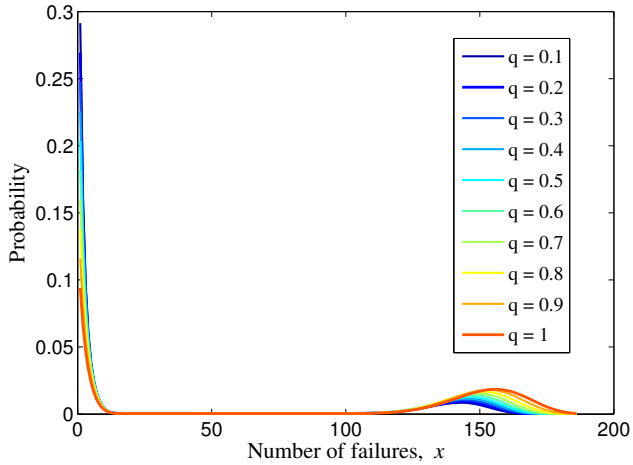

Figure 6.9: Probability mass function of the failure size in the power grid when P_{stop} has the bowl-shape form obtained from power-system simulations. The interdependencies between the power and communication system increase the size of the hump.

6.4.2 Individually reliable systems can behave unreliably when coupled

In the next study, we assume that we have two reliable systems with constant $p(x)$ and $q(y)$. We couple the two reliable systems using the interdependent Markov chain framework. In this study, we want to answer the following critical question: can two coupled reliable systems form a single unreliable system? To answer this question, we use the system of difference equations in (6.6) and assume that p and q are constant. We want to find function $d(y)$ such that the two reliable power and communication systems, result in the power-law distribution for the blackout size. To find such $d(y)$, we input the probability of the blackout size in the power grid

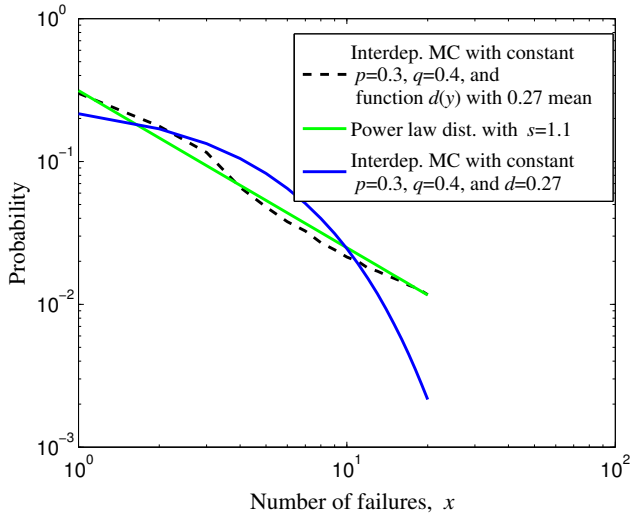

Figure 6.10: Probability mass function of the failure size in the power grid in an interdependent Markov chain model, when two reliable systems are coupled with interdependencies that lead to unreliable behavior.

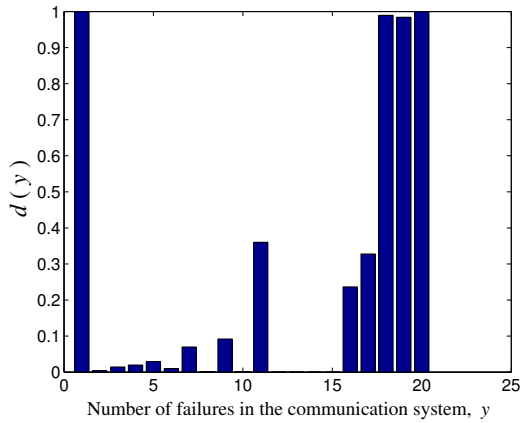

Figure 6.11: The $d(y)$ values that result in an unreliable behavior (power-law distribution) for the two coupled reliable systems.

in (6.12) based on the power-law distribution introduced in (4.19), i.e., $\mathcal{R}_p(x) = P(x, 1.1, m_1)$ introduced in (4.19). This implies that we have a system of m_1 non-linear equations for $d(y)$. We have solved this system of non-linear equations using an optimization approach, which minimizes the distance between $\mathcal{R}_p(x)$ and the

blackout size resulted from the system of difference equations, with the constraint $0 \leq d(\cdot) \leq 1$. In Fig. 6.10, we have shown the result of the distribution of the blackout size in a system with 20 components when the individual systems are reliable but the distribution of the failure size in the coupled power grid (dashed line) approximates the power-law distribution. We have also represented the distribution of the failure size when function d is constant (i.e., state independent) in the dark solid line, which results in exponential distribution. The $d(y)$ values that result in unreliable behavior for the two reliable systems is presented in Fig. 6.11. The results in Fig. 6.11 suggest the d values, which result in the power-law distribution also exhibit the three phase phenomenon observed in cascading failures, as described in Chapter 4. At the beginning, one failure in the communication system does not alter the cascade-stop probability but as the number of failures in the communication system increases their impact on the cascade-stop probability increases and thus d becomes smaller. The values of d rise again as the number of failures increases in the communication system as well as the power grid and cascading failures phase out. Using the results in Fig. 6.10, we showed that two individually reliable systems may behave unreliably when coupled as a result of interdependency between the individual systems. This important result confirms the importance of considering the interdependent systems as a single system for reliability analysis.

6.5 Summary and conclusions

In this chapter, we presented a novel interdependent Markov chain framework for modeling cascading failures in interdependent infrastructures. In this framework, we start from individual Markov chains that approximate the stochastic dynamics of each of the physical systems and developed a minimal Markov chain that encompasses the individual chains and approximates the stochastic dynamics of the entire

collection of systems as a single system while capturing the interdependencies among the systems. We presented the interdependent Markov chain framework in a general setting and then, as a specific example, derived an interdependent Markov chain model for cascading failures in electric-cyber infrastructures. We studied various scenarios of reliable and unreliable systems to characterize the distribution of the failure size in coupled systems. A key insight obtained from the interdependent Markov-chain model is that interdependencies between two systems can make two reliable systems behave unreliably when put together. For instance, we specifically showed that certain interactions among the systems can result in the power-law distribution for the size of failures in the coupled system when the two individual systems have exponential distributions for the failure size.

There are a wide range of interesting problems that can be studied based on the interdependent Markov chain framework. Examples of such problems are the analytical characterization of asymptotics of the interdependent Markov chain based on asymptotics of the individual chains and analytical characterization of the interdependencies that lead to critical behaviors. The problems addressed in this chapter are the ones that are relevant to the interdependent power and communication systems. Further analysis of the interdependent Markov chains and other examples are extensions of this work and are out of scope of this dissertation.

Chapter 7

Fundamental bounds on the information rate in information-centric power grids

In this chapter, we look at another aspect of smart grids, namely the information exchange in the communication system of the power grid, which enables efficient monitoring and control of the power grid. We develop an information-theoretic framework for characterization of the exchange of information in the sensor network that enables the monitoring of the power grid. Control rooms of power grids rely heavily on accurate estimate of the state of the system. As such, large number of sensors are employed in the power systems. The sensors collect samples of the state of power-system components with high frequency. Nonetheless, exchange of such state information from large number of sensors incurs a large communication cost on the communication network of the power grid. The framework presented in this chapter enables the characterization of the minimum required communication capacity for the sensor network in smart grids by compressing the data by exploiting the correlation among the data sources. In other words, the presented framework

captures the interplay between the information rate and the correlation among the state information of various components in the system.

In this chapter, we consider the sensor network that enables accurate state estimation of the power grid for monitoring and control purposes. In particular, we assume that sensors are located on transmission lines and measure the temperature and the power flow of the lines and update these information to the control center of the system. Note that this is a specific example of the application of sensors in power grids. Sensors can be employed to measure a wide range of attributes such as voltage, frequency and phase at different points of the system. In this chapter, *we characterize the minimum information rate that the sensors need to update their information to the control center in order to track the thermal state of the components accurately.* In other words, this study characterizes the minimum required communication capacity for this specific application of sensor networks in power grids.

The presented framework in this chapter is based on a lossless distributed source-coding framework. While distributed source coding theory has been widely used in sensor networks in the last decade, its utility has been limited to the context of distributed sensing, which the signal of the interest is an environmental signal that is independent of the system attributes [86]. Although tracking the state of components in a system can be viewed as a distributed-sensing problem, the signal of interest here is tied to the system characteristics, for example, power-flow distribution and customer demands in the power grid. For instance, the temperature of the lines is correlated with the power flow through the lines controlled and monitored by the control center. In other words, the temperature of the lines depends on the power distribution mechanism in the system and vice versa. In addition, the information about the power-flow through the line is available both at the line and the control center.

Here, the distributed source coding model may warrant extension or modifications

to capture the information characteristics and their availability in various parts of the system. In this research, we use the generality of distributed source coding theory to characterize the minimum information rate required by the sensor nodes communicating over the communication network to support accurate and real time state information of transmission lines by exploiting the correlation among state information of various lines. The model presented in this chapter provides a general framework for characterization of the minimum required information rate in sensors networks that sense correlated signals for which certain side information is available at the source and the destination of the information exchange. In particular, we have also applied this framework in the context of sensor networks with distributed sensing and computing purposes [87].

7.1 Related work

Recently, information theory has been adopted for characterizing the control overhead (rate of information exchange for monitoring and control purposes) in distributed systems. The pioneering work presented by Gallager [88] is one of the earliest contributions that used information theory in characterizing the network overhead for tracking source and receiver addresses. In [89] and [90] the minimum overhead of maintaining state information (link state and motion state, respectively) to be used in routing protocols across a mobile ad hoc network is formulated as a rate-distortion problem. The assumption in [89] and [90] is that the state information associated with various nodes/links are mutually independent; hence, the rate-distortion formulation is considered for a single component. The authors of [91] use rate-distortion theory to investigate the optimal timing for updating the bandwidth information of the links. In [92], the relation between network performance and information rate is captured by extending the definition of distortion measure to

capture network performance. All the models that are based on the rate distortion theory are based on the assumption that certain amount of error in the estimation of the state of components is acceptable.

All the aforementioned works consider point-to-point information theory in characterizing the interplay between the rate of information and distortion. Network information theory [93], on the other hand, provides a strong tool for characterizing the information exchange in a distributed fashion when there is correlation among the state information of different sources. As mentioned in the previous section, distributed source coding theory [86] has been widely used in sensor networks in the last decade but its application has been limited to standard distributed sensing problem. To the best of our knowledge, distributed source coding theory has not been employed in studying the information rate in distributed systems for control purposes, which the signal to be sensed is tied to the system attributes and the side information is available at different points of the system.

7.2 Sensor model

Recall that we assume sensors collect information about the thermal state of power-system transmission lines and update the information to the control center. We assume that sensors form clusters consisting of a cluster head (CH) and a set of geographically adjacent sensors. The sensors of each cluster update their temperature data to CH. We further assume that the clusters communicate together and to the control center over a communication network with lossless channels. We refer to the sensor nodes located on transmission lines simply by the nodes.

Here, the problem of investigating the information rate of the sensor network is broken down to the same problem for individual clusters of sensor nodes. Hence, we will focus on one cluster hereafter with the understanding that the same procedure

will be applied to all clusters of the sensor network.

We represent the n samples of the changes in the temperature of the transmission lines by $X_i^n = (X_{i1}, X_{i2}, \ldots, X_{in})$. The reason to consider the changes in the temperature of transmission lines is to have independent samples in time. The changes in the temperature of a transmission line is a function of the power flow through the line and the environmental factors. If we assume that power flow changes due to random changes in the customer demands and also environmental factors are random and independent in time then the samples of temperature changes will be independent in time. However, the X_{ij} values are correlated among different sensor nodes of a cluster both due to the geographical proximity (the same environmental effects) and correlation in the power flow data due to local changes in the customer demand and the physics of the power flow in a region. We can write the dynamics of line temperature changes as $X_i = Y_i + T_i$ where, Y_i is the random thermal change due to the power flow through the line and the T_i is the random thermal change due to the environmental factors that affect the temperature. Thus dynamics of the temperature of a line is governed by the random variables associated with the environmental factors and the power flow in the line.

We assume that sensors sample the state of the components at discrete time instants called *sampling instant*. We further assume that at the *update instant* sensor nodes send the state information to CH. We call the interval between two consecutive update instants an *update interval*. We further assume that an update interval consists of n sampling instants. Besides the temperature of the lines, we assume that the power flow through the line is also measured at the n sampling instances. The information about the power-flow through the line is also available at the control center of the system. In the next section, based on the introduced assumptions we develop a distributed source coding framework for exchanging information in which the information about the power flow through the lines serves as the side information.

7.3 Distributed source coding model

Assume that at each update instant node i uses its encoder to encode the samples of the states i.e., $X_i^n = (X_{i1}, X_{i2}, ..., X_{in})$ separately from other nodes and then sends it to the CH. We call the information about the power flow, Y_is, the *side information*. We assume that the statistical characteristics of X_i and Y_i are available. The CH uses its decoder to decode and reconstruct the state of nodes using the correlation among X_is and the side information Y_is. Specifically, the reconstructed state of node i is denoted by $\hat{X}_i^n = (\hat{X}_{i1}, \hat{X}_{i2}, \ldots, \hat{X}_{in})$ and the probability of error is $P_e^{(n)} \triangleq \mathsf{P}\big\{(\hat{X}_1^n, \ldots, \hat{X}_N^n) \neq (X_1^n, \ldots, X_N^n)\big\}$. Figure 7.1-a illustrates this formulation schematically for a cluster with N nodes. Our formulation is an extension of Slepian-Wolf Theorem [94] to distributed lossless source coding with multiple side information.

An N-tuple $(R_1, \ldots, R_N)$ is said to be *achievable* for distributed lossless source coding if there exists a sequence of codes with these rates such that $\lim_{n\to\infty} P_e^{(n)} = 0$.

For the ease of reference and discussion of the theory, we define:

Formulation 1. A distributed source coding problem that does not use Y_is and nor does it use the correlation among X_is. This formulation is equivalent to N separate Shannon's lossless source coding problems.

Formulation 2. A distributed source coding problem that uses Y_is but it does not use the correlation among X_is. This formulation is equivalent to N conditional lossless source coding problems (single source coding problem with side information at the encoder and the decoder [93]).

Formulation 3. A distributed source coding problem that uses the correlation among X_is but it does not use Y_is. This formulation is a Slepian-Wolf problem.

Formulation 4. A distributed source coding problem that uses both Y_is and the

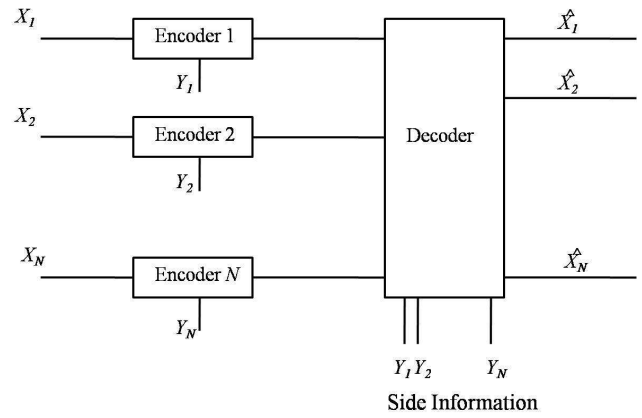

(a)

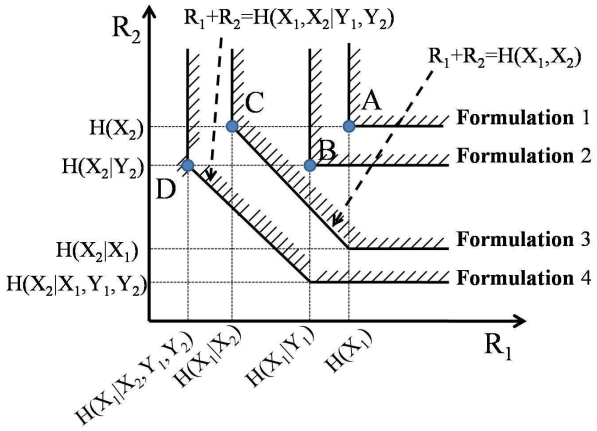

(b)

Figure 7.1: (a) The proposed distributed source coding model with side information to characterize the information rate in the sensor network of a power grid. (b) The achievable rate region of the four formulations.

correlation among X_is. This is our formulation in this research.

Note that Formulations 1 and 2 fall in the area of point-to-point information theory.

7.4 Characterizing the rate region

We begin the characterization of the rate region of Formulation 4 by considering the distributed source coding model for a cluster with two nodes. The achievable rate region of the formulations mentioned in the last section has been depicted in Fig. 7.1-b. Note that in Fig. 7.1-b, we have shown the rate region of Formulations 2 and 3 in the special case when $H(X_1|X_2) < H(X_1|Y_1)$ and $H(X_2|X_1) < H(X_2|Y_2)$, where $H(.|.)$ represents the conditional entropy. Characterization of the achievable rate region of Formulation 3 has been presented by Slepian and Wolf in [94]. The achievable rate region of Formulation 2 is also known [93].

Characterizing the achievable rate region of the Formulation 4 is straight forward and can be explained as follows. Consider a special case in which there is only one encoder that jointly encodes the state information of the two nodes while the CH decodes the code for both sources using side information. In this case the outer bound of the *sum-rate*, defined as $R_1 + R_2$, for Formulation 4 can be written as $R_1 + R_2 \geq H(X_1, X_2|Y_1, Y_2)$. In general, however, this bound may not be achievable since nodes are encoding the sources separately (this is why it is termed outer bound). Now consider the case when nodes encode the sources separately while each node having access to the other node's state information. In this case, the rate of a node should satisfy $R_1 \geq H(X_1|X_2, Y_1, Y_2)$ based on Formulation 2. Combining these bounds results in the outer bound for the optimal rate region of Formulation 4, which can easily be shown to be achievable and tight (with a proof similar to that of the Slepian Wolf Theorem [95]) and therefore improves the lower bound on the minimum information rates. Based on the above discussions, we present the rate region of this framework for two nodes in Theorem 7.4.1 and for the general N nodes in Theorem 7.4.2.

Theorem 7.4.1. *The optimal rate region for Formulation 4 with two nodes is*

$$\begin{aligned} R_1 &\geq H(X_1|X_2, Y_1, Y_2), \\ R_2 &\geq H(X_2|X_1, Y_1, Y_2) \text{ and} \\ R_1 + R_2 &\geq H(X_1, X_2|Y_1, Y_2). \end{aligned} \tag{7.1}$$

For proof see Appendix C. Theorem 7.4.1 can be extended to an arbitrary number of nodes in the cluster as follows.

Theorem 7.4.2. *Let $\mathcal{S} \subset \{1, 2, ..., N\}$. The optimal rate region for the problem in Formulation 4 with N nodes is*

$$\sum_{j \in \mathcal{S}} R_j \geq H\big(X(\mathcal{S})|X(\mathcal{S}^c), Y(\mathcal{S} \cup \mathcal{S}^c))\big),$$

where $\mathcal{S}^c$ represents the complement of the set $\mathcal{S}$ and $X(\mathcal{S})$ is the set of X_is for $i \in S$ and $X(\mathcal{S}^c)$ and $Y(\mathcal{S} \cup \mathcal{S}^c)$ are defined likewise.

We omit the proof of Theorem 7.4.2 since it is similar to that of Theorem 7.4.1.

Note that in this special case of the distributed source coding problem the rate region of the framework depicted in Fig. 7.1-a would be the same as the one stated by Theorems 7.4.1 and 7.4.2 even if the side information Y_is were only available at the decoder. However, in lossy distributed source-coding problems these two cases would result in different rate regions. The next point to note here is that the lower bounds derived based on these approaches, are asymptotically achievable (as the number of samples in an update interval goes to infinity, i.e., $n \to \infty$); hence, they provide bounds on the information rate of the sensor network [89–92].

7.5 Numerical evaluation

Theorems 7.4.1 and 7.4.2 provide analytical expressions of the lower bound for the minimum state information rate of nodes in a cluster. In this section, we consider a specific example of a sensor network and provide the numerical results calculated for the minimum information rate of the state estimation. For simplicity, we consider a cluster with two nodes.

We discussed that the Y_is of different lines may be correlated due to the physics of the power flow and customer demands. To model the dependency between Y_1 and Y_2 in our example we simply use $Y_1 = Y_2 + \Delta Y$. In this model ΔY affects the correlation between Y_1 and Y_2 (and consequently the correlation between X_1 and X_2). In a similar way, the correlation between T_is can be modeled by $T_1 = T_2 + \Delta T$. Note that the correlation among T_is also affect the correlation among X_is. In our example, we assume independent Poisson distributions for random variables with random-variable-specific Poisson parameters.

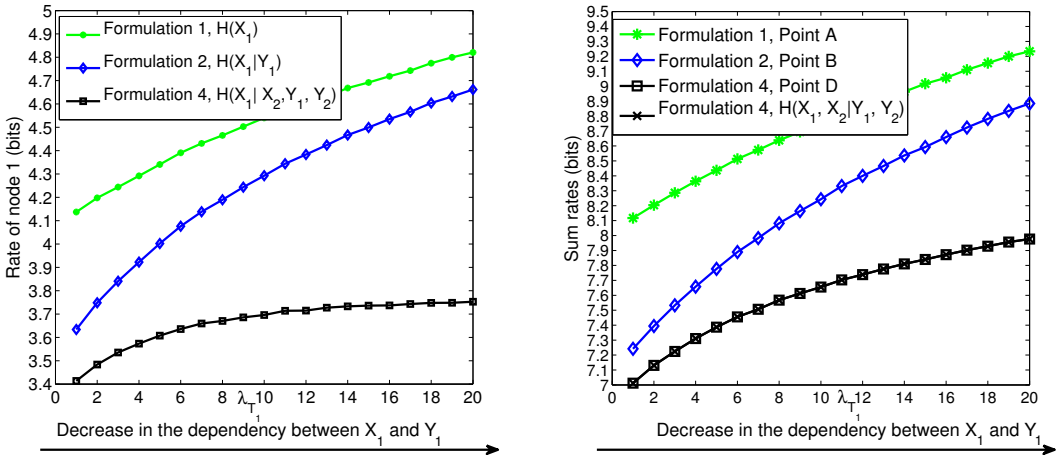

(a) (b)

Figure 7.2: (a) State information rate of node 1, and (b) total control overhead (sum of the rates of nodes) as a function of the dependency between X_1 and Y_1.

In our calculations, we have assumed $\lambda_{Y_2} = 4$, $\lambda_{T_2} = 3$, and $\lambda_{\Delta L} = \lambda_{\Delta T} = 1$. Since all the random variables have Poisson distributions, we can numerically calculate the entropy, joint entropy and conditional entropy for different combination of the presented random variables.

Figure 7.2-a depicts the minimum state-information rate of node 1 as a function of λ_{T_1}, for Formulations 1, 2, and 4 calculated at points A, B, and D shown in Fig. 7.1-b, respectively. In our calculations, we have only changed λ_{T_1}. From Fig. 7.2-a, we observe that as the dependency between X_1 and Y_1 decreases the rate of node 1 increases. The sum of the rates of nodes (total control overhead) for the formulations are calculated based on the sum-rate constraint in Theorem 4.1 and shown in Fig. 7.2-b. Figure 7.2-b also shows that the sum of the pair of rates shown in Fig. 7.2-a equals to the sum-rate constraint value calculated based on Theorem 4.1. This is due to the special position of the selected pair of rates (in Fig. 7.1-b).

We next investigate the effect of correlation between X_1 and X_2 on the control overhead. To see this effect in our example, we changed $\lambda_{\Delta Y}$ and $\lambda_{\Delta T}$ (we assume $\lambda_{\Delta Y} = \lambda_{\Delta T}$). The minimum state-information rate of node 1 for Formulation 3 (calculated at point C in Fig. 7.1-b) and Formulation 4 are represented in Fig. 7.3-a. The minimum total control overhead for Formulation 3 and 4 are shown in Fig. 7.3-b. Notably Formulation 4 provides the smallest lower bound among other formulations for the minimum information rate of the nodes.

7.6 Summary and conclusions

In this chapter, we developed an information-theoretic framework for characterization of the minimum rate of information for the sensor network that enables the monitoring of the power grid. This framework is based on distributed source coding model that enables the characterization of the minimum rate of information exchange

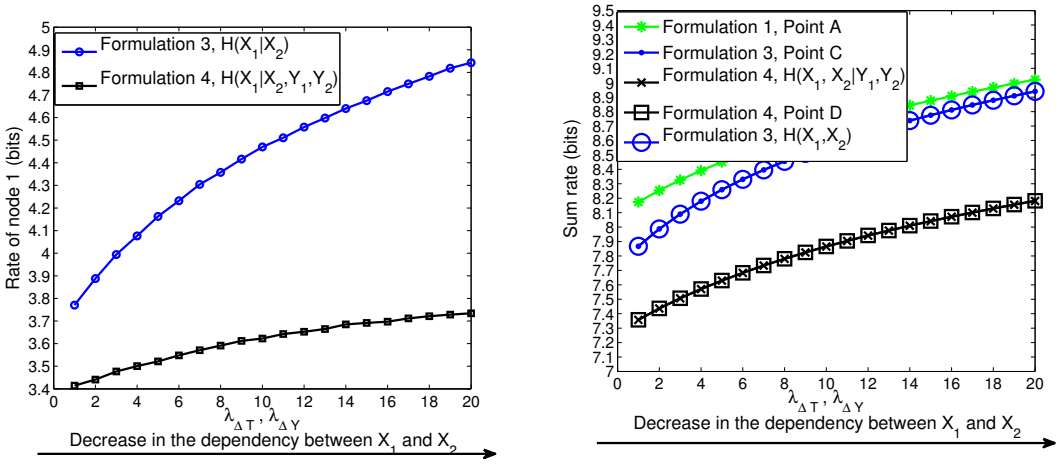

Figure 7.3: (a) State information rate of node 1, and (b) total control overhead (sum of the rates of nodes) as a function of the dependency between X_1 and X_2.

(minimum required capacity) in the communication network. The framework captures the interplay between the information rate and the correlation among the state information of various components. Moreover, using the proposed framework we presented an improved estimate of the lower bound for the minimum information rate necessary to accurately describe the state of components in the system. This improvement is achieved by exploiting the correlation among the state information of components as well as the available side information in the system. The model presented in this chapter provides a general framework for characterization of the minimum required information rate in sensors networks, that sense signals for which certain side information is available at the source and the destination of the information exchange.

Chapter 8

Future work

Understanding complex cascading phenomena in critical infrastructures is crucial in designing cascade-aware control mechanisms to ensure the resilience of infrastructures to large failures. The probabilistic frameworks presented in this dissertation for modeling cascading failures in power grids and interdependent infrastructures provide critical insight about the risk of blackouts and the factors affecting such risk. These probabilistic models can provide predictive capabilities to infrastructure operators to examine and analyze the risk of cascading failures as well as the critical system settings that may severely affect the risk of large failures. In this dissertation, we tackled multiple challenging problems regarding modeling, predicting and analyzing the risk of cascading failures and a number of interesting problems remain for future work. In this chapter, we present an overview of future research problem in this area.

Our simulation results presented in this dissertation suggest that the topological and spatial distribution of failures affect cascading failures. Understanding how failures propagate in infrastructures and how the spatial distribution of failures and the structure of the infrastructure affect the risk of failures is a future research problem.

Capturing the effects of the distribution of failures and the structure of the system in stochastic dynamics of cascading failures is also an extension of the work presented here. Our research group at the University of New Mexico is currently working on this problem. Also, we described that based on historical data human error plays a key role in the cascading behavior of the system. Capturing the effects of human error in characterization of the risk of large blackouts is another future work. Our research group at the University of New Mexico in collaborations with Fraunhofer USA Center for Sustainable Energy Systems is currently working on this problem as an extension of the work presented in this dissertation. In general, there are a large number of key factors in operating critical infrastructures that affect cascading failures. For instance, the available resources and use of microgrids in the distribution network of power grids can largely affect the cascading behavior in smart grids of the future by helping the system in mitigating the effects of contingencies. Although the stochastic nature of the introduced models in this dissertation enables capturing the effects of factors affecting cascading failures indirectly into the predictions of the risk of large failures, embedding such information directly in the model can improve the predictive capability of the model.

In addition, a key outcome of the presented probabilistic models in this dissertation is a roadmap for the identification of critical sub-regions of the parameter space of the system, corresponding to various severity levels of cascading behavior. Theoretical characterization of such critical regions allow for separation of the cascading behavior from non-cascading behavior in critical infrastructures. For instance, in this dissertation, we identified the bowl-shape function for the probability that cascading failures terminate, which leads to heavy tail in the distribution of the failure size. Studying the conditions that lead to high probability of failures in complex systems such as critical infrastructures using analytical approaches is another area of future work.

Further, as a future work, the theory developed in this dissertation, specifically the interdependent Markov chain model, can be extended for modeling cascading failures in other complex interdependent systems. Also, further analysis of the asymptotics of the interdependent Markov chain based on asymptotics of the individual chains and analytical characterization of the interdependencies that lead to critical behaviors are interesting problems to be investigated. Specifically, the interdependent Markov chain framework can be used to analytically characterize conditions that individually reliable systems may behave unreliably due to interdependencies with other systems. Additionally, as a future work, the introduced regeneration-based framework for modeling cascading failures can be used to derive the dynamics of complex systems with non-Markovian characteristics.

The information-theoretic model presented in this dissertation for characterizing the minimum information rate in sensor networks provides a general framework. It can be customized for various applications in which the rate of information exchange needs to be characterized in scenarios with correlated sources of information and available side information that are tied to the performance metrics of the system. Furthermore, this general framework can be extended using distributed lossy source coding framework to appropriate cases in which certain amount of error in the data to be tracked is acceptable.

Appendices

Appendix A

Derivation of equation (4.5)

We start by defining the following events: (1) E_{stop}, which is the event that cascade-stop transition occurs, (2) E_{F_i}, which is the event that the power grid has F_i failures, and (3) $E_{C_i^{\max}}$, which is the event that the maximum capacity of the failed lines in the power grid is $C_i^{\max}$. Note that $P_{\text{stop}}(S_i)$ is the conditional probability $\mathsf{P}\{E_{\text{stop}}|E_{F_i} \cap E_{C_i^{\max}}\}$. Next, we use the simple approach used in [82], in conjunction with certain reasonable assumptions to approximately represent $\mathsf{P}\{E_{\text{stop}}|E_{F_i} \cap E_{C_i^{\max}}\}$ in terms of a weighted superposition of $\mathsf{P}\{E_{\text{stop}}|E_{F_i}\}$ and $\mathsf{P}\{E_{\text{stop}}|E_{C_i^{\max}}\}$. We begin by noting that multiple application of Bayes rule yields

$$\mathsf{P}\{E_{\text{stop}}|E_{F_i} \cap E_{C_i^{\max}}\}=\frac{\mathsf{P}\{E_{\text{stop}} \cap E_{F_i}\}\mathsf{P}\{E_{C_i^{\max}}|E_{\text{stop}} \cap E_{F_i}\}}{\mathsf{P}\{E_{F_i} \cap E_{C_i^{\max}}\}}. \tag{A.1}$$

Using the representation in (A.1) we can write

$$\mathsf{P}\{E_{\text{stop}}|E_{F_i} \cap E_{C_i^{\max}}\} = \mathsf{P}\{E_{\text{stop}}|E_{F_i}\}\frac{\mathsf{P}\{E_{C_i^{\max}}|E_{\text{stop}} \cap E_{F_i}\}}{\mathsf{P}\{E_{C_i^{\max}}|E_{F_i})}. \tag{A.2}$$

With a similar approach, we can also write

$$\mathsf{P}\{E_{\text{stop}}|E_{F_i} \cap E_{C_i^{\max}}\} = \mathsf{P}\{E_{\text{stop}}|E_{C_i^{\max}}\}\frac{\mathsf{P}\{E_{F_i}|E_{\text{stop}} \cap E_{C_i^{\max}}\}}{P(E_{F_i}|E_{C_i^{\max}}\}}. \tag{A.3}$$

Appendix A. Derivation of equation (4.5)

Now using (A.2) and (A.3), we can write

$$\mathsf{P}\{E_{\text{stop}}|E_{F_i} \cap E_{C_i^{\max}}\} = w\mathsf{P}\{E_{\text{stop}}|E_{F_i}\}\frac{\mathsf{P}\{E_{C_i^{\max}}|E_{\text{stop}} \cap E_{F_i}\}}{\mathsf{P}\{E_{C_i^{\max}}|E_{F_i}\}} + (1-w)\mathsf{P}\{E_{\text{stop}}|E_{C_i^{\max}}\}\frac{\mathsf{P}\{E_{F_i}|E_{\text{stop}} \cap E_{C_i^{\max}}\}}{P(E_{F_i}|E_{C_i^{\max}}\}}, \tag{A.4}$$

where $w \in [0,1]$. In this dissertation, $\mathsf{P}\{E_{\text{stop}}|E_{F_i}\}$ and $\mathsf{P}\{E_{\text{stop}}|E_{C_i^{\max}}\}$ are denoted by $P^{(1)}_{\text{stop}}(F_i)$ and $P^{(2)}_{\text{stop}}(C_i^{\max})$, respectively.

Next, we assume that the dependence of the event $E_{C_i^{\max}}$ on the event E_{stop} is weaker than the dependence of the event $E_{C_i^{\max}}$ on the event E_{F_i}, which implies that $\mathsf{P}\{E_{C_i^{\max}}|E_{\text{stop}} \cap E_{F_i}\} \approx \mathsf{P}\{E_{C_i^{\max}}|E_{F_i}\}$. This simplifying assumption can be justified from the physical characteristics of power grids. Based on our simulation results, we know that given that F_i is large, there is a high probability that $C_i^{\max}$ is also large; on the other hand, when F_i is small then the probability of having large $C_i^{\max}$ is small. For example, when F_i is large the probability of high capacity line failures increases due to high stress on the system and the large ratio of the number of high capacity lines to the total number of lines in the system. Therefore, although the knowledge of event E_{stop} adds information about the occurrence of the event $E_{C_i^{\max}}$ we assume that it does not significantly alter the probability distribution of the event $E_{C_i^{\max}}$ given E_{F_i}. Similarly to the previous assumption, we assume that the dependence of the event E_{F_i} on the event E_{stop} is weaker than the dependence of the event E_{F_i} on the event $E_{C_i^{\max}}$. Hence, when $C_i^{\max}$ is small then the probability of F_i being large is small and E_{stop} does not alter this probability significantly. These assumptions enable us to approximate (A.4) by (4.5).

Appendix B

Proof of Theorem 6.3.1

For simplicity of notation, we denote the asymptotic probability of reaching a state, say $s = (x, i, y, m, \ell)$, from the initial state $\mathcal{I}$ by $\mathcal{P}(x, i, y, m, \ell)$.

Based on the structure of the interdependent Markov chain model introduced in Section 6.3, which is partially shown in Fig. 6.5, as well as the transition probabilities introduced in (6.5), we write $\mathcal{P}(x, 1, y, 0, 0)$ based on the asymptotic probabilities of reaching to its previous states as

$$\begin{aligned}
&\mathcal{P}(x,1,y,0,0) = p(x)\mathcal{P}_{\mathcal{I}}(x,0,y,1,0) + p(x)d(y)\mathcal{P}(x,0,y,1,1),\\
&= p(x)(1-q(y))\mathcal{P}(x,0,y,0,1) + p(x)d(y)q(y)\mathcal{P}(x,0,y-1,0,1)\\
&= p(x)(1-q(y))\Big((1-p(x-1))\mathcal{P}(x-1,0,y,1,0)\\
&+ (1-p(x-1)d(y)\mathcal{P}(x-1,0,y,1,1))\Big)\\
&+ p(x)d(y)q(y)\Big((1-p(x-1))\mathcal{P}(x-1,0,y-1,1,0)\\
&+ (1-p(x-1)d(y-1))\mathcal{P}(x-1,0,y-1,1,1)\Big),
\end{aligned} \tag{B.1}$$

where in the first line $\mathcal{P}(x, 1, y, 0, 0)$ has been written based on the probability of reaching to its two possible previous states and the second line is derived by writing the probabilities in the first line based on their possible previous states and similarly

for the next step. This means that we have written $\mathcal{P}(x,1,y,0,0)$ based on the asymptotic probabilities of reaching to its three-step past states. We also know that

$$\mathcal{P}(x-1,1,y,0,0) = p(x-1)\mathcal{P}(x-1,0,y,1,0) + p(x-1)d(y)\mathcal{P}(x-1,0,y,1,1), \tag{B.2}$$

and similarly,

$$\begin{aligned}\mathcal{P}(x-1,1,y-1,0,0) &= p(x-1)\mathcal{P}(x-1,0,y-1,1,0)\\ &+ p(x-1)d(y-1)\mathcal{P}(x-1,0,y-1,1,1).\end{aligned} \tag{B.3}$$

Now, if we substitute (B.2) and (B.3) in (B.1) then we have

$$\begin{aligned}\mathcal{P}(x,1,y,0,0) &= p(x)(1-q(y))\Big((1-p(x-1))\big(\mathcal{P}(x-1,1,y,0,1)\\ &- p(x-1)d(y)\mathcal{P}(x-1,0,y,1,1)\big)/p(x)\\ &+ (1-p(x-1)d(y)\mathcal{P}(x-1,0,y,1,1))\Big)\\ &+ p(x)d(y)q(y)\Big((1-p(x-1))\mathcal{P}(x-1,0,y-1,1,0)\\ &+ (1-p(x-1)d(y-1))\big(\mathcal{P}(x-1,1,y-1,0,1)\\ &- p(x-1)\mathcal{P}(x-1,0,y-1,1,0)\big)/(p(x)d(y-1))\Big).\end{aligned} \tag{B.4}$$

Next, we simplify (B.4) and substitute the definition of $\mathcal{P}(x-1,0,y-1,1,0)$ and $\mathcal{P}(x-1,0,y,1,1)$ based on $\mathcal{P}(x-1,0,y-1,0,1)$ in (B.4). As mentioned in Chapter 6, we denote $\mathcal{P}(x,1,y,0,0)$ by $\mathcal{F}(x,y)$ and $\mathcal{P}(x,0,y,0,1)$ by $\mathcal{G}(x,y)$. As such, after the simplifications of (B.4) we can write

$$\begin{aligned}\mathcal{F}(x,y) &= \alpha_1(x,y)\mathcal{F}(x-1,y) + \alpha_2(x,y)\mathcal{F}(x-1,y-1)\\ &\quad + \alpha_3(x,y)\mathcal{G}(x-1,y-1),\\ \mathcal{G}(x,y) &= \alpha_4(x,y)\mathcal{F}(x-1,y) + \alpha_5(x,y)\mathcal{G}(x-1,y-1),\end{aligned} \tag{B.5}$$

where its coefficients are functions of $p(.)$, $q(.)$ and $d(.)$. This proves the general case in Theorem 6.3.1. Based on the structure of the presented interdependent Markov

chain model, there are three special cases that the coefficients do not follow the general case presented in (6.8). This is because certain states do not have all the previous states that we used in the derivation of the above difference equations. For instance, when $y = 1$ the state $s = (x - 1, 0, y - 1, 1, 1)$ in the above equations does not have any previous state. Similarly, the cases where $y = x$ and $y = x - 1$ need to be considered as special cases due to the assumption that communication failures are triggered by power failures and thus certain states are not possible as previous states. This is because we cannot have more communication failures than power failures in the system based on the assumptions of the model. The derivation of the difference equations for special cases is similar to the general case and thus have been omitted here.

Appendix C

Proof of Theorem 7.4.1

Theorem 7.4.1 is an extension of Slepian-Wolf Theorem to the case with four sources that two of them are co-located with the decoder and the other two are remote. Similarly to [95], the proof of Theorem 7.4.1 consists of two parts. First, we show that for the pair of rates in the region described in Theorem 7.4.1, there exists a sequence of codes with $\lim_{n\to\infty} P_e^{(n)} = 0$ (the achievability proof). Next, we will show that for every sequence of codes with $\lim_{n\to\infty} P_e^{(n)} = 0$ the rates satisfy the constraints in Theorem 7.4.1 (the converse proof).

Achievability proof of Theorem 1: Here, we use random binning technique [95], and the notion of typical sequences [93]. For X with a pmf $p_X(x)$ and $\varepsilon \in (0, 1)$, define the set of ε-typical n-sequences x^n as

$$\mathcal{T}_\varepsilon^n(X) = \{\ x^n : |\pi(x|x^n) - p_X(x)| \leq \varepsilon p(x) \text{ for all } x \in \mathcal{X}\ \},$$

where, $\pi(x|x^n) = |\{i : x_i = x\}|/n$ for $x \in \mathcal{X}$, which $\mathcal{X}$ is the corresponding alphabet of X_i's. The notion of typicality can be extended to multiple random variables. To review of the properties of ε-typical sets see [93].

Codebook generation. Randomly and independently assign an index $m_1(x_1^n)$ to each sequence $x_1^n \in \mathcal{X}_1^n$ according to a uniform pmf over $[1 : 2^{nR_1}]$. Sequences with the same index m_i form a bin $\mathcal{B}_1(m_i)$. We do the same for the second source. The bin assignments are revealed to nodes and the CN.

Encoding. Upon observing $x_1^n \in \mathcal{B}_1(m_1)$, encoder 1 sends m_1. Similarly, for $x_2^n \in \mathcal{B}_1(m_2)$, encoder 2 sends m_2.

Decoding. Given the received index pair (m_1, m_2), the decoder declares $(\hat{x}_1^n, \hat{x}_2^n)$ to be the estimate of the sources if it is the unique pair in the product bin $\mathcal{B}_1(m_1) \times \mathcal{B}_2(m_2)$ such that $(x_1^n, x_2^n, y_1^n, y_2^n)$ is jointly typical; otherwise it declares an error.

Analysis of the probability of error. We bound the probability of error averaged over bin assignments. Let M_1 and M_2 denote the random bin indices for X_1^n and X_2^n, respectively. The decoder makes an error if and only if one or more of the following events occur:

$$
\begin{aligned}
\mathcal{E}_1 &= \{(X_1^n, X_2^n, Y_1^n, Y_2^n) \notin \mathcal{T}_\varepsilon^n \}, \\
\mathcal{E}_2 &= \{\tilde{x}_1^n \in \mathcal{B}_1(M_1) \text{for some } \tilde{x}_1^n \neq X_1^n, (\tilde{x}_1^n, X_2^n, Y_1^n, Y_2^n) \in \mathcal{T}_\varepsilon^n\}, \\
\mathcal{E}_3 &= \{\tilde{x}_2^n \in \mathcal{B}_2(M_2) \text{for some } \tilde{x}_2^n \neq X_2^n, (\tilde{x}_2^n, X_1^n, Y_1^n, Y_2^n) \in \mathcal{T}_\varepsilon^n\}, \\
\mathcal{E}_4 &= \{\tilde{x}_1^n \in \mathcal{B}_1(M_1), \tilde{x}_2^n \in \mathcal{B}_2(M_2) \\
&\quad \text{for some } \tilde{x}_1^n \neq X_1^n, \tilde{x}_2^n \neq X_2^n, (\tilde{x}_1^n, \tilde{x}_2^n, Y_1^n, Y_2^n) \in \mathcal{T}_\varepsilon^n\}.
\end{aligned}
$$

Then by the union of events bound, the average probability of error is upper bounded as

$$
\mathsf{P}\{\mathcal{E}\} \leq \mathsf{P}\{\mathcal{E}_1\} + \mathsf{P}\{\mathcal{E}_2\} + \mathsf{P}\{\mathcal{E}_3\} + \mathsf{P}\{\mathcal{E}_4\}. \tag{C.1}
$$

Now, we bound each probability of error term. By the law of large numbers and definition of ε-typical sets, $\mathsf{P}\{\mathcal{E}_1\}$ tends to zero as $n \to \infty$. For the second term,

using symmetry of the codebook construction, we have

$$\begin{aligned}
&\mathsf{P}\{\mathcal{E}_2|X_1^n \in \mathcal{B}_1(1)\} \\
&= \sum_{(x_1^n,x_2^n,y_1^n,y_2^n)} \Bigg(p_{(X_1^n,X_2^n,Y_1^n,Y_2^n)}((x_1^n,x_2^n,y_1^n,y_2^n)|X_1^n \in \mathcal{B}_1(1)) \times \\
&\mathsf{P}\{\tilde{x}_1^n \in \mathcal{B}_1(M_1) \text{ for some } \tilde{x}_1^n \neq X_1^n, (\tilde{x}_1^n, X_2^n, Y_1^n, Y_2^n) \in \mathcal{T}_\varepsilon^n| \\
&x_1^n \in \mathcal{B}_1(M_1), (X_1^n,X_2^n,Y_1^n,Y_2^n) = (x_1^n,x_2^n,y_1^n,y_2^n)\} \Bigg) \\
&= \sum_{(x_1^n,x_2^n,y_1^n,y_2^n)} \Bigg(p_{(X_1^n,X_2^n,Y_1^n,Y_2^n)}(x_1^n,x_2^n,y_1^n,y_2^n) \times \sum_{\tilde{x}_1^n \in \mathcal{T}_\varepsilon^n(X_1|x_2^n,y_1^n,y_2^n)} \mathsf{P}\{\tilde{x}_1^n \in \mathcal{B}_1(1)\} \Bigg) \\
&\leq 2^{n(H(X_1|X_2,Y_1,Y_2)+\delta(\varepsilon))} 2^{-nR_1}, \qquad \text{(C.2)}
\end{aligned}$$

which tends to zero as $n \to \infty$ if $R_1 > H(X_1|X_2,Y_1,Y_2) + \delta(\varepsilon)$. Similarly, $\mathsf{P}\{\mathcal{E}_3\}$ and $\mathsf{P}\{\mathcal{E}_4\}$ tend to zero as $n \to \infty$ if $R_2 > H(X_2|X_1,Y_1,Y_2) + \delta(\varepsilon)$ and $R_1 + R_2 > H(X_1,X_2|Y_1,Y_2) + \delta(\varepsilon)$. Therefore, there exists a sequence of bin assignments with $\lim_{n\to\infty} P_e^{(n)} = 0$. This completes the achievability proof of the theorem.

Converse proof of Theorem 1: Given a sequence of codes with $\lim_{n\to\infty} P_e^{(n)} = 0$, let K_1 and K_2 denote the indices from encoders 1 and 2, respectively. By Fano's inequality [93], we have

$$\begin{aligned}
&H(X_1^n|K_1,K_2,Y_1^n,Y_2^n) \leq H(X_1^n|\hat{X}_1^n) \qquad \text{(C.3)} \\
&\leq 1 + nP_e^{(n)} \log|\mathcal{X}| = n\varepsilon_n,
\end{aligned}$$

where ε_n tends to zero as $n \to \infty$ by the assumption that $\lim_{n\to\infty} P_e^{(n)} = 0$. Now consider

$$
\begin{aligned}
nR_1 &\geq H(K_1) \qquad\qquad (C.4)\\
&\geq H(K_1|K_2, Y_1^n, Y_2^n)\\
&= H(K_1|K_2, Y_1^n, Y_2^n) + H(X_1^n|K_1, K_2, Y_1^n, Y_2^n)\\
&- H(X_1^n|K_1, K_2, Y_1^n, Y_2^n)\\
&= H(X_1^n, K_1|K_2, Y_1^n, Y_2^n) - H(X_1^n|K_1, K_2, Y_1^n, Y_2^n)\\
&\geq H(X_1^n, K_1|K_2, Y_1^n, Y_2^n) - n\varepsilon_n\\
&= H(X_1^n|K_2, Y_1^n, Y_2^n) - n\varepsilon_n\\
&\geq H(X_1^n|X_2^n, K_2, Y_1^n, Y_2^n) - n\varepsilon_n\\
&= H(X_1^n, K_2|X_2^n, Y_1^n, Y_2^n) - H(K_2|X_2^n, Y_1^n, Y_2^n) - n\varepsilon_n\\
&= H(X_1^n|X_2^n, Y_1^n, Y_2^n) + H(K_2|X_1^n, X_2^n, Y_1^n, Y_2^n) - n\varepsilon_n\\
&= nH(X_1|X_2, Y_1, Y_2) - n\varepsilon_n.
\end{aligned}
$$

Here, we have used $H(A_1, A_2|A_3) = H(A_1|A_3) + H(A_2|A_1, A_3)$, a property of the conditional entropy, multiple times, where A_i's are arbitrary random variables. Now, by taking $n \to \infty$, we can conclude that $R_1 \geq H(X_1|X_2, Y_1, Y_2)$. This completes the converse proof of Theorem 7.4.1.

References

[1] D. E. Newman B. A. Carreras, V. E. Lynch and I. Dobson. Blackout mitigation assessment in power transmission systems. In *36th Annual Hawaii International Conference on System Sciences, HICSS*, 2003.

[2] Final report on the august 14th, 2003 blackout in the united states and canada. *U.S.-Canada System Outage Task Force*, 2004.

[3] Pual Hines. *A Decentralized Approach to Reducing the Social Costs of Cascading Failures*. PhD Dissertation,Carnegie Mellon University, 2007.

[4] 1992-2009 system disturbances reports. *North American Electric Reliability Council*, 2009.

[5] I. Dobson, B. A. Carreras, and D. E. Newman. Branching process models for the exponentially increasing portions of cascading failure blackouts. Jan. 2005.

[6] Final report of the investigation committee on the 28 september 2003 blackout in italy. *Union for the Coordination of Transmission of Electricity*, 2004.

[7] S Robinson. The power grid as complex system. *SIAM: Society for Industrial and Applied Mathematics:*, 12(1), 2002.

[8] Alexander Veremyev, Alexey Sorokin, Vladimir Boginski, and Eduardo L. Pasiliao. Minimum vertex cover problem for coupled interdependent networks with cascading failures. *European Journal of Operational Research*, 232(3):499 – 511, 2014.

[9] R. Baldick et al. Initial review of methods for cascading failure analysis in electric ieee pes cams task force on understanding, prediction, mitigation and restoration of cascading failures. *Power and Energy Society General Meeting - Conversion and Delivery of Electrical Energy in the 21st Century*, Jul. 2008.

[10] P. Hines, E. Cotilla-Sanchez, and S. Blumsack. Topological models and critical slowing down: Two approaches to power system blackout risk analysis. *44th Hawaii International Conference on System Sciences (HICSS)*, pages 1–10, 2011.

[11] Christopher L. DeMarco. A phase transition model for cascading network failure. *IEEE Control Systems Magazine*, 21(6):40–51, Dec. 2001.

[12] V. Latora P. Crucitti and M. Marchiori. Model for cascading failures in complex networks. *Physical Review E*, 69(4), 2004.

[13] Hongda Xiao and E.M. Yeh. Cascading link failure in the power grid: A percolation-based analysis. *IEEE International Conference on Communications Workshops (ICC)*, pages 1–6, 2011.

[14] I. Dobson, B. A. Carreras, and D. E. Newman. A loading-dependent model of probabilistic cascading failure. *Probability in the Engineering and Informational Sciences*, 19(1):15–32, Apr. 2005.

[15] I. Dobson, B. A. Carreras, and D. E. Newman. A branching process approximation to cascading load-dependent system failure. Jan. 2004.

[16] I. Dobson, K. R. Wierzbicki, B. A. Carreras, V. E. Lynch, and D. E. Newman. An estimator of propagation of cascading failure. Jan. 2006.

[17] Zhifang Wang, A. Scaglione, and R.J. Thomas. A markov-transition model for cascading failures in power grids. *45th Hawaii International Conference on System Science, HICSS*, pages 2115–2124, 2012.

[18] A. Pievatolo, E. Tironi, and I. Valade. Semi-markov processes for power system reliability assessment with application to uninterruptible power supply. *IEEE Transactions on Power Systems*, 19(3):1326–1333, Aug. 2004.

[19] Hui Ren and I. Dobson. Using transmission line outage data to estimate cascading failure propagation in an electric power system. *IEEE Transactions on Circuits and Systems II: Express Brief*, 55(9):927–931, Sep. 2008.

[20] I. Dobson. Estimating the propagation and extent of cascading line outages from utility data with a branching process. *IEEE Transactions on Power Systems*, 27(4):2146–2155, Nov. 2012.

[21] Massoud Amin. Toward secure and resilient interdependent infrastructures. *Journal of Infrastructure Systems*, 8(3):67–75, 2002.

[22] Richard G. Little. Controlling cascading failure: Understanding the vulnerabilities of interconnected infrastructures. *Journal of Urban Technology*, 9(1):109–123, 2002.

[23] S.M. Rinaldi. Modeling and simulating critical infrastructures and their interdependencies. In *37th Annual Hawaii International Conference on System Sciences, HICSS*, Jan. 2004.

[24] S.M. Rinaldi, J.P. Peerenboom, and T.K. Kelly. Identifying, understanding, and analyzing critical infrastructure interdependencies. *IEEE Control Systems*, 21(6):11–25, Dec. 2001.

[25] Hyeung-Sik J. Min, Walter Beyeler, Theresa Brown, Young Jun Son, and Albert T. Jones. Toward modeling and simulation of critical national infrastructure interdependencies. *IIE Transactions*, 39(1):57–71, 2007.

[26] J. Craig L. Dueas-Osorio and B. Goodno. Probabilistic response ofinterdependent infrastructure networks. *2nd Annual meeting of the Asian pacific network of center*, 2004.

[27] B. J. Goodno L. Dueas-Osorio, J. I. Craig and A. Bostrom. Interdependent response of networked systems. *Journal of Infrastructure Systems*, 13(3):185–194, 2007.

[28] J. I. Craig L. Dueas-Osorio1 and B.J. Goodno. Seismic response of critical interdependent networks. *Earthquake Engineering and Structural Dynamics*, 36:285–306, 2007.

[29] Min Ouyang, Liu Hong, Zi-Jun Mao, Ming-Hui Yu, and Fei Qi. A methodological approach to analyze vulnerability of interdependent infrastructures. *Simulation Modelling Practice and Theory*, 17(5):817 – 828, 2009.

[30] D.A. Reed, K.C. Kapur, and R.D. Christie. Methodology for assessing the resilience of networked infrastructure. *IEEE Systems Journal*, 3(2):174–180, Jun. 2009.

[31] S. V. Buldyrev et al. Catastrophic cascade of failures in interdependent networks. *Nature*, 464:1025 –1028, Apr. 2010.

[32] S.V. Buldyrev H.E. Stanley S. Havlin W. Li, A. Bashan. Cascading failures in interdependent lattice networks: the critical role of the length of dependency links. *Phys. Rev. Lett,*, 108:228702, 2012.

[33] Jianwei Wang, Chen Jiang, and Jianfei Qian. Robustness of interdependent networks with different link patterns against cascading failures. *Physica A: Statistical Mechanics and its Applications*, 393(0):535 – 541, 2014.

[34] K. Hopkinson et al. Epochs: a platform for agent-based electric power and communication simulation built from commercial off-the-shelf components. *IEEE Transactions on Power Systems*, 21(2):548–558, 2006.

[35] Hua Lin et al. Power system and communication network co-simulation for smart grid applications. In *Innovative Smart Grid Technologies (ISGT), 2011 IEEE PES*, pages 1–6, 2011.

[36] F. Tiriticco S. Meloni S. De Porcellinis R. Setola V. Rosato, L. Issacharoff. Modeling interdependent infrastructures using interacting dynamical models. *International Journal of Critical Infrastructures*, 4:6379, 2008.

[37] E. Zio and G. Sansavini. Modeling interdependent network systems for identifying cascade-safe operating margins. *IEEE Transactions on Reliability*, 60(1):94–101, Mar. 2011.

[38] Jin Wei, D. Kundur, T. Zourntos, and K. Butler-Purry. A flocking-based dynamical systems paradigm for smart power system analysis. In *IEEE Power and Energy Society General Meeting*, pages 1–8, 2012.

[39] D.E. Newman, B. Nkei, B.A. Carreras, I. Dobson, V.E. Lynch, and P. Gradney. Risk assessment in complex interacting infrastructure systems. In *38th Annual Hawaii International Conference on System Sciences, HICSS*, Jan. 2005.

[40] B.A. Carreras et al. Interdependent risk in interacting infrastructure systems. In *40th Annual Hawaii International Conference on System Sciences, HICSS*, pages 112–112, 2007.

[41] Charles D. Brummitt, Raissa M. DSouza, and E. A. Leicht. Suppressing cascades of load in interdependent networks. *Proceedings of the National Academy of Sciences*, 109(12):E680–E689, 2012.

[42] Marian Anghel, Kenneth A. Werley, and Adilson E. Motter. Stochastic model for power grid dynamics. Jan. 2007.

[43] I. Dobson, B.A. Carreras, and D.E. Newman. Branching process models for the exponentially increasing portions of cascading failure blackouts. Jan. 2005.

[44] I. Dobson, K.R. Wierzbicki, Janghoon Kim, and Hui Ren. Towards quantifying cascading blackout risk. *Bulk Power System Dynamics and Control - VII. Revitalizing Operational Reliability, iREP Symposium*, Aug. 2007.

[45] Janghoon Kim and I. Dobson. Approximating a loading-dependent cascading failure model with a branching process. *IEEE Transactions on Reliability*, 59(4):691 –699, Dec. 2010.

[46] H. Hermanns. *Interactive Markov Chains and the Quest for Quantified Quality*. 2002.

[47] A. Ponse J.A. Bergstra and S.A. Smolka. *Handbook of Process Algebra*. 2001.

[48] J. Hillston A. Clark, S. Gilmore and M. Tribastone. Stochastic process algebras. *Formal Methods for Performance Evaluation*, 4486:132179, 2007.

[49] A. J. Wood and B. F. Wollenberg. *Power Generation, Operation, and Control*. New York: Wiley, second edition, 1996.

[50] Ye Yan, Yi Qian, H. Sharif, and D. Tipper. A survey on smart grid communication infrastructures: Motivations, requirements and challenges. *IEEE Communications Surveys Tutorials*, 15(1):5–20, 2013.

[51] Fangxing Li et al. Smart transmission grid: Vision and framework. *IEEE Transactions on Smart Grid*, 1(2):168–177, 2010.

[52] J. Duncan Glover, Mulukutla S. Sarma, and Thomas Jeffrey Overbye. *Power system analysis and design*. Cengage Learning, fourth edition, 2008.

[53] I. Dobson, B. A. Carreras, V. E. Lynch, and D. E. Newman. Complex systems analysis of series of blackouts: cascading failure, critical points, and self-organization. *Chaos*, 17(2), 2007.

[54] Quan Chen and L. Mili. Composite power system vulnerability evaluation to cascading failures using importance sampling and antithetic variates. *IEEE Transactions on Power Systems*, 28(3):2321–2330, Aug. 2013.

[55] M. Bockarjova and G. Andersson. Transmission line conductor temperature impact on state estimation accuracy. *IEEE Lausanne Power Tech*, pages 701–706, 2007.

[56] K. Turitsyn R. Ptzner and M. Chertkov. Controlled tripping of overheated lines mitigates power outages. *arXiv:1104.4558v2*, 2011.

[57] Jie Chen, James S. Thorp, and Ian Dobson. Cascading dynamics and mitigation assessment in power system disturbances via a hidden failure model. *International Journal of Electrical Power and Energy Systems*, 27(4):318 – 326, 2005.

[58] R.D. Zimmerman, C.E. Murillo-Sanchez, and R.J. Thomas. Matpower: Steady-state operations, planning, and analysis tools for power systems research and education. *IEEE Transactions on Power Systems*, 26(1):12–19, 2011.

[59] M.J. Eppstein and P.D.H. Hines. A random chemistry algorithm for identifying collections of multiple contingencies that initiate cascading failure. *IEEE Transactions on Power Systems*, 27(3):1698–1705, Aug. 2012.

[60] A. Bernstein, D. Bienstock, D. Hay, M. Uzunoglu, and G. Zussman. Power grid vulnerability to geographically correlated failures-analysis and control implications. *arXiv preprint arXiv:1206.1099*, 2012.

[61] A. Bernstein, D. Bienstock, D. Hay, M. Uzunoglu, and G. Zussman. Power grid vulnerability to geographically correlated failures - analysis and control implications. 2014.

[62] S. Neumayer, G. Zussman, R. Cohen, and E.Modiano. Assessing the impact of geographically correlated network failures. In *IEEE MILCOM*, 2008.

[63] Vito Latora and Massimo Marchiori. Reliability modeling and analysis of communication networks with dependent failures. *IEEE Transactions on Communications*, 34(1):82–84, 1986.

[64] D. Papadimitriou et al. Inference of shared risk link groups.

[65] H. Lee and E. Modiano. Diverse routing in networks with probabilistic failures. In *Proc. IEEE INFOCOM*, 2009.

[66] S. Neumayer, G. Zussman, R. Cohen, and E. Modiano. Assessing the vulnerability of the fiber infrastructure to disasters. In *Proc. IEEE INFOCOM*, 2009.

[67] P. Erdös and A. Rényi. Some generalized max-flow min-cut problems in the plane. *Mathematics of Operations Research*, 16(2):310–333, 1991.

[68] P.K. Agarwal, A. Efrat, S.K. Ganjugunte, D. Hay, S. Sankararaman, and G. Zussman. Network vulnerability to single, multiple, and probabilistic physical attacks. In *Proceedings of IEEE MILCOM*, 2010.

[69] D. Magoni. Tearing down the internet. *IEEE Journal on Selected Areas in Communications*, 21(6):949–960, Aug. 2003.

[70] R.L. Church, M.P. Scaparra, and R.S. Middleton. Identifying critical infrastructure: The median and covering facility interdiction problems. *Annals of the Association of American Geographers*, 94(3):491–502, Aug. 2004.

[71] Z. Kong and E.M. Yeh. Resilience to degree-dependent and cascading node failures in random geometric networks. *IEEE Transactions on Information Theory*, 56(11):5533–5546, 2010.

[72] K. Goseva-Popstojanova and K.S. Trivedi. Failure correlation in software reliability models. *IEEE Transactions on Reliability*, 49:37–48, Mar. 2000.

[73] Y.-S. Dai, G. Levitin, and K.S. Trivedi. Performance and reliability of tree-structured grid services considering data dependence and failure correlation. *IEEE Transactions on Computers*, 56:925–936, 2007.

[74] M. Gallet, N. Yigitbasi, B. Javadi, D. Kondo, A. Iosup, and D. Epema. *A Model for Space-Correlated Failures in Large-Scale Distributed Systems*. Springer, 2010.

[75] Amin S. Schwartz G. Johansson K. Sandberg H. Andreasson, M. and S. Sastry. Correlated failures of power systems: Analysis of the nordic grid. pages 9–17, 2011.

[76] D.J. Daley and David Vere-Jones. *An Introduction to the Theory of Point Processes*. Springer, second edition, 2003.

[77] D.J Strauss. A model for clustering. *Biometrika*, 62:467–475, 1975.

[78] B. D. Ripley. Algorithm as 137: Simulating spatial patterns: Dependent samples from a multivariate density. *Journal of the Royal Statistical Society. Series C (Applied Statistics)*, 28:109–112, 1979.

[79] Paolo Crucitti, Vito Latora, Massimo Marchiori, and Andrea Rapisarda. Efficiency of scale-free networks: error and attack tolerance. *Physica A: Statistical Mechanics and its Applications*, 320:622–642, 2003.

[80] Bonneville power administration transmission services operations and reliability.

[81] S. Karlin and H. M. Taylor. *A First Course in Stochastic Processes*. 1975.

[82] G. Journel. Combining knowledge from diverse sources: An alternative to traditional data independence hypotheses. *Mathematical Geology*, 34(5):573–596, 2002.

[83] D. P. Nedic, I. Dobson, D. S. Kirschen, B. A. Carreras, and V. E. Lynch. Criticality in a cascading failure blackout model. In *Fifteenth Power Systems Computation Conference, Liege Belgium*, 2005.

[84] J.E. Pezoa and M.M. Hayat. Performance and reliability of non-markovian heterogeneous distributed computing systems. *IEEE Transactions on Parallel and Distributed Systems*, 23(7):1288–1301, Jul. 2012.

[85] M.M. Hayat and J.A. Gubner. A two-step markov point process. In *IEEE International Symposium on Information Theory*, Sep. 1995.

[86] T. Berger, Zhen Zhang, and H. Viswanathan. The ceo problem [multiterminal source coding]. *IEEE Transactions on Information Theory*, 42(3):887 –902, May 1996.

[87] Mahshid Rahnamay-Naeini, Nasir Ghani, and Majeed Hayat. On the interplay between resource-management overhead and performance in sensor networks: An information theoretic approach. In *IEEE Global Telecommunications Conference, GLOBECOM*, 2013.

[88] R. Gallager. Basic limits on protocol information in data communication networks. *IEEE Transactions on Information Theory*, 22(4):385 – 398, Jul. 1976.

[89] Di Wang and A.A. Abouzeid. Link state routing overhead in mobile ad hoc networks: A rate-distortion formulation. In *The 27th Conference on Computer Communications, IEEE INFOCOM*, April 2008.

[90] Di Wang and A.A. Abouzeid. On the cost of knowledge of mobility in dynamic networks: An information-theoretic approach. *IEEE Transactions on Mobile Computing*, 11(6):995 –1006, June 2012.

[91] Gang Cheng and Nirwan Ansari. Rate-distortion based link state update. *Computer Networks*, 50(17):3300–3314, Dec. 2006.

[92] Jun Hong and V.O.-K. Li. Impact of information on network performance - an information-theoretic perspective. In *IEEE Global Telecommunications Conference GLOBECOM*, pages 1–6, 2009.

[93] Abbas El Gamal and Young-Han Kim. *Network Information Theory*. Cambridge University Press, 2012.

[94] D. Slepian and J. Wolf. Noiseless coding of correlated information sources. *IEEE Transactions on Information Theory*, 19(4):471 – 480, July 1973.

[95] T. Cover. A proof of the data compression theorem of slepian and wolf for ergodic sources (corresp.). *IEEE Transactions on Information Theory*, 21(2):226 – 228, Mar. 1975.